Title
Understanding Charge Transport in Polymers for Thermoelectric Applications

Author
Glaudell, Anne

Publication Date
2016

University of California
Santa Barbara

Understanding Charge Transport in Polymers for Thermoelectric Applications

A dissertation submitted in partial satisfaction
of the requirements for the degree

Doctor of Philosophy
in
Materials

by

Anne Marie Glaudell

Committee in charge:

Professor Michael Chabinyc, Chair
Professor Ram Seshadri
Professor Rachel Segalman
Professor Bradley Chmelka

June 2016

The Dissertation of Anne Marie Glaudell is approved.

Professor Ram Seshadri

Professor Rachel Segalman

Professor Bradley Chmelka

Professor Michael Chabinyc, Committee Chair

March 2016

Understanding Charge Transport in Polymers for Thermoelectric Applications

by

Anne Marie Glaudell

Acknowledgements

I would first like to extend my utmost gratitude to my advisor, Prof. Michael Chabinyc, for recruiting me to his research lab, and for his academic guidance and patience throughout my time at UC Santa Barbara. Thank you to Professors Ram Seshadri, Rachel Segalman, and Brad Chmelka for their time and effort on my dissertation committee and for helpful discussions and advice. I would gratefully acknowledge my financial support that enabled me to pursue this research, as well as for funding to participate in academic conferences in the US and abroad: AFOSR MURI program under FA9550-12-1-0002, ConvEne IGERT Program of the National Science Foundation under NSF-DGE 0801627, IRG 2 under MRSEC Program of the National Science Foundation under Award No. DMR 1121053.

I sincerely appreciate the knowledgeable and helpful administrative staff of Materials and MRL, who keep track of the important things so we all may focus on the science. Thank you to the technical staff of Materials, MRL, and CNSI for their valuable expertise and assistance in measurement acquisition and analysis. The wonderful people at the Physics Machine Shop were also absolutely essential in the completion of this work, for their expertise and creative solutions for the instrumentation build, and seemingly endless emergency spare parts to keep lab equipment in commission.

I could not have asked for a better research group than Chabinyc lab members, who contributed to a wonderful environment in which to work, on both the professional and personal level. I would especially like to thank Justin Cochran, former fellow graduate student in the Chabinyc group, for being my mentor and introduction to the Chabinyc lab, and teaching me enough chemistry to prevent me from accidentally blowing my self up. I also thank fellow physics person Dr. Chris Takacs for the many insanely useful discussions and occasionally commiserations on building instrumentation, always over a

cup of expertly-brewed coffee. And to the remaining Chabinyc group post-docs, fellow graduate students, and collaborators, I have learned so much from you all.

In writing this acknowledgements section, I have found it a surprisingly monumental task to individually mention and thank each person that has had a meaningful impact on the completion of this Ph.D, without leaving someone out. Thank you to the innumerable unnamed people that have inspired and supported me along the way, including friends, family, friends that have become family, colleagues, collaborators, and mentors.

Finally, I am forever grateful to my family especially my parents for their unwavering and unconditional love, support, and patience, and to whom I dedicate this dissertation.

Curriculum Vitæ Anne Marie Glaudell

Education

2010 - 2016	Doctor of Philosophy (Ph.D.) in Materials (Expected) University of California Santa Barbara.
2006 - 2010	Bachelor of Science (B.S.) in Physics University of Illinois at Urbana-Champaign

Research

2010 - 2016	**Graduate Student Researcher**, Prof. M. L. Chabinyc Materials Dept., UC Santa Barbara NSF Convene IGERT Fellow
2009	**Research Intern**, Stuart S. Parkin Laboratory Science & Technology Division, IBM Almaden, San Jose CA American Physical Society/IBM Research Internship for Undergraduate Women
2008 - 2009	**Undergraduate Researcher**, Prof. Laura H. Greene Materials Research Laboratory, U. Illinois

Teaching

Winter 2013	**Teaching Assistant** Crystallography and Diffraction Fundamentals, MATRL 209A Graduate Level Course, Materials, UC Santa Barbara
Spring 2010	**Discussion Teaching Assistant** College Physics - Mechanics Undergraduate Level Course, Physics, U. Illinois
Fall 2009	**Laboratory Teaching Assistant** College Physics - E&M and Modern Undergraduate Level Course, Physics, U. Illinois

Publications

- B. Russ, **A. M. Glaudell**, J. J. Urban, M. L. Chabinyc, and R. A. Segalman, ”Organic Thermoelectrics for Conformal Energy Harvesting and Personal Comfort,” *Nature Reviews Materials*, in revisions (2016).
- S. N. Patel, **A. M. Glaudell**, D. Kiefer, and M. L. Chabinyc, ”Increasing the Thermoelectric Power Factor of a Semiconducting Polymer by Doping from the Vapor Phase.” ACS Macro Letters 5 (Feb., 2016) 268272.

- **A. M. Glaudell**, J. E. Cochran, S. N. Patel, and M. L. Chabinyc, ”Impact of the Doping Method on Conductivity and Thermopower in Semiconducting Polythiophenes.” Advanced Energy Materials 5 (Oct., 2015) 1401072
- S. Bubel, A.J. Hauser, **A.M. Glaudell**, T.E. Mates, S. Stemmer, M.L. Chabinyc. The Electrochemical Impact of Electrostatic Modulation of the Metal-Insulator Transition in Nickelates. Applied Physics Letters (2015), 106, 122102
- J. E. Cochran, M. J. N. Junk, **A. M. Glaudell**, P. L. Miller, J. S. Cowart, M. F. Toney, C. J. Hawker, B. F. Chmelka, and M. L. Chabinyc, ”Molecular Interactions and Ordering in Electrically Doped Polymers: Blends of PBTTT and F_4TCNQ .” Macromolecules 47 (Oct., 2014) 68366846.
- **A.M. Glaudell**, M.L. Chabinyc. Electrically Conductive Polymers Convert Heat to Electricity. SPIE Newsroom. 28 July 2014.
- R. A. Schlitz, F. G. Brunetti, **A. M. Glaudell**, P. L. Miller, M. A. Brady, C. J. Takacs, C. J. Hawker, and M. L. Chabinyc, Solubility-Limited Extrinsic n-Type Doping of a High Electron Mobility Polymer for Thermoelectric Applications, Advanced Materials 26 (May, 2014) 28252830.
- **A. M. Glaudell**, R. A. Schlitz, M. L. Chabinyc, Seebeck Coefficient and Electrical Conductivity Optimization in Polymers in Innovative Thermoelectric Materials; H. E. Katz and T. O. Poehler, ed. Imperial College Press, England, In press

Abstract

Understanding Charge Transport in Polymers for Thermoelectric Applications

by

Anne Marie Glaudell

There is a great need to recycle energy wasted as heat into usable energy using clean, low-cost, and innovative technologies. Thermoelectric materials convert between heat and energy with no moving parts, and can be used to passively capture waste heat from industrial processes and for local fast temperature control. Traditional inorganic thermoelectric materials are efficient at high temperature and large temperature gradients, but are brittle and inflexible, often using environmentally harmful materials. Organic semiconductors have proved successful in commercial applications such as light-emitting diodes (OLEDs), solar cells (OPVs), and thin film transistors (OTFTs or OFETs), and there has recent been a significant research effort on organic materials for thermoelectric applications. Organic thermoelectric materials have the potential to fill voids that inorganic thermoelectric devices cannot. These materials can be solution deposited near room temperature onto flexible substrates, and generally perform well at room temperature. Flexible devices open up new applications for near room temperature thermoelectrics, and enable creative solutions for current applications. The challenge for efficient organic thermoelectrics is developing highly doped, stable p- and n-type materials, as intrinsic disorder in organic semiconductors makes predictive design non-trivial.

The effort is two fold: to assess the viability of high-mobility semiconducting polymers for thermoelectric applications, and to gain a deeper understanding of the underlying transport mechanism that governs electronic, thermoelectric, and optical properties. First, we evaluate the thermoelectric properties of a consistent set of polythiophenes

varying the dopant molecule and method. By comparing the electronic and thermoelectric properties studied here and the many existing OTE compounds in the literature, we demonstrate that a general relationship between electrical conductivity σ and thermopower α, $\alpha \propto \sigma^{-1/4}$, emerges over a large range of conductivity, polymers, and doping schemes. This empirical relationship can function as an approximate metric for assessing new materials as well as to guide improvements in thermoelectric performance in organics. Next, the temperature-dependent electronic and thermoelectric transport properties of the well-studied high-mobility polymer poly(2,5-bis(3-tetradecylthiophen-2-yl)thieno- [3,2-b]thiophene) (PBTTT-C_{14}) were studied for a range of processing conditions, dopants, and doping methods. In conjunction with microstructural characterization, we demonstrate how rational processing improves performance above what is expected from the empirical relationship, a key result in interpreting the transport measurements and understanding charge transport in PBTTT-C_{14} and other semiconducting polymers.

Contents

List of Figures

List of Tables

Chapter 1

Introduction

Portions of this chapter are published in or adapted from the following authored publications, with the appropriate permissions:

[5] B. Russ, **A. M. Glaudell** (*co-first author*), J. J. Urban, M. L. Chabinyc, and R. A. Segalman, Organic Thermoelectrics for Conformal Energy Harvesting and Personal Temperature Control, *Nature Reviews Materials*, in revisions, 2016.

[6] **A. M. Glaudell**, R. A. Schlitz, and M. L. Chabinyc, Innovative Thermoelectric Materials, ch. Seebeck Coefficient and Electrical Conductivity Optimization in Polymers. Imperial College Press, England.

Organic semiconductors have been studied extensively for applications in conductors and thin film electronics.High-performance organic photovoltaics (OPVs) with power conversion efficiencies near 10%,[7] all-printed circuits with both p- and n-type thin film transistors (TFTs),[8] and highly efficient organic light-emitting diodes (OLEDs)[9] have been demonstrated. These applications have driven the synthesis of a large range of materials with varying electronic structures[10–13] and an extensive study of the relationship of processing methods to their electrical performance.[14,15] The ability to process organic semiconductors using simple methods such as ink-jet printing make them attractive for the fabrication of thermoelectric devices.

Both organic semiconducting molecules and polymers have been studied as thermoelectrics. Foundational work on single co-crystals of electron donor and acceptors revealed that organic semiconductors can have metallic behavior, high electrical conductivity (~1-10 S-cm^{-1}) and signatures of 1D transport.[16–18] Such materials have exciting physical and electrical behavior, but they are challenging to process into devices due to their solubility and the difficulty of tuning their carrier concentration because of the need to maintain fixed stoichiometry between the donor and acceptor. Electrically doped semiconducting polymers provide a pathway toward greater processability because of the ability to tune the carrier concentration.16Iodine-doped polyacetylene has very high electrical conductivity (>1000 S-cm^{-1}) and thermoelectric performance rivals that of bismuth telluride at room temperature.[19] However, iodine-doped polyacetylene is known to be unstable.[20] Recent improvements in the synthetic chemistry of semiconducting polymers and stable doped polymers such as those based on 3,4-ethylenedioxythiophene (PEDOTs) suggest that these problems may be overcome.[21] However, the scope of this Dissertation will focus on the high mobility polymer poly(2,5-bis(3-tetradecylthiophen-2-yl)thieno[3,2-b]thiophene)(PBTTT-C$_{14}$), and polymers similar to it.

1.1 Basic Elements of Thermoelectrics

1.1.1 Physics & Characterization

Thermoelectric materials exhibit the Seebeck effect, in which carriers move in response to a temperature gradient. Charge carriers diffuse across the temperature gradient, creating a charge build up and thus a potential difference ΔV. The magnitude of this effect is the Seebeck coefficient or thermopower, and is simply the ratio of the potential built up divided by the applied thermal gradient: $\alpha = -\Delta V/\Delta T$. The overall thermoelectric performance of a material is generally benchmarked by ZT, the dimensionless thermoelectric figure of merit. ZT is comprised of the electrical conductivity σ, the thermopower α (also commonly S), and the thermal conductivity κ, and depends on the temperature T:

$$ZT = \frac{\alpha^2\sigma}{\kappa}T \tag{1.1}$$

A good thermoelectric material has a high ZT, and should be a good electrical conductor (high σ) and a poor thermal conductor (low κ). The three thermoelectric parameters σ, α, and κ are inter-related with carrier concentration, and decoupling these parameters is non-trivial, especially for disordered materials.

The Seebeck coefficient is directly related to the density of states, while the electrical conductivity can be limited by electronic and morphological defects. Electrical conductivity increases with carrier concentration n as $\sigma = e\mu n$, where e is the elementary charge (1.602×10^{-19} C), and μ is the carrier mobility. The Seebeck coefficient reflects the average entropy transported per charge carrier, and thus decreases with increasing carrier concentration. The thermal conductivity is comprised of a lattice contribution and an electronic contribution, $\kappa = \kappa_L + \kappa_E$, the latter of which increases with carrier concentration, as charge carriers can also transport heat.

To accurately assess a materials's thermoelectric performance, σ, α, and κ must be evaluated in the same direction as the temperature gradient. This is especially relevant for organic thermoelectric materials as the anisotropy of polymer chains tends to lead to macroscopic anisotropies in the material after processing, where the in-plane and out-of-plane properties may differ greatly. In solution-processed thin-film organic thermoelectric materials, the electrical conductivity and thermopower are measured in the in-plane direction. Practically, measuring the in-plane thermal conductivity of thin films is quite difficult. Thermal conductivity κ of thin films is measured using the 3-ω method or by

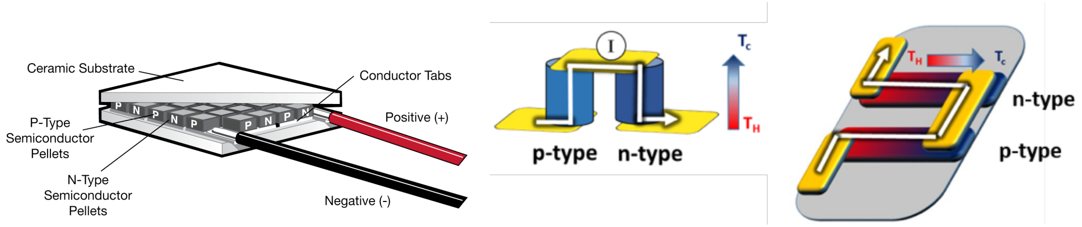

Figure 1.1: Schematic of a Peltier element (left),[22] a typical inorganic thermoelectric device used for local temperature control, with the temperature gradient shown perpendicular to the substrate (center). Solution processed devices lend to in-plane transport, with a temperature gradient parallel to the substrate (right).[5]

time domain thermal reflectance (TDTR), both of which extract the out-of-plane thermal conductivity.

1.1.2 Devices

The efficiency η of a thermoelectric device (for either power generation or cooling) is related to the figure of merit ZT of the material and the Carnot limit $\eta_C = \Delta T/T_{hot}$ via the following:

$$\eta = \eta_C \frac{\sqrt{1+ZT}-1}{\sqrt{1+ZT}+1} \tag{1.2}$$

A prototypical thermoelectric device consists of legs of alternating p- and n-type thermoelectric material that are electrically in series and thermally in parallel, as well as being ZT-matched. Traditional inorganic thermoelectric devices consist of bulk pellets tiled in two dimensions on a ceramic substrate that is patterned with electrical contacts, where the thermal gradient across the material is perpendicular to the substrate. This geometry is not well suited to many organics and other solution-processed materials, for which in-plane architectures are advantageous as the major direction of carrier transport is in the plane of the substrate. In this geometry, the thermal gradient across the material is parallel to the substrate. This necessitates the development of alternative device geometries to accommodate this processing restriction, and additionally takes advantage of the ability for OTEs to be printed on flexible substrates.

1.2 Electronic Properties of Organic Semiconductors

The fundamental difference in developing new organic materials compared to inorganic thermoelectrics is the approach to optimizing the thermoelectric figure of merit ZT. A good thermoelectric material is often described as an electronic crystal and a phonon glass.[23–25] Inorganic semiconductors are generally the former, thus the focus is on reducing the thermal conductivity κ by increasing phonon scattering to reduce the lattice contribution.[24] On the other hand, organic semiconducting materials, particularly polymers, are closer to a phonon glass in most cases. Thus, much of the organic literature focuses on increasing conduction and maximizing the power factor $\alpha^2\sigma$.

Organic materials form van der Waals solids with relatively weak electronic coupling between molecules compared to covalent solids, therefore molecular properties are frequently used as a basis for understanding the solid state electronic structure.[26] For molecules these are the highest occupied and lowest unoccupied molecular orbitals (HOMO and LUMO) that lead to the valence and conduction states in solids.[27] Depending on the molecular design, the gap between these electronic levels typically ranges from ∼1 to 3 eV and the position of the ionization energy (IE) and electron affinity (EA) with respect to vacuum can be shifted as well. Detailed descriptions of synthetic approaches for effectively modifying energetic levels in organic electronic materials can be found in a number of excellent reviews.[10, 28–30]

Organic semiconductors generally have low intrinsic carrier concentration as synthesized and, due to their relatively wide band gaps, require doping to increase their electrical conductivity. The addition or removal of electrons from the π-system of organic molecules causes intramolecular geometric distortions and also distortions of the arrangement of neighboring molecules or polymer chains.[27] For this reason, the carriers in organic materials are frequently described as polarons. The polaronic nature of organic materials can be observed using various methods, but optical spectroscopy is the simplest due to the substantial shift in the main optical absorption due to formation of polaronic electronic levels; due to the geometric relaxation sub-gap states are formed leading to a red-shift in the optical aborption upon doping.[27]

The introduction of carriers in itself does not necessarily lead to high electrical conductivity due to the role of structural order from the molecular scale to the on transport properties.[31] Within crystalline domains, charge transport can be highly anisotropic due to differences in the electronic coupling between molecules.[32] The need to couple π-electronic levels of molecules requires close intermolecular contacts to allow efficient charge transfer between molecules. The rigidity of conjugated units leads to molecules with planar functionalities that stack against each other, π-stacking, for strongest coupling. In polymers, the conjugated repeat units are strongly electronically coupled along the backbone and have weaker electronic coupling between stacked chains.[33,34] Functional moieties, e.g. alkyl sidechains, are added to improve solubility are highly insulating and prevent electronic communication between molecules through the chains. Because of these factors, orienting the backbone of polymers along the direction of transport can lead to improved delocalization of charge and significant enhancement of the electrical conductivity relative to non-oriented samples.[32] The ordered domains in organic semiconductors are small (∼100s nm) in many cases, therefore carriers must traverse many domains during transport, and as a result, apparent charge mobilities can be markedly diminished relative to what might be expected for a perfect single crystal.[34] Because of the structural disorder, along with the polaronic nature of the charge carriers, transport is not well described by band theories used for crystalline inorganic semiconductors and in many cases theories from disordered semiconductors are more successful in rationalizing their behavior.

1.3 Properties of Organic Thermoelectrics

Reported room-temperature ($\sim$ 300K) metrics of OTEs as a function of electrical conductivity are captured in Figure 1.2 for a broad range of state-of-the-art doped organic materials in comparison to the benchmark room-temperature material Bi_2Te_3. Clearly, performance of OTE materials operating at near room temperature conditions is rapidly approaching that of inorganic TE counterparts. Because the majority of OTE studies work to optimize the power factor, we will discuss the latest advances for enhancing the electrical conductivity and the Seebeck coefficient in OTEs and how collectively these studies are helping to future design rules. We also discuss the potential consequences of enhancements in the power factor on the resulting thermal conductivity, which is a strong function of morphology for most materials.

Considering the vast range of available molecular structures of organic materials, it is helpful to consider the performance requirements for potential room temperature thermoelectrics. Because the electrical conductivity must be relatively high in practical thermoelectrics ($>\sim$ 10 S/cm), one can estimate the requirements for the charge carrier mobility and carrier concentration in organic materials near room temperature. Given that the carrier concentration is limited by the molecular density ($\sim 10^{22}$ cm^{-3} in organic systems), the carrier mobility cannot be lower than $\sim$ 0.01 cm^2/Vs to achieve reasonable electrical conductivity at the highest doping physically possible. The observed mobilities of polymers based on field-effect measurements, which may measure across many domains, are $\sim$1 to 10 cm^2/Vs[57–60] Although field-effect measurements are confined to thin film interfaces, these mobilities are comparable to bulk doped materials. Whether the mobility measured at an interface by TFTs will translate directly to that in the bulk in the

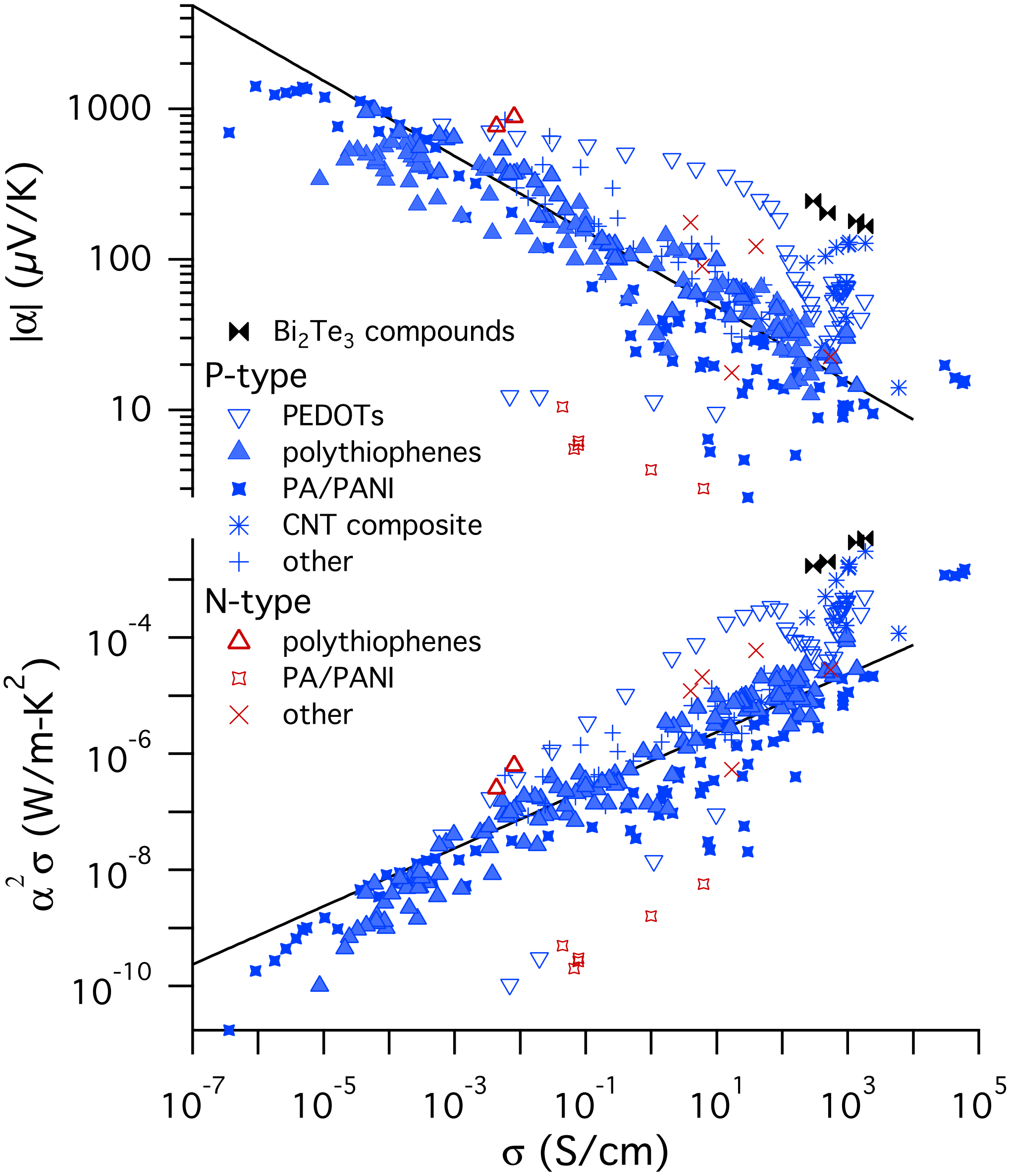

Figure 1.2: (from [5]) Literature compilation of the room-temperature thermoelectric properties of a variety of doped polymers and composites. Thermopower (Seebeck coefficient) α (top) and power factor $PF = \alpha^2\sigma$ (bottom) vs. electrical conductivity σ. The solid line indicates the empirical relationships $\alpha \propto \sigma^{-1/4}$ and $PF \propto \sigma^{1/2}$ from [35]. The plot highights PEDOTs,[2–4] polythiophenes,[1,35–39] polyacetylenes and polyanilines (PA/PANI),[40–43] carbon nanotube (CNT) composites,[44–49] and other organics.[38,50–53] The best room-temperature inorganic Bi_2Te_3 compounds are also included for reference.[54–56]

presence of dopant ions is uncertain, however one expects that similar trends will likely be observed. While these figures help determine the needs for the electrical conductivity, the dependence of the Seebeck coefficient on carrier concentration is difficult to predict for many materials making it the largest unknown for organic materials. As a requisite, TE materials must have high conductivities and tunable charge carrier concentrations. Here, we highlight important factors influencing how to introduce carriers into organic semiconductors, how these carriers are transported and their resulting thermopower.

1.3.1 Doping

Electrical doping of organic materials relies on forming a material that is chemically stable upon addition or removal of an electron by a dopant.[61] It is important to understand that in the literature, the terms p-type and n-type are frequently used to describe which apparent carrier mobility is largest in a material rather than the position of the Fermi level. Organic semiconductors can be ambipolar, and in some cases the hole and electron mobilities are comparable, but one sign of carrier may be preferred due to the ability to inject or stably dope the material.[62] The stability of electrically doped materials is determined in part by the IE and EA. The EA of many organic materials is relatively small leading to chemical instabilities of negatively charged molecules due to reactions with the environment, e.g. H2O and O2.[63,64] Stable introduction of electron carriers into materials requires the EA to be larger than $\sim$ 3.98 eV to avoid reaction with water and oxygen and associated trap states. Because of this requirement, stable n-type materials are frequently based on units with relatively large EA such as perylene diimide (PDI), naphthalene diimide (NDI), and fullerene derivatives.[28,65–67] For stable introduction of holes, the IE of the semiconductor should be larger than $\sim$5.0 eV for similar reasons. One of the most widely studied stable p-type polymers, PEDOT, is based on the ethylenedioxythiophene (EDOT) monomer because of its simple chemistry and resulting IE of ∼5.1 eV. EDOT can be oxidatively polymerized water in the presence of an acidic polyelectrolyte, typically polystyrenesulfonic acid (PSS), to form a water processable dispersion PEDOT:PSS.[68] EDOT can also be polymerized with oxidants from the vapor phase leading to other variants, for example the oxidant Fe(III) tris-p-toluenesulphonate (TOS) can be used to synthesize PEDOT:Tos.[2,69]

Because efficient charge transfer relies on favorable alignment of the frontier electronic levels of the dopant relative to those of the active semiconducting organic material (smaller ionization energies for n-type dopants or larger electron affinities for p-type dopants), significant efforts have focused on molecular design of dopants.[67,70–72] Overall, there are more known p-type dopants than n-type because of the demands for chemical stability of reduced conjugated materials. While much work has focused on dopants having clear exothermic charge transfer based on the IE and EA of the species in the separated materials,[61] there is recent work demonstrating good conductivity with dopants where such charge transfer would be expected to be less efficient.[73]

New classes of stable dopants for n-type materials have recently emerged. Organometallic dopants have led to impressive performance in both polymers and small molecules. Reactive organic dopants have also been developed.[74–76] For example, reagents that lead to hydride transfer, such as DMBI, are efficient dopants for soluble fullerenes and n-type polymers.[67,70,77,78] Addition of trialkylamino functionalized sidechains to compounds with relatively high EAs has also proven effective using a latent approach by thermally driven transformation of ammonium hydroxide substituents.[66,79]

The dopant, or counterion, to the carrier can be bulky relative to the conductive unit of the material causing distortions in the packing structure that is necessary for charge transport between molecules.[61,80–83] The nominal molar ratio of dopant to conductive unit can be as large as 1:4 in highly conductive materials (conductivity above 10 S/cm).[35]

Even simple dopants such as I_2 are known to cause significant changes in the ordered structures of polymers such as poly(3-hexylthiophene).[84] Incorporation of large amounts of dopant can lead to phase segregation of the doped phase from the undoped phase, which can lower the conductivity.[67,78] In conjugated polyelectrolytes the counterion to the carrier is covalently attached to the backbone, e.g. a sulfonic acid group for a p-type polymer.[85,86] This structure has not generally lead to high electrical conductivity (values <1 S/cm), but these materials demonstrate the tunability of the electrical conductivity with small changes. For example the change from Na_+ to K_+ as a counter ion to the sulfonic acid group can lead to greater than 5× drop in conductivity for a donor-acceptor backbone.[86] The development of structure property relationships to understand how to control the packing in a the electrically doped state is an important direction of future research.

1.3.2 Electrical Conductivity σ

Organic electronic materials are dominantly studied as disordered or polycrystalline form. The mobility of carriers in organic materials is related microscopically to the electronic coupling between molecules and interchain transport in polymers, and also macroscopically to the ability of these carriers to cross domain boundaries, similar to polycrystalline semiconductors. Thus, the observed electrical conductivities of organic materials are generally a sample-dependent property.

Because transport can depend on filling trap states and domain boundaries, the concentration of dopant is a major factor in determining electrical transport. For example, non-linear increases in electrical conductivity with increasing concentration of dopants are frequently observed when doping semiconducting polymers with molecular dopants such as F_4TCNQ[87] or with chemical dopants such as $NO\text{-}PF_6$.[36] Conduction in lightly doped disordered organic materials occurs through thermally assisted processes, with an Arrhenius-type relation with respect to temperature: $\sigma \propto \exp(-E_A/k_BT)$, characteristic of charge hopping between nearest neighbors.[61,87] Such temperature dependence can also occur due to barriers at domain boundaries in polycrystalline materials. At high carrier concentrations, a temperature dependence suggesting variable range hopping may also emerge where $\sigma = \sigma_0 \exp[-(T_0/T)^\gamma]$, where γ is related to the dimensionality of the system (0.25 for 3-D VRH, 0.5 for 2-D VRH).[32,40,41,88–90] While these trends can be attributed to filling of the electronic density of states, it is also known that the conductivity can be affected by non-uniformity in materials leading to phase-separated domains that may have high and low conductivity.[91] A clear example of phase separation is seen in P3HT doped from solution by F_4TCNQ where two types of domains are observed by X-ray diffraction.[81] The majority of work on microstructure of organic materials so far has been carried out on undoped materials making it challenging to separate these two effects.

Processing methods are known to have as significant an influence as the carrier concentration on the electrical conductivity of organic materials. The electrical conductivity of bulk samples of polymers such as polyacetylene and poly(thiophene) can be increased by many orders of magnitude by mechanical stretching leading to alignment of polymer chains.[59] In solvent-cast materials, processing during coating also affects the resulting conductivity. For example, addition of co-solvents to solution PEDOT:PSS in water can change the electrical conductivity by $> 100\times$ without obvious changes in the carrier concentration.[92,93] Another approach taken is to simply remove excess PSS from the blend thereby reducing the amount of insulator.[3,94] Because of these changes, it can be difficult to understand the upper limits of the conductivity of organic materials, particularly polymers.

Dopants are frequently introduced after synthesis of the molecular material leading to changes in properties due to processing methods. For solution processable materials, a dopant may be added to the casting solution leading to charge transfer, i.e. doping, in the solution phase prior to formation of the solid.[80,81] Dopants may also be added after casting by infiltration from solvent.[95–98] There have not been extensive comparisons of the effects of doping from both methods for the same materials system. There has been significant effort in studying how F4TCNQ, a molecule with a relatively deep EA, dopes polymers such as P3HT.[81,96,99] In this materials system, when doped from solution charge transfer occurs in solution and the resulting conductive film has two phases (heavily and lightly or undoped phases).[81] The charge transfer reaction in solution limits the solubility of the material leading to difficulties in casting thicker films directly.[96] Addition of the F_4TCNQ by a sequential spin-coating process can improve uniformity and resulted in somewhat higher electrical conductivities than achieved with the traditional blend and cast method.[96]

Efficient design of TE modules (see Section 1.1) requires the integration of both highly conductive p-type and n-type materials. Currently, conductivities >100 S/cm are readily realized with p-type polymers using various doping methods and values exceeding 4000 S/cm have been recently reported.[4,35,37,68,100] These high conductivities have been achieved through a combination of improved doping methods and processing methods. While there are high reported n-type conductivities for alkali doped fullerenes (as high as 550 S/cm)101-103 and for poly(metal 1,1,2,2-ethenetetrathiolate)s (∼40 S/cm),[53] typical conductivities are below 1 S/cm.[66,67,101] Because most effort has been placed on the study of p-type systems, it is not clear yet whether the lower conductivity of n-type materials is intrinsic or a matter of improving materials processing and stable dopant strategies.

1.3.3 Thermopower α

Because of the complex dependence on carrier concentration and microstructure, the thermopower and electrical conductivity in organic materials have a different coupling than in many inorganic materials. If we consider the most basic model of thermopower in homogeneous materials, the electrical conductivity and thermopower are dictated by the density of states (DOS) of the system and the location of the Fermi level E_F. Only carriers near in energy to the chemical potential (E_F) will participate in transport. The Seebeck coefficient can be defined as the average entropy per charge carrier weighted by the carriers contribution to conduction, and thus directly relates to the conductivity density of states $\sigma(E)$:[102]

$$\alpha = -\frac{k_B}{e}\int \frac{E-E_F}{k_B T}\frac{\sigma(E)}{\sigma}dE \tag{1.3}$$

Depending on the type of transport present in the system, α can take on various temperature dependent forms as in the case of conductivity. For lightly doped organic semiconductors, the thermopower is roughly independent of temperature and is consistent with hopping behavior for a homogeneous system.[103] Such behavior is not observed in heavily doped polymers where the thermopower increases with temperature.[38,39,42,104] Complicating understanding of electronic transport processes is experimental evidence that clearly does not follow a single transport mechanism, where the conductivity is thermally activated but the Seebeck coefficient exhibits metallic behavior with temperature.[105] Transport models applied to polymers have for the most part assumed a homogenous medium, where carriers are distributed homogenously throughout with the same transport mechanism everywhere.[57,59] The morphology of many doped polymers is poorly understood, but it is known that in some case doping can be inhomogeneous and structural order can vary at the nanoscale. A heterogeneous treatment of electrical conductivity has been previously addressed in light of mixed transport indicated by conductivity and thermopower measurements, with a form similar to how one would treat competing transport mechanisms in a homogenous disordered material.[43] The overall resistivity $\rho = \sigma^{-1}$ of the material is the sum of the contributions of the disordered (σ_d) and ordered regions (σ_m), each weighted by a general geometrical factor f that reflects the relative amount of each material and the average macroscopic path a carrier takes through the material:

$$\sigma^{-1} = f_m \sigma_m^{-1} + f_d \sigma_d^{-1} \tag{1.4}$$

The behavior of the Seebeck coefficient is more complex and it can also be treated using a heterogeneous model.[105] Importantly, the electrical conductivity and Seebeck coefficient can be shown to be weighted differently in the ordered and disordered regions given different transport processes in heterogenous phases. Figure 1.3 demonstrates how mixed transport behavior may be attributed to varying degrees of heterogeneity and order in the microstructure. Development of models that encompass the heterogeneity of many of the high-performing polymers should help to improve predictive power for the performance of thermoelectric materials.

Direct measurement of the carrier concentration in organic materials is difficult due to their low mobility and presence of energetic disorder. While Hall coefficient measurements historically have been unreliable, new reports have been recently appeared for a number of organic materials, suggesting that in the future it may be possible to use such measurements with well-ordered organic semiconductors.[90] Because of the lack of a predictive model and the difficulty of directly measuring the carrier concentration, it is simplest to discuss observations of thermopower as a function of electrical conductivity. Using recent literature data for a broad range of doped organic materials (shown in Figure 1.2), a striking empirical relationship between the electrical conductivity and

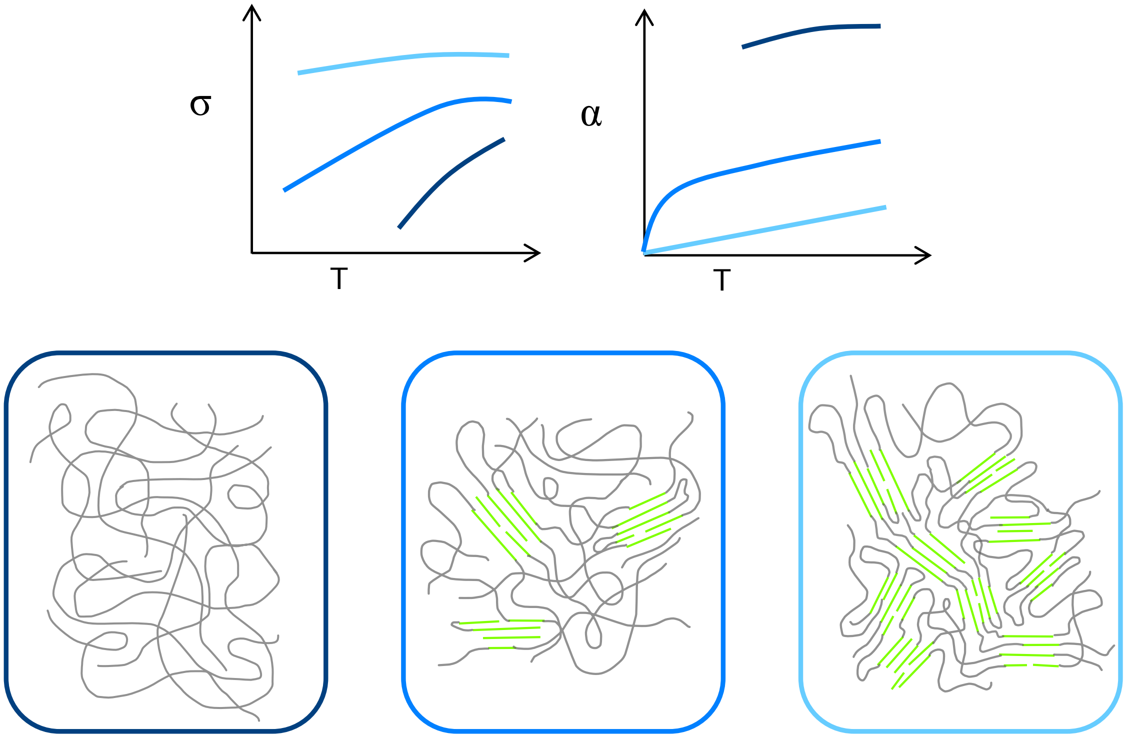

High % Disordered Regions
Disordered transport dominates

Ordered/Disordered Mix
Both regions contribute
Limited by disordered regions

High % Ordered Regions
Ordered transport dominates

Figure 1.3: In semiconducting polymeric materials, ordered regions/lamellae/fiber bundles are connected by disordered chains. Illustrated are variations in the temperature dependence for σ and α with a spatially homogenous carrier distribution, but with varying degrees of morphological disorder. The three illustrated materials scenarios are: (left) highly disordered microstructure, (right) a highly ordered microstructure, and (center) and intermediate microstructure where both highly ordered and highly disordered domains exist. Carrier conduction in highly ordered domain occurs via band conduction with some electronic disorder, while carrier conduction in the highly disordered region is assumed to be thermally-assisted hopping. From left to right, as the volume fraction of ordered domains increases relative to disordered domains, conductivity increases simply because the average mobility increases. Because of the presence of disordered domains, the overall conductivity would not be metallic-like in temperature even if the ordered regions had metallic bands.(from [5])

thermopower emerges, similar to initial observations on polyacetylene, where $\alpha \propto \sigma^{-1/4}$ ($PF \propto \sigma^{1/2}$).[35,43] Particularly notable is the fact that these materials exhibit transport mechanisms ranging from hopping to near metallic conduction. It is unclear why such a relationship occurs because it is not readily predicted from existing transport models. One possibility is that the materials are single band conductors and the electronic DOS is similar, leading to the observed scaling with electrical conductivity. At this point, this relationship appears only to be consistently defied by PEDOT-based systems and polyaniline, suggesting a fertile area for exploration to uncover the origin of the apparent empirical relationship. It is important to note that the approaches for measuring material thermoelectric properties, especially the Seebeck coefficient, vary widely in literature. For example, applied thermal gradients have varied from ~ 0.1°C to 10s°C as measured across distances varying from microns to cms in length.[2–4,78,106,107] Additionally, measurement of the temperature where the Seebeck voltage is measured is often difficult to do directly. These differences can lead to difficulties in direct comparison of extracted parameters and should be taken into account for fundamental studies.

Tuning the degree of doping and morphology is critical for optimization of TE properties in a given system. For example, there are widely varying reported values of the power factor for PEDOT derivatives due to changes in processing and modification of the level of doping.[2–4,106,108] In PEDOT:Tos, for example, the oxidation level was tuned from 15% to 40% through chemical de-doping with the maximum PF of 350 µW/m-K^2 achieved at 23% oxidation. Effects of doping on electronic properties in organic materials are multi-faceted. In addition to increasing charge carrier concentration, increased doping tends to increase carrier mobility, due to filling of trap states caused by energetic disorder. Removal of PSS using an ethylene glycol rinse, for example, improved all parameters associated with ZT (σ, α, κ), leading to a PF = 469 µW/m-K^2 and a ZT = 0.42, which is the highest reported ZT for solution-processable OTEs to date.[3]

Tuning the shape of the electronic density of states is a route that could provide enhancements in the thermopower. For example, narrowing the DOS can help enhance the asymmetry about the Fermi energy and improve the Seebeck coefficient. Relatively high Seebeck coefficients have been reported based on field effect measurements in highly crystalline small molecule systems, such as rubrene and pentacene,[109] and polymers with relatively small energetic disorder.[34] The DOS can also potentially be tailored in more complex systems. In an effort to simultaneously increase σ and α, an additive poly(3-hexylthiothiophene) (P3HHT) was added to poly(3-hexylthiophene) (P3HT) to deliberately modify the DOS due to the differing IE of the two polymers.[1] In this case, P3HHT defines the Fermi level, whereas it is assumed that most of the current is carried in the bulk P3HT. A regime was observed where both thermopower and conductivity increase with doping modulation via F_4TCNQ , which is not observed in the neat P3HT system. While the PF was quite low compared to other systems, this was proof of concept that deliberately introducing DOS asymmetries can help to decouple σ and α.

The polaronic nature of the carriers in organic materials can potentially lead to enhancements in thermopower. The formation of bipolarons from two polarons is considered energetically favorable in homopolymers, such as poly(thiophene) and PEDOT, due to the release of the structural distortion in the backbone.[59] A significant enhancement of the Seebeck coefficient (55 μV/K at electrical conductivity of $\sim$ 1000 S/cm) in highly ordered vapor deposited PEDOT-Tos was suggested to occur due to formation of a bipolaron band.[4] The formation of the bipolaron band was based on temperature dependent transport and photoemission characteristics similar to a semi-metal. Quite different behavior has been observed in other materials such as polyaniline, which has polaronic carriers and an exceptionally low thermopower ($\leq$ 10 μV/K), at electrical conductivities comparable to PEDOT suggesting that there is still much to be learned about transport in polymers with high carrier densities.

Additionally, strategies that scatter low-energy carriers, while allowing high-energy carriers to pass, can increase the asymmetry of mobile carriers above and below the Fermi energy boosting the Seebeck coefficient.[25,110] The reduction of the total number of charge carriers decreases the electrical conductivity, but since the power factor scales as α^2, a net increase in the power factor can be realized in appropriate carrier concentration regimes. To find conditions conducive to these filtering effects, interface engineering efforts have focused on selecting material component combinations whose transport bands are slightly mismatched in energy level alignment.[107,111–114] This phenomena has been suggested in helping explain properties of some organic/inorganic composite systems,[113] but definitive demonstration of energy filtering is not trivial, however.

1.3.4 Thermal conductivity κ

While the thermal conductivity of organic thermoelectric materials is often not discussed, and is beyond the scope of this dissertation, it is important to acknowledge the limits of the assumption that it is low and unchanging. The thermal conductivity of amorphous, isotropic, undoped organic materials tends to be around 0.3 W/m-K, but it is not clear how the thermal conductivity of these disordered materials changes with doping and morphology. It is useful to look at the limits of thermal conductivity in organic materials as a whole, to get a sense of the possible ranges of thermal conductivity in OTE materials.

Thermal conductivity, as with any transport property, is a tensor. The most common techniques in use for measuring thermal conductivity (3ω and TDTR) are most easily employed to measure thermal conductivity out-of-plane κ_Z. However, since polymeric materials can possess considerable anisotropy, measuring κ_{XY} is of paramount importance, and challenging. Mathematical modeling may be done within 3ω or TDTR measurements of thin films to estimate an anisotropy factor for the thermal conductivity,[3,115] the validity of which depends on the κ itself. Another option is secondary sample preparation to enable re-orientation of the film for compatibility with the TDTR measurement capability (i.e. the in-plane direction becomes the out-of-plane direction). The latter method often requires the ability to make a significantly thick film that maintains the order seen in the thin films of interest, ways of which are not necessarily compatible with doping methods, especially post-processing ones.

At the low end of the range, fullerene-based molecules have the lowest thermal conductivity of organic matter, from 0.03 - 0.06 W/m-K. C_{60} has a thermal conductivity of $\sim$ 0.1 W/m-K, while the addition of functional groups to make soluble fullerenes can further lower the thermal conductivity; PCBM and PCBNB exhibit thermal conductivity 40% lower, at 0.06 W/m-K.[116,117] At the higher end of thermal conductivity of organic materials are aligned polymer fibers, where order is induced mechanically by stretching or fiber pulling. Insulating liquid crystalline polymer fibers can have axial thermal conductivities as high as 30 W/m-K, but also as low as 1 W/m-K[118] illustrating the complexity of estimating anisotropy in κ based on morphology. Inducing order not only reduces phonon scattering, but in electronic polymers, may increase carrier mobility (and thus κ_e) by aligning the polymer backbones, reducing traps, and increasing connectivity between polymers in the fast-transport direction.

Due to the significant hurdle of being able to directly measure thermal conductivity of organic thin films in-plane, often the thermal conductivity reported is the out-of-plane component κ_Z, if reported at all. As demonstrated in fibers and mechanically aligned films, it is clear that anisotropy can significantly affect thermal conductivity in the direction of transport. It is difficult to pin down where many classes of the high-performing thermoelectric polymers sit on the thermal conductivity spectrum. Many of these materials are locally ordered, some with a degree of long-range order, but have no macroscopic alignment in the x-y plane in the absence of mechanical assistance (stretching or directional blade coating, for example). Conversely, polymers are often highly anisotropic out of plane in the z-direction, with backbones either face-on or edge-on to the substrate continuing through the thickness of the film. Equally of a concern as phonon scattering is the electronic component to thermal conductivity,[119, 120] as the high conductivities obtained in PEDOTs and other polymers are measured in the direction of fast transport (in-plane). If carrier transport is extremely anisotropic, κ_{XY} may have a non-negligible electronic component compared to κ_Z. In the case that κ is only measured perpendicular to the direction of carrier transport, it is possible that ZT may be misrepresented by up to an order of magnitude or more if significant anisotropy exists.

The effect of anisotropy on thermal conductivity is demonstrated in PEDOT, which is currently the best-performing OTE reported. It has been reported that the thermal conductivity of PEDOT:PSS is highly anisotropic when using DMSO as a cosolvent, with κ_{XY} as much as $2\times$ higher than κ_Z in undoped films of PEDOT, and $3\times$ higher in treated/doped films.[119] The difference in thermal conductivity anisotropy in doped vs. undoped films is attributed to a significant contribution of the carriers to thermal conductivity, κ_e, at high electrical conductivity, and follows the Weidemann-Franz law. Another study of PEDOT:PSS with ethylene glycol (EG) as a both cosolvent and secondary post-processing step found the thermal transport to be even more anisotropic, $\kappa_{XY} \approx 5.6\kappa_Z$.[121] In this case, the anisotropy is attributed to the PSS isolating transport between PEDOT nanocrystals in the out-of-plane direction. In a comparison between DMSO vs EG co-solvents, use of DMSO was found to result in a lower anisotropy factor, $\kappa_{XY}/\kappa_Z = 1.4$ and 1.6 respectively, while κ_Z was independent of co-solvent.[3] This paper reported a record ZT for organics using the calculated in-plane κ_{XY}, with ZT = 0.42 for the DMSO co-solvent and ZT = 0.28 for EG. While there was no speculation on the reason for the difference in thermal anisotropy between DMSO and EG co-solvents, this illustrates a promising route of rational control of thermal asymmetry to enhance ZT, in addition to controlling electronic properties.

1.4 Permissions

Portions of this chapter are published in or adapted from the following authored publications, with the appropriate permissions:

[5] B. Russ, **A. M. Glaudell** (*co-first author*), J. J. Urban, M. L. Chabinyc, and R. A. Segalman, Organic Thermoelectrics for Conformal Energy Harvesting and Personal Temperature Control, *Nature Reviews Materials*, in revisions, 2016.

[6] **A. M. Glaudell**, R. A. Schlitz, and M. L. Chabinyc, Innovative Thermoelectric Materials, ch. Seebeck Coefficient and Electrical Conductivity Optimization in Polymers. Imperial College Press, England.

Chapter 2

Impact of the Doping Method on Conductivity and Thermopower in Semiconducting Polythiophenes

Reprinted with Permission from [35]:

> **A. M. Glaudell**, J. E. Cochran, S. N. Patel, and M. L. Chabinyc. "Impact of the Doping Method on Conductivity and Thermopower in Semiconducting Polythiophenes." *Advanced Energy Materials*, vol. 5, p. 1401072, Oct. 2015. Copyright 2014 WILEY-VCH Verlag GmbH & Co. KGaA, Weinheim.

The development of organic semiconductors for use in thermoelectrics requires the optimization of both their thermopower and electrical conductivity. Here two fundamentally different doping mechanisms are used to investigate the thermoelectric properties of known high hole mobility polymers: poly 3-hexylthiophene (P3HT), poly(2,5-bis(3-tetradecylthiophen-2-yl)thieno[3,2-b]thiophene) (PBTTT-C_{14}), and poly(2,5-bis(thiphen-2-yl)-(3,7-diheptadecantyltetrathienoacene)) (P2TDC$_{17}$-FT4). The small molecule tetrafluorotetracyanoquinodimethane (F_4TCNQ) is known to effectively dope these polymers, and the thermoelectric properties are studied as a function of the ratio of dopant to polymer repeat unit. Higher electrical conductivity and values of the thermoelectric power factor are achieved by doping with vapor-deposited fluoroalkyl trichlorosilanes. The combination of these data reveals a striking relationship between thermopower and conductivity in thiophene-based polymers over a large range of electrical conductivity that is independent of the means of electrical doping. This relationship is not predicted by commonly used transport models for semiconducting polymers and is demonstrated to hold for other semiconducting polymers as well.

2.1 Introduction

Organic electronic materials have found recent success in applications from solar cells to transistors and displays.[7–9] Semiconducting polymers can be deposited on flexible substrates, and processed at room temperature, thus reducing the energy needed to manufacture devices compared to inorganic materials. These features also lend themselves to alternative manufacturing techniques for electronics: inkjet printing, roll-to-roll processing, and screen printing.[122] Despite the recent progress in applications, charge transport is still not well understood in semiconducting polymers. An improved understanding of transport will lead to the ability to design new materials and open new applications for organic materials.

A critical need for organic semiconductors is the ability to control their electrical conductivity. In addition to measurements of conductivity, the thermopower (Seebeck coefficient) offers a unique view into transport; it provides direct access to the entropy per carrier.[102,123] Thermopower measurements combined with conductivity measurements can offer a clearer picture of transport mechanisms than what is offered by electrical measurements alone.

Unlike conventional inorganic semiconductors, doping of organic materials usually requires introduction of a large molecular species that may disrupt the molecular organization. Here, we examine how doping using two approaches leads to a surprising trend in the thermopower as a function of electrical conductivity for a series of organic semiconducting polymers. This relationship is compared to predictions from several transport models commonly applied to organic semiconductors. The empirical trend provides guidance by which to determine improvements in the thermoelectric performance of organic semiconductors. One may use this trend to see if new materials have thermoelectric properties consistent with those previously studied. For instance, if a new material had a lower electrical conductivity than expected for the measured thermopower, this may be indicative of morphology-limited conductivity.

Only recently have organic electronic materials been seriously considered for thermoelectrics and they could enable fabrication of flexible thermal energy scavengers and heating/cooling devices.[2,124] Traditional thermoelectric modules consist of rigid and brittle materials rendering them relatively fragile limiting their application in some cases. The ability to process organic electronic materials on a flexible substrate opens up the possibility of conformal device geometries for niche applications such as comfortable wearables and portable/roll out thermoelectric generators or coolers. The challenge for organic thermoelectric materials lies in enhancing and controlling the electronic properties, as well as adapting device morphology for solution-processable semiconducting materials.

The power conversion efficiency of a thermoelectric material is related to the thermoelectric figure of merit $ZT = (\alpha^2\sigma/\kappa)T$, where α is the Seebeck coefficient, σ is electrical conductivity, κ is thermal conductivity, and T is temperature. The sign of the thermopower α indicates the type of the majority carrier. The three parameters α, σ, and κ are counter-indicated and interrelated as a function of carrier concentration, resulting in a maximum ZT at an intermediate carrier concentration. The thermal conductivity κ is the sum of two components: κ_L from the lattice, and κ_E, the electronic component from the charge carriers. The main challenge for the development of inorganic thermoelectric materials is lowering the thermal conductivity while maintaining their electrical properties. Polymers on the other hand, have a low lattice thermal conductivity due to their disordered morphology. Because the electronic component of the thermal conductivity is unlikely to contribute until very high electrical conductivities (>1000 S-cm^{-1}), the main emphasis currently is to understand how to optimize their electrical properties, i.e., the power factor $PF = \alpha^2\sigma$.

The thermopower α is directly related to the electronic density of states (DOS) of a material. Fritzche derived a general expression for thermopower in relation to the conductivity DOS $\sigma(E)$:[102]

$$\alpha = \frac{k_B}{e}\int \frac{E - E_F}{k_B T}\frac{\sigma(E)}{\sigma}dE \tag{2.1}$$

where E_F is the Fermi energy, σ is the absolute conductivity, and k_B/e is a natural unit of thermopower equal to 86.17 μV-K^{-1}. The conductivity density of states $\sigma(E)$ can be represented in the following way, given $\sigma = e\mu n$, where μ is carrier mobility, and n is carrier concentration:[102]

$$\sigma(E) = e\mu(E)g(E)f(E)[1 - f(E)] \tag{2.2}$$

Here, $\mu(E)$ is the mobility as a function of energy, $g(E)$ is the density of states, and $f(E)$ is the Fermi distribution. Deriving a relation of thermopower as a function of conductivity for various transport mechanisms is non-trivial, and many proposed relations of $\alpha(\sigma)$ are not derived from models, but fit the data and qualitatively related to transport.[105,125,126] The reason being that while the DOS has been studied for many materials in diodes and thin film transistors, it is unclear how parameters in Equation 4.3 change as a function of doping, especially in the case of molecular doping, which may significantly change molecular ordering. Semiconducting polymers complicate the determination of a relation due to their heterogeneous morphology because they are composed of both ordered and disordered regions that may exhibit different fundamental transport mechanisms.

Studies of the thermoelectric properties of foundational semiconducting polymers including polyacetylene, polyaniline, and polypyrrole have been made in the context of fundamental transport mechanisms. Much of this work addressed aligned or highly anisotropic polymers doped with ions such as iodine, enabling metallic levels of conductivity. Although the thermoelectric figure of merit ZT and power factor PF were often not calculated or addressed, these materials turn out to have relatively high power factors, up to 1.49 mW-m^{-1}K^{-2} for iodine-doped stretch-aligned polyacetylene at 6.1×10^4 S-cm^{-1}.[42] However, this class of polymers is a poor choice for applications. The metallic levels of conductivity are in general temporary, reliant upon an overpressure or constant presence of the dopant vapor. The high anisotropy due to alignment of these polymers is shown to significantly increase the thermal conductivity of the material in the direction of transport, possibly negating the advantage of polymers in the first place and limiting ZT.[127] More recently, poly(3,4-ethylenedioxythiphene) (PEDOT) derivatives dominate the research on organic and hybrid thermoelectric materials.[128] These are widely used as an environmentally stable transparent conducting electrode in organic photovoltaic devices, and there are many well-documented methods to vary the conductivity of the film.

Here, we study the role of the doping method on the electrical conductivity and thermopower of a series of structurally related semiconducting polymers. These materials are all known to have high carrier mobilities in thin film transistors and help to provide a benchmark for understanding the performance of polymers for thermoelectrics. By comparing our work to data from the literature, we find an unusual trend in the PF over a very large range ($10^{-5} - 10^{3}$ S-cm^{-1}) of electrical conductivity, which differs from conventional inorganic thermoelectric materials.

2.2 Results

There have been few investigations into the effect on thermoelectric properties of various doping mechanisms with a consistent set of polymers.[38] Here, we examine a structurally similar series of polymers known to perform well in thin-film transistors. Three polymers were investigated in this study (shown in Figure 2.1): poly 3-hexylthiophene (P3HT), poly(2,5-bis(3-tetradecylthiophen-2-yl)thieno[3,2-b]thiophene) (PBTTT-C_{14}), and poly(2,5-bis(thiphen-2-yl)-(3,7-diheptadecantyltetrathienoacene)) (P2TDC_{17}-FT4). These polymers have known high hole-mobility and possess crystalline, ordered regions as well as amorphous, disordered regions.[14] P3HT and PBTTT-C_{14} have similar trap-free mobilities (∼1 to 10 cm^{2}-V^{-1}s^{-1});[33, 129–131] by extension, we also chose P2TDC_{17}-FT4.[132] Experimentally measured carrier mobilities in these polymers differ due to microstructural ordering and processing.[14, 132–134]

The polymers were doped in two separate ways: in solution with the small molecule tetrafluorotetracyanoquinodimethane (F_4TCNQ), and via vapor deposition of the alkyl silane (tridecafluoro-1,1,2,2,-tetrahydrooctyl)-trichlorosilane (FTS) onto the surface of the polymer thin film. F_4TCNQ is known to effectively hole-dope these polymers via charge transfer.[81, 87] FTS has also been shown to dramatically enhance conductivity in PBTTT-C_{14} and P3HT, far beyond 10 S-cm^{-1}.[139] There is evidence that F_4TCNQ inserts itself into the ordered regions of the polymer, disrupting the molecular packing of the neat material.[14, 81, 87, 140] By contrast, it is thought that the vapor-deposited FTS forms

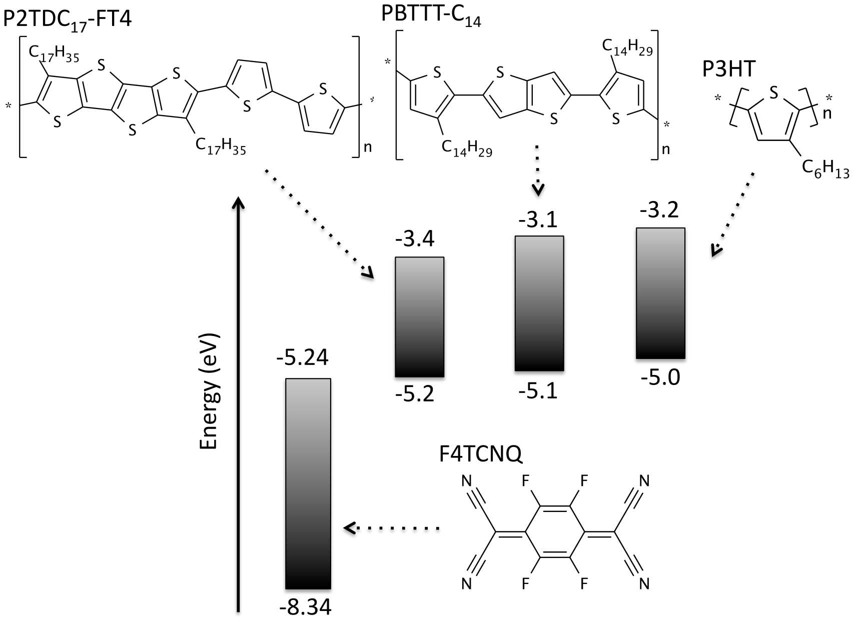

Figure 2.1: Molecular structure and highest occupied molecular orbital (HOMO)/lowest unoccupied molecular orbital (LUMO) levels of polymers P3HT,[87, 135, 136] PBTTT-C_{14} ,[133, 137] and P2TDC_{17}-FT4 ,[132] in addition to the small molecule F_4TCNQ .[138]

a self-assembled monolayer, or at least a thin film, on the surface of the semiconducting film leading to doping stabilized by a surface dipole.[139] The precise mechanism of doping is still uncertain. Grazing-incidence wide angle X-ray scattering (GIWAX) results on FTS-doped PBTTT-C_{14} films indicate that the FTS causes a small disruption of the crystallite size, but does not incorporate into the ordered crystalline domains as observed with F_4TCNQ doping (see Supporting Information and Figure 2.S7 therein).

For polymers doped with F_4TCNQ, a wide range of conductivities was obtained by varying the weight ratio of dopant to polymer in solution. For all three polymers, conductivity increases by increasing the weight ratio of dopant to polymer in solution. A 10-fold increase in dopant concentration from 2.5 mol% (1 wt%) to 25 mol% (10 wt%)

for PBTTT-C$_{14}$ resulted in an increase of conductivity by nearly four orders of magnitude, from 6.37×10^{-4} S-cm^{-1} to 2.08 S-cm^{-1} . P3HT and P2TDC$_{17}$-FT4 followed similar trends, with the results summarized in Figure 2.2. This finding agrees with previous studies of F4TCNQ-doped polythiophenes.[87]

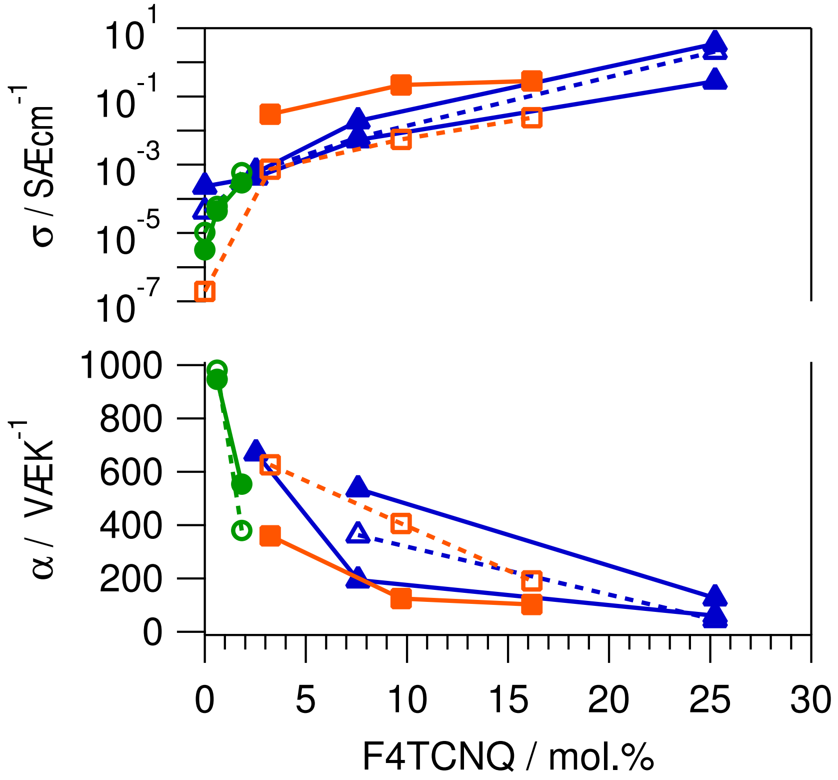

Figure 2.2: Conductivity (top) and thermopower (bottom) as a function of molar ratio of F$_4$TCNQ to polymer repeat unit (mol%) for P3HT (●), PBTTT-C$_{14}$ (▲), and P2TDC$_{17}$-FT4 (■). Samples are either as cast (open symbols, dashed lines), or annealed at 150°C for 10 minutes (solid symbols and lines). The two solid traces for annealed PBTTT-C$_{14}$ are from films made from different solutions to show the reproducibility of the measurement.

The thermal stability of the F$_4$TCNQ -doped films can be seen in electrical conductivity measurements of as-cast and annealed thin films of each doping level and polymer (Figure 2.2). For P3HT and PBTTT-C$_{14}$ at the doping levels reported, there were only small changes between samples measured as cast versus annealed at 150 °C for 10 min

Table 2.1: Activation energy and Arrhenius parameters extracted from temperature-dependent conductivity measurements

Polymer	**F_4TCNQ** mol.%	σ_{RT} S/cm	E_A meV	σ_0 S/cm
PBTTT-C_{14}	2.5	5.1×10^{-4}	170	0.40
	7.6	8.7×10^{-3}	140	3.3
	12	2.6×10^{-1}	78	11
	25	5.2×10^{-1}	50	8.2
	FTS	1.3×10^{-1}	130	23
	FTS	1.1×10^{-1}	150	34
P3HT	0.60	8.1×10^{-5}	210	0.31
	1.8	2.5×10^{-4}	180	0.25
	3.0	4.5×10^{-3}	130	0.63
	FTS	1.8×10^{-1}	100	7.7

under dry nitrogen, and similarly small differences from solution-to-solution. F_4TCNQ was less compatible as a dopant in P2TDC$_{17}$-FT4, as the film conductivity values were not stable to annealing, even at lower annealing temperatures. As cast films exhibited variation in conductivity across different solutions, indicating that F_4TCNQ is a less stable dopant in P2TDC$_{17}$-FT4 solution than in P3HT or PBTTT-C$_{14}$ solutions. For more details refer to the Supporting Information (Figure 2.S10). Further processing optimization may be necessary for future studies using this polymer/dopant system.

An Arrhenius plot of temperature-dependent electrical conductivity measurements confirm that the conductivity is thermally activated below 270 K for the F_4TCNQ -doped polymers (Supporting Information Figure 2.S8), and below 300 K for FTS-doped polymers (Figure 2.S9), with activation energies determined by the Arrhenius expression for activated transport: $\sigma = \sigma_0 \exp(E_A/k_B T)$. Furthermore, a plot of the calculated activation energies E_A shows that E_A is proportional to the absolute value of $\ln(\sigma_{RT})$, where σ_{RT} is the conductivity at room temperature (300 K) (Figure 2.3). The parameter σ_0 slightly increased with increasing conductivity, with no clear trend between samples. Table 2.1 summarizes the Arrhenius fitted parameters for each sample measured.

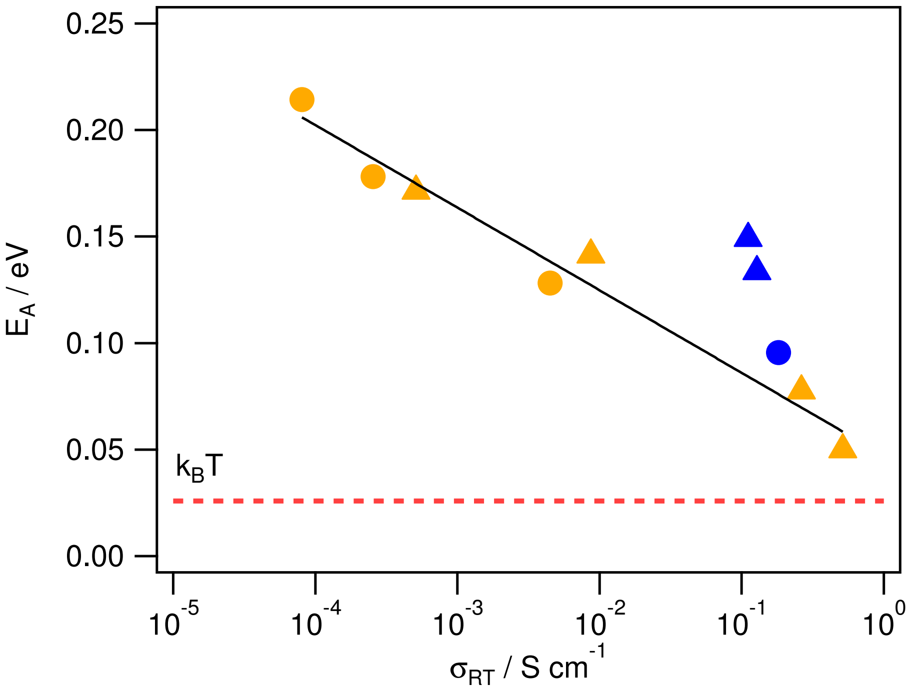

Figure 2.3: Activation energies as a function of room-temperature conductivity σ_{RT} for F_4TCNQ -doped (yellow) and FTS-doped (blue) P3HT (●) and PBTTT-C14 (▲). The solid line is a log fit to the F_4TCNQ -doped polymer data. Activation energies were determined by the slope of an Arrhenius plot of temperature dependent conductivity.

Thermopower was measured in identically and simultaneously processed samples as conductivity to maintain accurate comparison between conductivity and thermopower. For P3HT, PBTTT-C_{14} , and P2TDC$_{17}$-FT4 doped with F_4TCNQ , the thermopower decreased with increasing dopant ratio, as expected for semiconductors. Thermopower showed similar stability as conductivity for as-cast and annealed films, with little change upon annealing for P3HT and PBTTT-C_{14} , and larger changes for P2TDC$_{17}$-FT4 (Figure 2.2).

For the polymer thin films doped with FTS, a wide range of conductivities was obtained by partially doping films, or by exposing fully doped films to ambient atmosphere, humidity and illumination, for varying amounts of time, thereby de-doping the film over

Table 2.2: Conductivity, thermopower, and calculated power factor for the highest-performing films measured.

Polymer	**Dopant**	σ_{RT} S/cm		α_{RT} μV/K		PF_{RT} μW/m-K^2	
PBTTT-C_{14}	F_4TCNQ (25 mol.%)	3.51	± 0.05	60	± 9	1.3	± 0.4
P3HT	FTS	27.7	± 0.1	60	± 9	10	± 3

time (see Supporting Information for more details). Kept under inert conditions (nitrogen environment), the films maintain the conductivity resulting from the processing method, i.e., returning de-doped films to inert conditions halts the de-doping process. The electrical conductivities reached as high as 27.7 S-cm^{-1} for P3HT and 604 S-cm^{-1} for PBTTT-C_{14} . These values are nearly as high as those reported elsewhere for FTS doping ($\sim$50 S-cm^{-1} for P3HT, $\sim$1100 S-cm^{-1} for PBTTT-C_{14}).[139] We attribute this difference to brief exposure to atmosphere, which is unavoidable in the current experimental setup. The thermopower is also inversely correlated with doping, indicated by in inverse correlation with conductivity discussed later. There seems to be no difference in performance for intermediate-doped versus de-doped films, as there is no hysteresis evident in the thermopower vs conductivity curve (Figure 2.4). The thermoelectric parameters of the highest-performing compositions are summarized in Table 2.2.

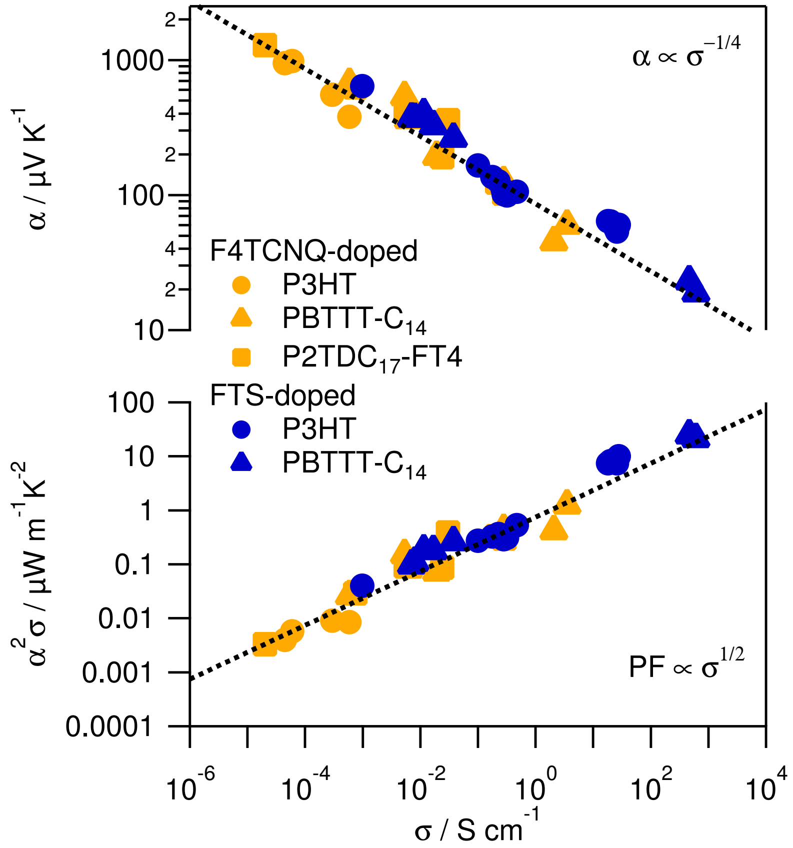

Figure 2.4: Thermopower (top) and power factor (bottom) as a function of electrical conductivity for F$_4$TCNQ -doped polymers (yellow) P3HT (●), PBTTT-C$_{14}$ (▲), and P2TDC$_{17}$-FT4 (■) and FTS-doped polymers (blue) P3HT (●), and PBTTT-C14 (●). The dashed lines indicate an empirical fit of α proportional to $\sigma^{-1/4}$ and PF proportional to $\sigma^{1/2}$.

2.3 Discussion

The relationship between the thermopower and electrical conductivity in a semiconductor can best be understood if the carrier concentration is known. However, the carrier concentration cannot be measured directly in polymer films via traditional measurements over a wide range of conductivities due to energetic disorder.[90,105] Poorly conducting films have carrier mobilities that are too low for the Hall effect measurement to be useful and at high conductivity the interpretation of the Hall coefficient is difficult in disordered materials.[90] While electronic spin resonance (ESR) can be used at low carrier concentration to measure spin concentrations, the more highly conducting films exhibit both polarons and spinless bipolarons, the latter of which are silent in ESR.[141,142] It is also unclear if the molar ratio of the dopant to the polymer is representative of the free carrier concentration. As a consequence, we compare the thermopower α and power factor PF to the electrical conductivity σ instead of to the carrier concentration p or nominal molar percent doping. This method has proven to be successful for providing an understanding of the behavior of inorganic semiconductors, although it is not as widely applied for organic materials.[143]

A clear trend emerges when comparing thermoelectric properties of all three polymers across both doping schemes Figure 2.4. The thermopower curve is fit to an empirical power law:

$$\alpha = \frac{k_B}{e}\left(\frac{\sigma}{\sigma_\alpha}\right)^{-1/4} \tag{2.3}$$

Here, k_B/e is the Boltzmann constant divided by unit charge, or the natural unit of thermopower 86.17 μV-K^{-1}. The parameter σ_α is an unknown conductivity constant independent of carrier concentration in the range covered, and fit to approximately 1 S-cm^{-1} . It is unclear as to what physical significance σ_α carries from this empirical fit. An additive constant to Equation 2.3 does not change the value of σ_α dramatically. On a double logarithmic plot, adjusting σ_α shifts the thermopower trend line up or down. Increasing σ_α causes the fit to overestimate the thermopower with the absolute effect largest in the lower conductivity region; decreasing σ_α underestimates the thermopower similarly. The power factor consequently then has a square root dependence on conductivity, inline image. We have compiled thermoelectric data from the literature and show a comparison of those to the data reported here in Figure 2.5; this further demonstrates this empirical relationship. Previous studies of optimization of the thermoelectric properties of P3HT doped with F_4TCNQ^1 and PF_{6^-} anions[36] also appear to follow the trend line, although the range of electrical conductivity was limited. Data from a recent study of PBTTT, P3HT, and other polythiophenes doped with ferric salt with bis(trifluoromethane)sulfonimide (TFSI) also follows the empirical trend over a large conductivity range.[38]

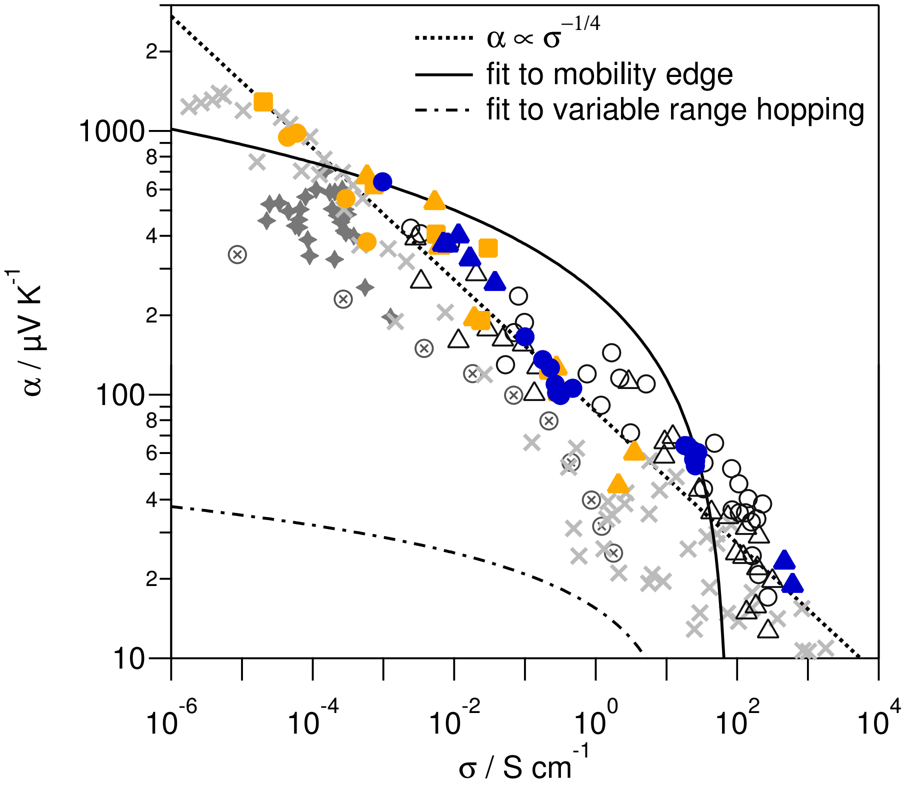

Figure 2.5: Compilation of thermopower vs conductivity data from this study: F4TCNQ-doped polymers (yellow) P3HT (●), PBTTT-C_{14} (▲), and P2TDC$_{17}$-FT4 (■) and FTS-doped polymers (blue) P3HT (●), and PBTTT-C_{14} (▲), and select literature data: P3HT doped with PF_{6^-} (⊗),[36] P3HT:P3HHT doped with F_4TCNQ (✦),[1] P3HT (○) and PBTTT (△) doped with TFSI-,[38] and polyacetylene with various dopants (×) (compiled from ref. [105]). The dotted line indicates the empirical fit; the solid line indicates a mobility edge model using the activation energies measured for F_4TCNQ doped P3HT and PBTTT-C_{14} .

It is startling that this trend fits over 9 orders of magnitude of conductivity, for both doping mechanisms, and across semiconducting polymers. It can be safely assumed that the transport mechanism at the lowest end of the conductivities measured is much different than at the highest end of conductivities measured, even if only considering the F_4TCNQ -doped films. A measure of the activation energies of the F_4TCNQ -doped polymers shows that at the highest doping loads, the activation energy approaches k_BT, near which the transport mechanism is expected to change dramatically (Figure 2.3). Additionally, the two doping mechanisms are fundamentally different at a microstructural level. As stated earlier, the F_4TCNQ intercalates in between the ordered polymer chains and may or may not be present in the disordered regions. Adding more F_4TCNQ from dilute to saturation concentrations changes the morphology of the film. The FTS films are doped to saturation, and de-doped with humidity and illumination, with no evidence that the FTS is leaving the surface of the film.[139] The morphology of the doped and de-doped films is assumed to be identical within the active region. Partially doping the films with incomplete coverage of FTS is indistinguishable from a de-doped film when comparing measured conductivity and Seebeck coefficient.

Previous analyses of thermopower as a function of conductivity in other studies of semiconducting polymers have found one of two empirical relations: either inline image or the same inline image exhibited by our systems. A few models for charge transport in polymers do yield inline image. A $\ln \sigma$ dependence of thermopower emerges from bipolaron hopping within the Holstein-Hubbard model for molecular crystals.[36] This model results in inline image and inline image, where c is the concentration of charge-carrying polarons and bipolarons, thus inline image. This analysis was suggested to qualitatively explain the $\ln \sigma$ dependence found for PF_{6-} doped P3HT by Xuan et al. over a wide range of conductivities ~1 S-cm^{-1} down to ~10^{-5} S-cm^{-1} (data included in Figure 2.5).[36] However, experimental data were shown to have a much stronger doping dependence of thermopower and conductivity than what is predicted by this model.[36]

Analysis of stretch-aligned polyacetylene, polypyrrole, and polyaniline by Mateeva et al. shows the following $\ln\sigma$ relation:[126]

$$\alpha = -\frac{k_B}{e}\frac{1}{\beta}\ln\left(\frac{\sigma}{\sigma_{max}}\right) \tag{2.4}$$

It was found that inline image and is dependent on the chemical nature of the dopant, with no universal trend for different dopants across various polymers. Additionally, different values of β and σ_{max} were found depending on whether properties were measured parallel or perpendicular to aligned films. This relationship can also be derived from statistical mechanics, valid for the light doping limit, for a material with only one carrier type, and a material that exhibits a ?max such that inline image.[126] This trend does not exceed the thermopowers measured in this study, and power factor flattens out upon increasing dopant concentration. If $\beta = 1$, we are left with the Mott-Heike formula for thermopower in semiconductors: $\alpha = (k_B/q)\ln(c/(1-c))$.[36, 126] This model has been successful in describing transport in inorganic semiconductors including Bi_2Te_3, but is inappropriate for polymers due to disorder.[36, 143]

A 2001 review by Kaiser noted a inline image dependence of thermopower on conductivity for a multi-source compilation of polyacetylene data over a similarly wide range of conductivities as this study (Figure 2.5).[43, 103, 105, 144–151] These data were qualitatively related to the variable range hopping model, which describes thermopower as the following:

$$\alpha = -\frac{k_B}{e}(T_0T)^{1/2}\frac{d\ln N}{dE}\bigg|_{E_F} \tag{2.5}$$

The variable T_0 is found via the temperature dependent Mott relation for conductivity, with $\gamma = 1/3$ chosen in Kaiser's analysis: $\sigma = \sigma_0\exp\left[-(T_0/T)^{\gamma}\right]$.[123] It was found that the thermopower did track to $T_0^{1/2}$, as expected from Equation 2.5, and $(d\ln N/dE)$ at the Fermi energy is equal to about 2 eV^{-1}.[43]

The mobility edge model is also often used to describe transport of disordered polymer systems.[14,134] The mobility-edge model for thermopower gives the following temperature-dependent relation for hole transport:[14,102,123]

$$\alpha = \frac{k_B}{e}\left(\frac{E_F - E_V}{k_B T}\right) + A \tag{2.6}$$

Here, A is dimensionless and greater than 1 and is related to the weighted conductivity density of states, E_F is the Fermi energy, and E_V is the valence energy.[102,123] The activation energy E_A, while not equal to $E_F - E_V$, is correlated to this difference and is used as an estimate, although the activation energy for the thermopower is not necessarily the same as for the electrical conductivity.[152] The activation energy E_A measured for the F_4TCNQ -doped polymers shows $E_A \propto \ln\sigma$, as indicated by the trendline in Figure 2.3. If we apply the dependence of E_A on conductivity, we find that $\alpha \propto \ln\sigma$ in the mobility edge model:

$$\alpha = \frac{k_B}{e}\left(\frac{B\ln\sigma + C}{k_B T}\right) + A \tag{2.7}$$

Here, B and C are given by the fit of activation energy to conductivity, shown in Figure 2.3: $E_A = B\ln\sigma + A$. We see that the mobility edge model (solid line in Figure 2.5) as used does not fit our data well over many orders of magnitude, regardless of the value chosen for A.

We can also consider variable range hopping in three dimensions, as described in Equation 2.5. Restricting the parameter $T_0 = E_A/k_B$ to the activation energy relation found experimentally, and assuming that the shape of the density of states at the Fermi level $(d\ln N/dE)_{E=E_F}$ does not vary dramatically with doping, we can see that our data does not strictly fit the VRH hopping model either (long dashed line, Figure 2.5). The effect of molecular doping on the density of states in semiconducting polymers is not well known, therefore we use the simplest assumption here. We expect this assumption to be reasonable for higher carrier densities, where the Fermi energy is away from the trap states. This fit is displayed for a choice of $(d\ln N/dE)_{E=E_F} = 10\text{eV}^{-1}$. Decreasing this parameter moves the trace down, further away from the data.

It is not obvious that the theoretical models should fit the striking trend observed over the whole range of conductivities. The transport mechanism changes dramatically as carrier concentration increases from intrinsic levels to metallic levels. One possible explanation for the trend across this wide range of conductivities is that there is a smooth transition from a model that represents transport well at low carrier concentrations to one that represents carrier concentrations at very high carrier concentrations. Such a fit would also require a consistent DOS for the materials over the wide range of electrical conductivity studied. Surprisingly the same trend is observed for polyacetylene, which has a degenerate ground state, and the thiophene-based materials, which have non-degenerate ground states. Such behavior may indicate a connection between the electronic structure and morphology required to achieve high electrical conductivity, but it is premature to speculate on the necessary physical origin.

It is seen via temperature-dependent conductivity measurements that transport is activated at higher conductivities in the semiconducting polymers. The presence of activated transport is indicative of disorder but may not describe transport in the ordered regions. The temperature-dependence of the thermopower varies more dramatically between transport mechanisms and may reveal more about transport than is limited by conductivity measurements. For example, as the activation energy approaches k_BT, the thermopower is linear in temperature.[123] For mobility-edge hopping, it is inversely proportional to temperature (Equation 2.6). It has been suggested that FTS-doping induces enough charge carriers in P3HT to induce an insulator-to-metal transition, which may be apparent in future studies of the temperature-dependence of the thermopower and the electrical conductivity.

2.4 Conclusions

We have studied the thermopower of a series of semiconducting polymers using two doping methods. Examination of the power factor over electrical conductivities ranging from $\sim$10^{-5} S-cm^{-1} to $\sim$10^{3} S-cm^{-1} shows no obvious maximum in the power factor for these polymers, unlike what is typically observed for inorganic semiconductors. We have not yet seen a maximum power factor where any improvement in the electrical conductivity would be dominated by a loss in thermopower due to an increase in the number of charge carriers. Developing additional doping mechanisms that yield higher conductivities may provide a means to probe the maximum power factor for this class of materials, thus establishing the upper limit of the power factor and thermoelectric figure of merit.

The empirical relationship presented allows a method to determine if new materials exceed the performance of existing materials as thermoelectrics. We also note that to effectively screen materials as good thermoelectric materials, one must measure all the transport properties in the same direction of transport, i.e., in plane or out of plane. In our case, the chain axis of the polymers is known to be along the substrate although it is not oriented over the length scale of the measurements. It is possible that for some materials there is high anisotropy in one, two, or all the transport parameters σ, α, and κ. Device geometries and polymer processing can be chosen to take advantage of the most highly favorable direction for applications.

The surprising correlation of thermopower to electrical conductivity for two very different doping methods and also across polymers raises questions as to the mechanism of charge transport and role of a physical dopant within a polymer blend. This suggests that transport and thermoelectric properties are dominated primarily by the polymer and not by the specific doping mechanism. Temperature-dependent measurements of thermopower of both F_4TCNQ - and FTS-doped polymers are necessary to further explore the mixed transport in these heterogeneous semiconducting polymers.

2.5 Experimental Section

Samples were prepared by solution casting onto electrically insulating substrates of quartz, glass, or sapphire. Both thick (~1 μm) and thin (~50 nm) films were prepared via drop casting in a nitrogen atmosphere or spin-coating in ambient conditions, respectively. All samples were soft-baked at 80°C in a nitrogen atmosphere for 10 min to remove excess solvent. Annealed samples were baked at 150°C for 10 min, also under nitrogen.

Gold electrical contacts (45 - 90 nm thick) were deposited via controlled thermal evaporation through a shadow mask, at an average rate of 1 Å-s^{-1}. Two contact geometries were used on simultaneously and identically prepared samples, one each for electrical conductivity and thermopower measurements. Electrical conductivity was measured with a co-linear four-point-probe bar geometry. Thermopower measurement contacts consisted of 1 mm^2 gold pads adjacent to 0.2 mm x 1 mm electrical contact bars, 3 to 5 mm apart (Supporting Information Figure 2.S1). Measurements of thermopower and electrical conductivity were performed under nitrogen, with the exception of temperature-dependent measurements, which were performed under vacuum.

The thermopower was measured via the differential method: a temperature gradient is established across the sample and after a set settling time, five consecutive measurements are taken 1s apart. The temperature gradient was incremented between approximately ±5 K. Larger stable temperature gradients are possible with the choice of substrate, but the measurement assumes the Seebeck coefficient did not change significantly over T

±ΔT, so ΔT was kept under 5 K. Each sample was measured multiple times to account for the high percentage of error inherent with thermopower measurements in this system (15%) and in general.[153]

Polymer solutions were made at 5 mg-mL^{-1} in a solution of 1:1 chlorobenzene:dichlorobenzene. Solutions were filtered with 0.45 μm PTFE filter at 80°C. F_4TCNQ -doped samples were made by adding a relative wt% of F_4TCNQ to the polymer solution before casting. FTS-doped samples were doped in a post-processing step by exposing the cast films to FTS vapor in a vacuum oven at 80°C overnight. Saturation of the doping was assumed to be reached when the films are visibly completely transparent, after which the samples were removed from the chamber. In the short amount of time between the vacuum oven and moving the films to the inert environment, a slight but visible re-coloration of the film indicated slight de-doping, which was unavoidable with the current setup.

2.6 Acknowledgements

The authors gratefully acknowledge support through the AFOSR MURI program under FA9550-12-1-0002. A.M.G. received partial support from the ConvEne IGERT Program of the National Science Foundation under NSF-DGE 0801627. J.E.C. received partial support from DOE BES under Award DE-777SC0005414. This work was partially supported by the MRSEC Program of the National Science Foundation under Award No. DMR 1121053. Use of the Stanford Synchrotron Radiation Lightsource, SLAC National Accelerator Laboratory, is supported by the U.S. Department of Energy, Office of Science, Office of Basic Energy Sciences under Contract No. DE-AC02-76SF00515. The authors wish to thank Prof. Vitaly Podzorov (Rutgers U.) for helpful conversations about doping polymers with FTS vapor.

2.S Supporting Information

2.S1 Geometry of thermopower measurement setup

Figure 2.S1 shows the general set up of the thermopower (Seebeck coefficient) measurement. Peltier elements 5mm apart provided the temperature differential $\Delta T = T_H - T_C$. Gold contact pads were 5, 4, or 3mm apart (d in Figure 2.S1), and sample was placed such that the midline between the left and right pads was approximately the midline of the gap between the Peltier elements. The largest spacing was used to obtain the largest voltage measurement for a given Peltier power and to reduce error, unless film defects interrupted the continuity between the measurement probes. Thermocouples and voltage probes were aligned so that an accurate Seebeck coefficient could be obtained. The thermocouple bead was dipped in heat sink compound to ensure good thermal contact between the thermocouple and the sample. However, thermal anchoring issues cannot be completely avoided, and the measurement system has a systematic error of 15%, which is comparable to other systems.

The Peltier elements are wired together such that sourcing 1V makes one side hot and one side cold, and sourcing -1V reverses the temperature gradient. There was a $75 - 100$ s delay time between source and measure, such that a steady-state temperature gradient was reached. A typical Seebeck voltage scan is shown in Figure 2.S2.

2.S2 Dedoping of FTS doped polymers

FTS doping was done in a vacuum oven. Pristine samples were placed around a dish in the vacuum oven. A few drops of FTS were introduced to the dish, and the vacuum oven was evacuated to < -30Torr with a roughing pump. After 1 minute of active vacuum, the valve to the pump was closed, and the oven was heated to 80°C. Sam-

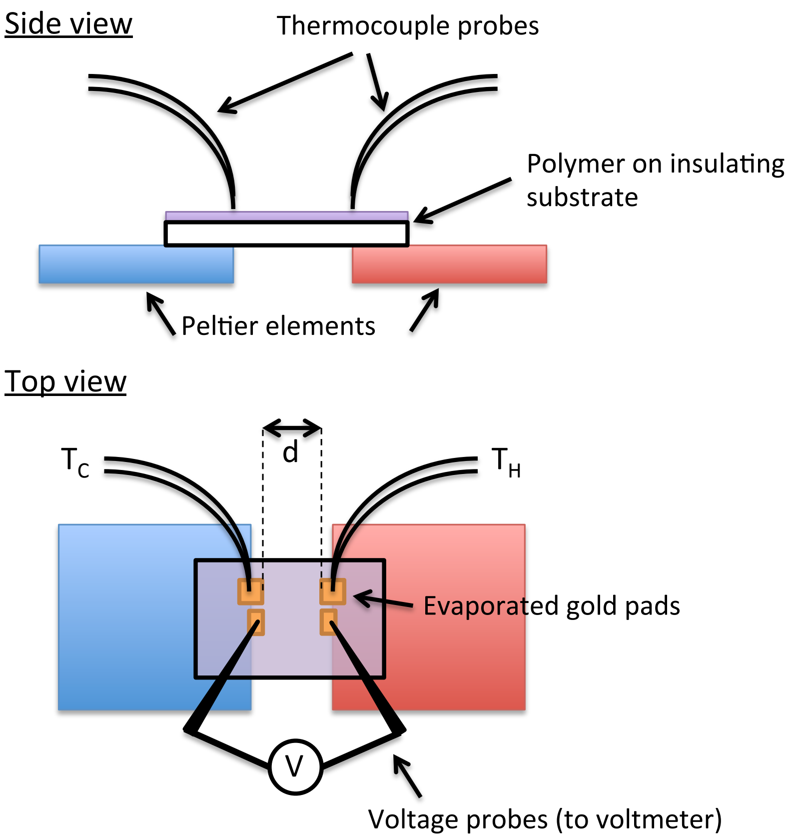

Figure 2.S1: Schematic of thermopower measurement apparatus. The spacing between the contacts is d.

ples were left overnight or until they appeared transparent. Samples were immediately transferred to a nitrogen glovebox under a foil-covered dish to reduce de-doping from ambient humidity and illumination. Samples were measured after various treatments and over time. Samples were measured immediately after being brought into the inert environment, and 12-24hours later. Samples were later annealed at 80°C for 30 minutes to test thermal stability, then again after 12-24 hours. Finally, samples were de-doped to reduce conductivity and measured again. To de-dope, samples were brought out of

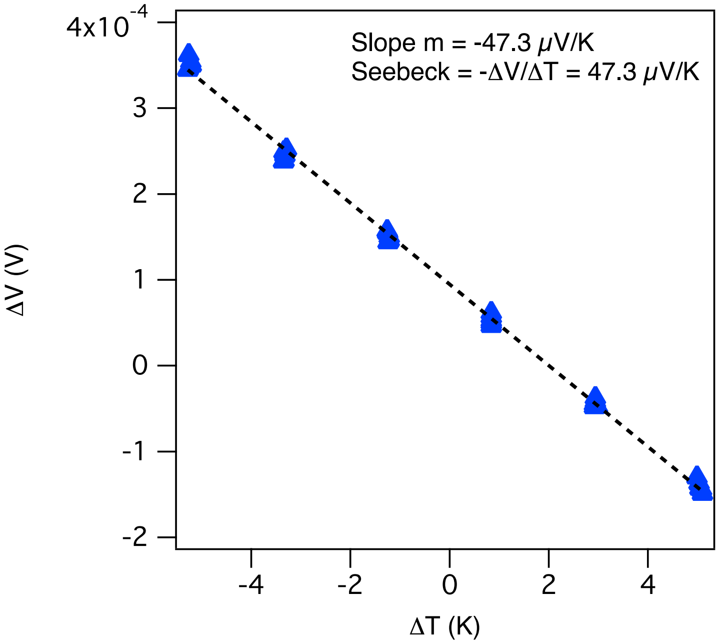

Figure 2.S2: Typical differential Seebeck measurement curve. The thermopower is calculated from the slope of a linear fit through the (ΔT, ΔV) points. At least 5 measurements for each steady-state ΔT are recorded.

the inert nitrogen glovebox and placed in an illuminated fume hood for 30 minutes to an hour+, then returned to the glove box and measured. An example measurement series is shown in Figure 2.S3. Under nitrogen atmosphere, samples were stable and showed no significant degradation over 24 hours. Annealing the doped samples at 80°C did not significantly degrade the conductivity. Conductivity dropped over 2 orders of magnitude when exposed to ambient humidity and illumination for 120 minutes, and thermopower increased by 1 order of magnitude.

2.S3 Topography of FTS doped polymers

As mentioned in the article body, FTS doping is achieved by exposing a pristine polymer film to a vapor of FTS for a certain period of time. Figure 2.S4 shows a representative atomic force microscopy (AFM) image showing the topography of a pristine sample of

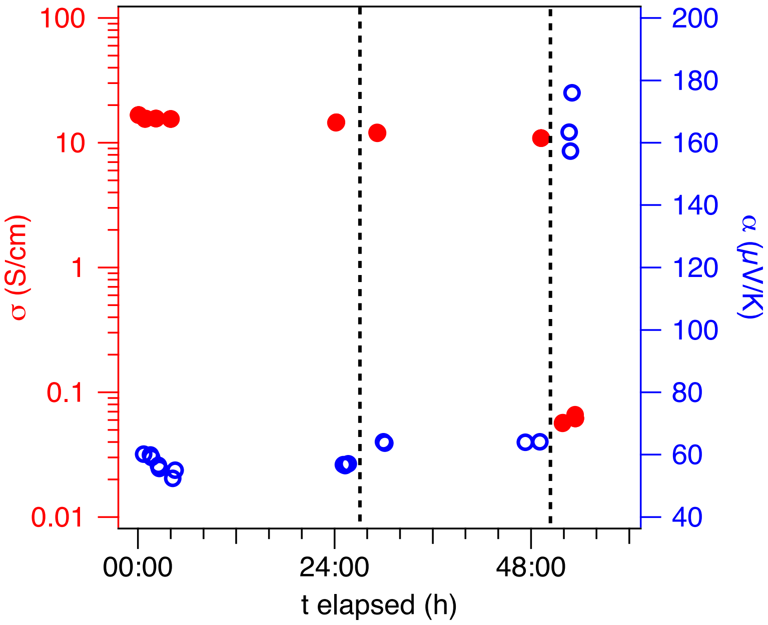

Figure 2.S3: Measurement series of an FTS-doped P3HT sample. (1) Sample baked at 80°C / 30mins in N_2. (2) Sample removed to ambient conditions (air + illumination) for 120 minutes and then returned to N_2 environment for measurements.

PBTTT-C_{14} . Figure 2.S5 shows an AFM image of a film that was not exposed to the FTS vapor long enough for continuous surface coverage. In between the large features, the texture is similar to that of the pristine PBTTT-C_{14} , indicating that the FTS does not infiltrate the polymer surface. Figure 2.S6 shows a film that has been overexposed to FTS. The height of the aggregates compared to the height of the FTS structure on the partially covered film indicates that the FTS does not form a perfect SAM, nor does it swell the film noticeably.

2.S4 Grazing Incidence Wide-Angle X-ray Scatter (GIWAXS) of FTS Doped PBTTT-C_{14}

Figure 2.S7 shows the GIWAXS patterns for pristine and FTS-doped PBTTT-C_{14} . For the FTS-doped film, we observe scattering reflections consistent with the PBTTT

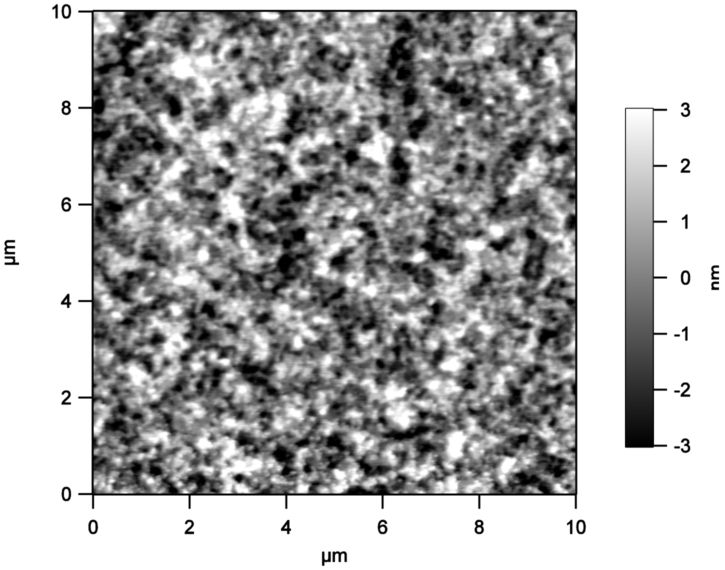

Figure 2.S4: AFM image of undoped PBTTT-C_{14} .

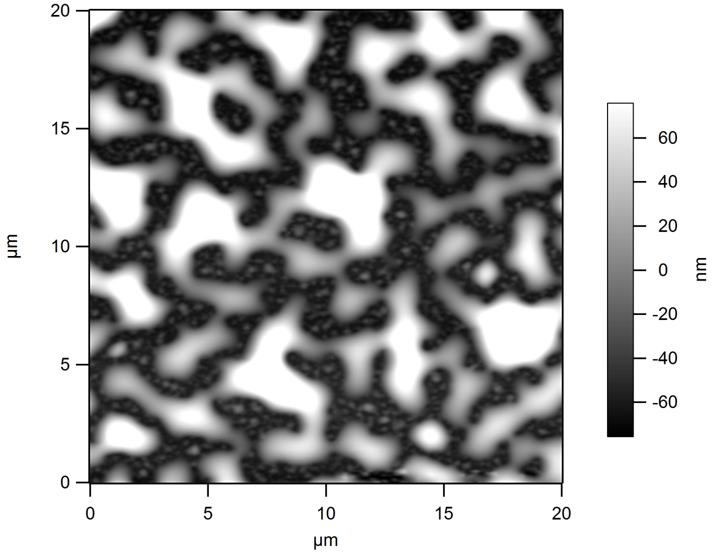

Figure 2.S5: AFM image of PBTTT-C_{14} that was partially exposed to FTS vapor

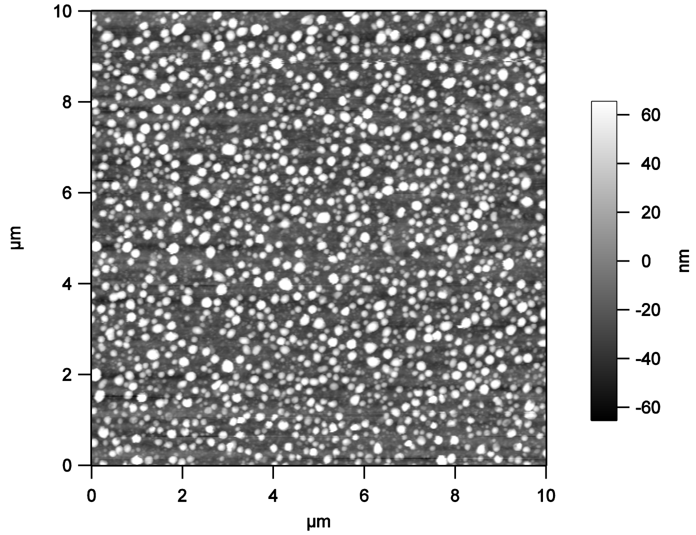

Figure 2.S6: AFM image of PBTTT-C_{14} that has been completely exposed to FTS vapor

crystal structure (the broad amorphous ring corresponds to FTS). However, we observe a small change in crystalline orientation and a small disruption in the crystallite size relative to the pristine film. The calculation of the crystallite correlation length (CCL) of the (110) peak corresponding to the - stacking indicates a small decrease in crystallite size (Table 2.S1). In addition, we do not observe a significant change in peak position for the out-of-plane (200) peak and in-plane (110) peak, which suggests the FTS does not insert itself in the ordered crystalline domains. This is in stark contrast to the observed mechanism of F$_4$TCNQ doping. When the film is dedoped (i.e. exposure to air for 1 hour), the GIWAXS pattern (not shown) is indistinguishable to the doped film. As shown in Table S1, the peak positions and CCL value remain very close to the doped film, thus indicating the FTS doping effect is irreversible with respect to the crystalline structure.

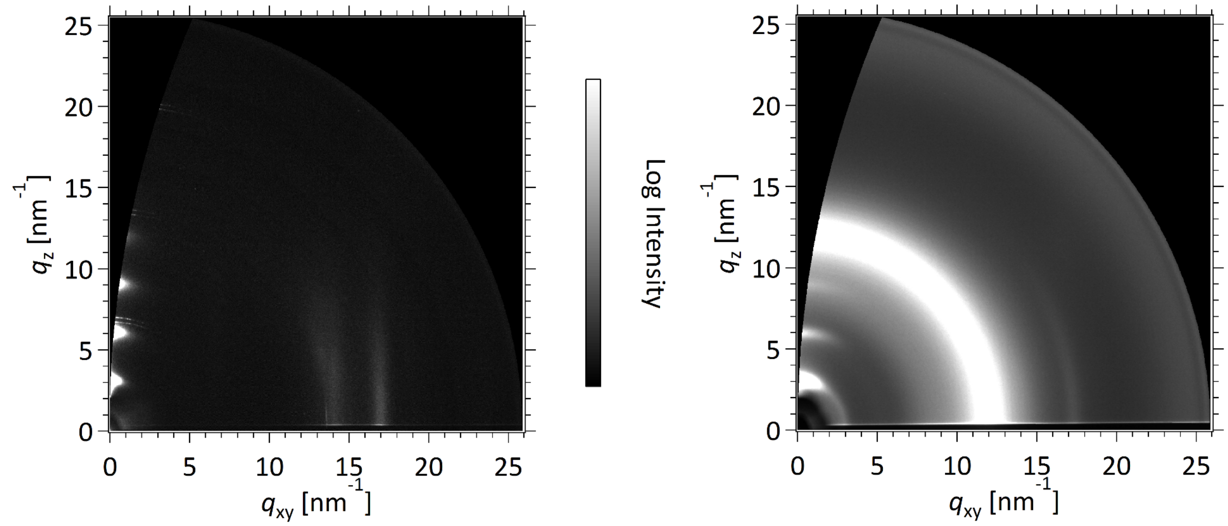

Figure 2.S7: Grazing Incidence Wide-Angle X-ray Scattering (GIWAXS) of a) Pristine PBTTT-C$_{14}$ vs. b) FTS-doped PBTTT-C$_{14}$. The broad amorphous ring seen on the FTS-doped film image is from the FTS layer on top of the film. GIWAXS patterns were obtained on beamline 11-3 at Stanford Synchrotron Radiation Lightsource (SSRL).

Table 2.S1: GIWAX peaks for pristine, FTS-doped, and dedoped PBTTT-C_{14}

	(200)		**π-π stacking (110)**		
	q (nm^{-1})	FWHM (cm^{-1})	q (nm^{-1})	FWHM (cm^{-1})	CCL* (nm)
Pristine	6.09	0.469	17.2	0.808	7.78
Doped	6.03	0.665	17.4	0.924	6.80
Dedoped	5.95	0.667	17.3	0.936	6.71

2.S5 Temperature-dependent conductivity

Conductivity was measured at temperatures below 300K to obtain the activation energy for both F_4TCNQ -doped (Figure 2.S8) and FTS-doped (Figure 2.S9) samples. Activation energy was found via fitting the curves to the Arrhenius expression for activated transport: $\sigma = \sigma_0 \exp(E_A/k_B T)$ below 270K (F_4TCNQ) and 300K (FTS).

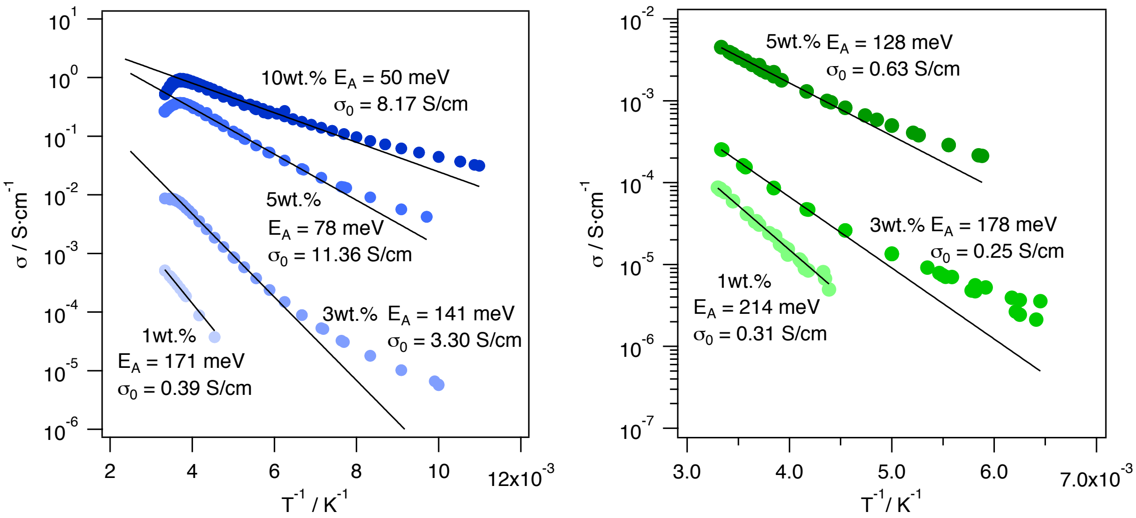

Figure 2.S8: Temperature-dependent conductivity of a) PBTTT-C_{14} and b) P3HT doped with various wt.% of F_4TCNQ . Samples were measured below 300K under vacuum

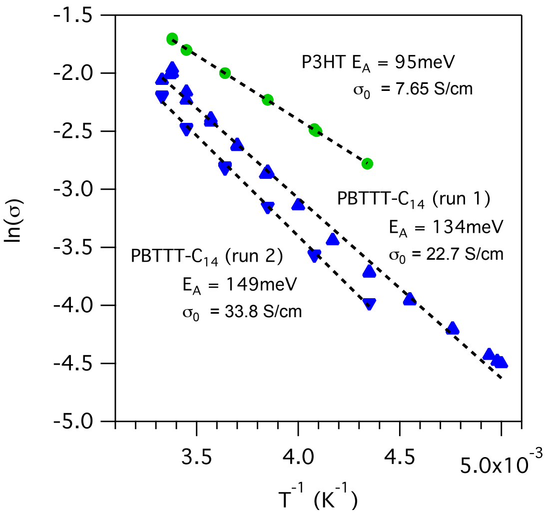

Figure 2.S9: Temperature dependent conductivity of FTS-doped P3HT (green circles) and PBTTT-C_{14} (blue triangles). Run 2 was obtained by de-doping the PBTTT-C_{14} sample (run 1) for 30 minutes in ambient humidity and illumination.

2.S6 Temperature Stability of Doped Polymers

Polymers P3HT and PBTTT-C_{14} doped with F_4TCNQ showed only slight changes to conductivity upon annealing at the mol.% dopants shown. P2TDC_{17}-FT4 showed much more change upon annealing, and un-annealed films had inconsistent conductivities across batches, compared to P3HT and PBTTT. We suggest this is because F_4TCNQ is much less stable in the FT4 solution and heated thin film, such that the solution age and film environmental history play a more important role in the nominal mol.% F_4TCNQ in the film, and aggregation of F_4TCNQ such that it cannot contribute to charge-transfer.

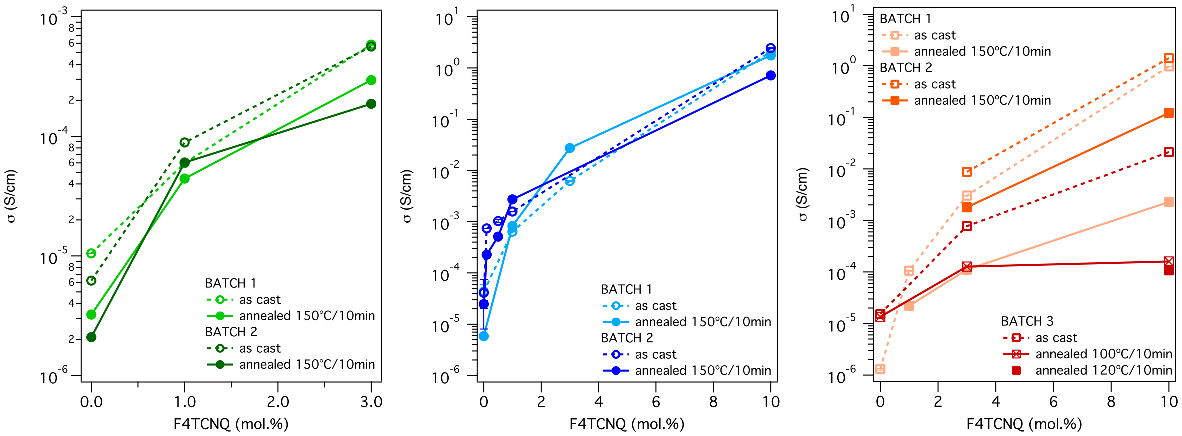

Figure 2.S10: Typical conductivity vs. mol% doping series for as cast and annealed polymer samples, over multiple batches of solution: a) P3HT b) PBTTT-C_{14} c) P2TDC_{17}-FT4 . Doped P3HT and PBTTT-C_{14} behaved consistently between as cast and annealed, over multiple batches. P2TDC_{17}-FT4 was inconsistently sensitive to annealing.

Chapter 3

Experimental Procedures & Instrumentation

Polymer thermoelectric research was new to the Chabinyc lab, so prior to studying the thermoelectric properties of organic materials. it was necessary to build instrumentation to measure electrical conductivity and Seebeck coefficient of thin films. By the end of this Ph.D. work, I developed instrumentation and hardware necessary to thermoelectric measurements. Virtual instruments (.vi's) were created from the bottom up in LabView, using GPIB protocol. Below is a list of the capabilities of our lab that were nonexistent prior to this work, some of which will be discussed in detail in this chapter:

Room Temperature

- Hardware & Instrumentation
  1. Modular probe station in N_2 glovebox
  2. Thin film electrical conductivity (linear 4PP)
  3. Thermopower
  4. Local temperature
- Measurements in LabView
  1. Electrical conductivity (linear 4PP)

2. Thermopower
3. Gated Thermopower

Variable Temperature Probe Station

- Hardware & Instrumentation
  1. TE Measurement stage
  2. Local surface temperature
  3. Thin film electrical conductivity
  4. Thermopower
- Measurements in LabView
  1. Variable temperature electrical conductivity
  2. Variable temperature thermopower
  3. Variable temperature semi-automated I-V measurements

3.1 Electrical Conductivity

Electrical conductivity of thin film materials was measured using a standard linear four-point probe (4PP) technique with current being sourced and voltage being measured. Four probes are spaced evenly apart on the surface of the sample, the outer contacts are for the current source while voltage is measured across the inner contacts. Current is stepped from a negative value to a positive value and the steady state voltage is recorded. The sheet resistance R_s is given from the slope of the V-I curve: $dV/dI = R_s$. The conductivity of a semiconductor using this method is calculated using the following equation, where g is a geometrical constant:

$$\sigma = \frac{dI}{dV} g \tag{3.1}$$

The geometric factor g depends on sample geometry and has been worked out analytically for a variety of different geometries.[154] A common simple case is a bar-shape or resistor geometry, in which the current is sourced at the end of a sample with uniform cross section (Figure 3.1a). The voltage probes need not be spaced evenly with the current source, but should be located where there is uniform current flux. The geometric constant in this case is l/A, where the cross-sectional area $A = w \times d$, where d is the thickness of the bar and w is the width, giving the familiar conductivity equation $\sigma = 1/\rho = (dI/dV)l/A$. For thin films, an appropriate approximation of the geometry is an infinite sheet, where the geometric constant has previously been solved: $g = \ln(2)/\pi d$, giving the equation below for calculating conductivity for thin films.

$$\sigma = \frac{\ln(2)}{\pi d}\left(\frac{dI}{dV}\right) \tag{3.2}$$

The error for an actual sample (i.e. non-infinite) is less than 1% provided that the thickness is less than 1/2 the probe spacing s, and that the dimensions of the sample are much greater than the linear span of the probes ($3s$).[154]

For organic thin films studied here it is necessary, due to the softness of the material, to deposit electrical contacts for the probe needles to make electrical contact with the film. Contacts are made via thermal evaporation through a physical mask. The typical arrangement used for this body of work comprises of 1 mm long x 0.1 mm wide strips evenly spaced in the center of the sample, as shown in Figure 3.2(left). The metal (generally $\sim$ 50nm of Au) layer ensures good electrical contact and the strips enable the probe needles to contact the sample multiple times reliably (vs. a square 0.5mm point contact pad). Alternatively, a bottom-contact geometry can also be used by evaporating a thin adhesion layer (Ti or Cr, 5nm) and then the metal (45nm of Au) before the polymer is spin-cast on the substrate (Figure 3.2(right)). Contact is made by scratching the needle through the thin polymer layer, with the adhesion layer of the metal preventing the needle probe from locally scratching off the metal and compromising electrical contact between

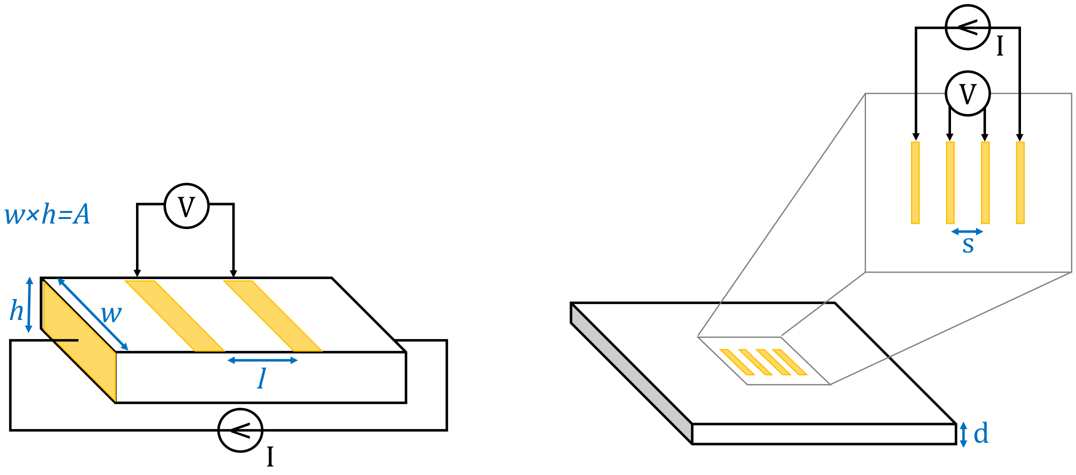

(a) Bar / resistor geometry (b) Infinite thin film geometry

Figure 3.1: Sample and contact geometries for measuring four-point probe conductivity. The infinite thin film geometry (b) was used for the films studied here.

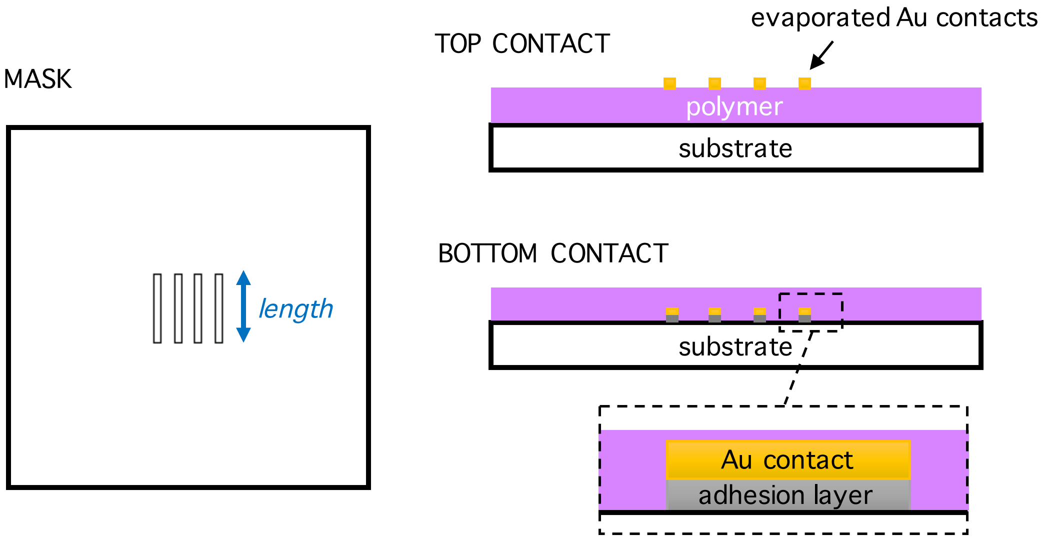

Figure 3.2: Schematic of shadow mask (left) and top-contact and bottom-contact (right) geometries for measuring electrical conductivity by the linear 4PP method. Features enlarged to show detail

the metal pads and the polymer thin film. The choice of bottom or top contact geometries may be dictated by necessary sample processing steps or stability requirements, or simply the ability to pre-fabricate substrates with contacts in bulk for later use.

3.2 Seebeck Coefficient (Thermopower)

The thermopower of material is measured by creating a laterally-uniform temperature gradient across the sample and measuring the induced Seebeck voltage. The Seebeck coefficient (thermopower) of the material is simply the Seebeck voltage over the temperature differential, measured at the same points:

$$\alpha = -\frac{\Delta V}{\Delta T} \tag{3.3}$$

The majority carrier is indicated by the sign of the Seebeck coefficient: α is negative for electrons, and positive for holes. If both carriers are mobile in the system, the Seebeck coefficient is the average of that of electrons and holes weighted by their contribution to conductivity.

Care must be taken to set up the measurement system such that the measurement of ΔV and ΔT are in the same direction, i.e.: $\alpha = -(V_2 - V_1)/(T_2 - T_1)$. Failing to ensure this is the case will not give the correct sign of the Seebeck coefficient. This point is especially important for new materials where the majority carrier is not known, one should not assume that the sign is always positive due to the assumption of hole-majority carriers (or negative due to electron-majority carriers).

Ideally, the Seebeck voltage and the temperature should be measured at the same points, as close as possible perpendicular to the temperature gradient if not on the exact same spot. For inorganic materials, often the copper lead of the thermocouple is used

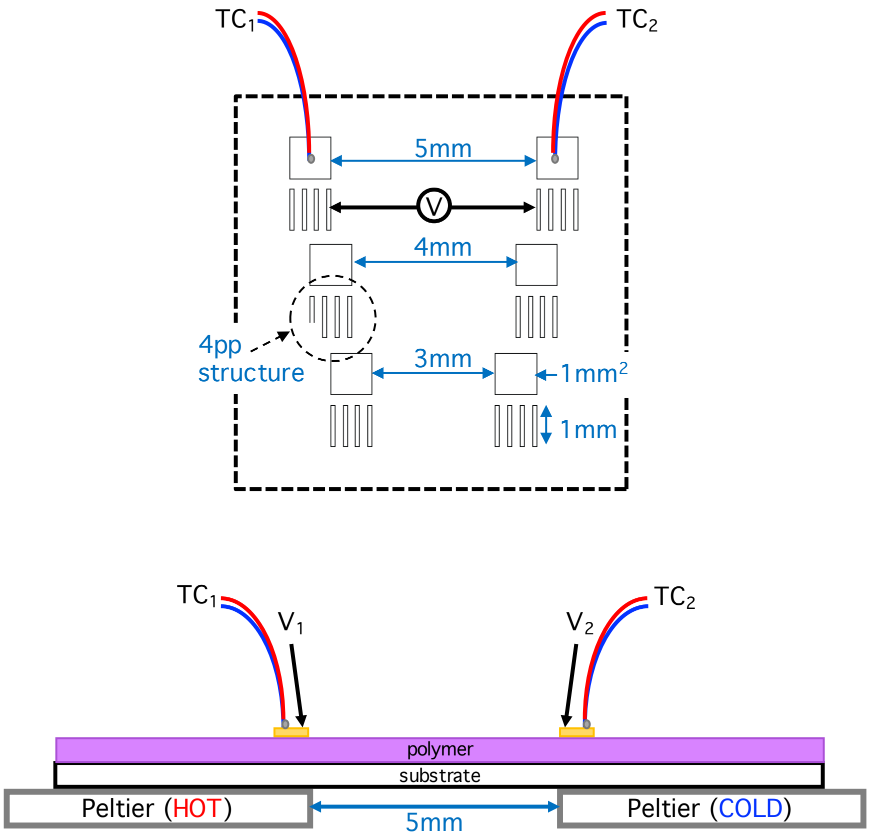

Figure 3.3: Schematic for measuring Seebeck coefficient. Mask (top) and top-contact geometry (bottom).

as the voltage lead, pressed onto the sample, ensuring that the temperature and the voltage are measured with the same junction. This method is often not practical, and for thin films the thermocouples can be placed laterally to the voltage probes, taking into consideration that the temperature gradient is linear.

The contact geometry for used for this body of work incorporated contacts for measuring 4pp conductivity as well as the Seebeck coefficient, as shown in Figure 3.3-right. On one side of the substrate, $1 \times 1\text{mm}^2$ contact pads sit adjacent to the same 4pp pattern used for measuring conductivity. On the opposite side of the substrate another set of contacts is placed, spaced 5mm away from the first. Two more sets of pads, spaced 4mm and 3mm, are also patterned on the substrate. These extra sets of contacts allow the sample to be measured in multiple places in case of damage or a non-uniform film. Additionally, the differently spaced contacts can be used for verification of the measurement because the Seebeck coefficient, a materials property, should be the same regardless of spacing.

3.3 Inert N2 Atmosphere Probe Station

3.3.1 Peltier elements

In order to create a temperature gradient, two Peltier elements (19811-9L31-02CN1, 200°C-rated, Custom Thermoelectric) were placed 5mm apart and secured to a copper plate using double-sided thermal tape (TCDT1, ThorLabs) on the entirety of the bottom surface. The elements were wired in series such that upon being supplied power, the top surface of one element heated above ambient temperature and the top surface of the other element cooled below ambient temperature. This can be achieved one of two ways, either mirroring the elements in series (Figure 3.4a) or placing one element upside down and wiring normally in series (Figure 3.4b). The pelter elements are prepped for the sample with some thermal interface material to ensure good thermal contact. Initially the thermal interface material was a light application of the same heat sink compound used for the thermocouple probe tips, but later a cleaner alternative of silicone interface sheets was used, cut to the sample size or larger. The silicone interface sheets (GapPad®1500, 0.010", Bergquist) were tacky on both sides to enable easy sample placement and removal, and when worn out after multiple uses, easy sheet replacement. The silicone interface sheets did not appear to noticeably affect the time of thermal equilibration of the sample when compared to using heat sink compound.The sample is placed across the gap such that the electrical contacts are at or within the 5mm gap and squared off.

3.3.2 Electrical Probes

The probe station is equipped with 4 micromanipulator electrical probes (SemiProbe MA-8005 plus magnetic base) with 5-25 µm tungsten needles. Two probes are reserved for sourcing current I in the four-point probe conductivity measurements. The other two probes are reserved for measuring potential, either the voltage V for the 4pp electrical conductivity measurement or the Seebeck voltage ΔV for the Seebeck measurement.

3.3.3 Thermocouple Probes

The temperature difference was measured by directly placing thermocouples on the samples. Thermocouple probes were made by attaching a Signature probe arm holder with a paperclip / bendable wire probe arm, to which a thermocouple was held against the wire support with heat shrink tubing. The tubing allowed the thermocouple to be adjusted against the wire support and removed easily. The thermocouple wire was secured to the base of the probe with tape, and terminated with a male type-T miniature

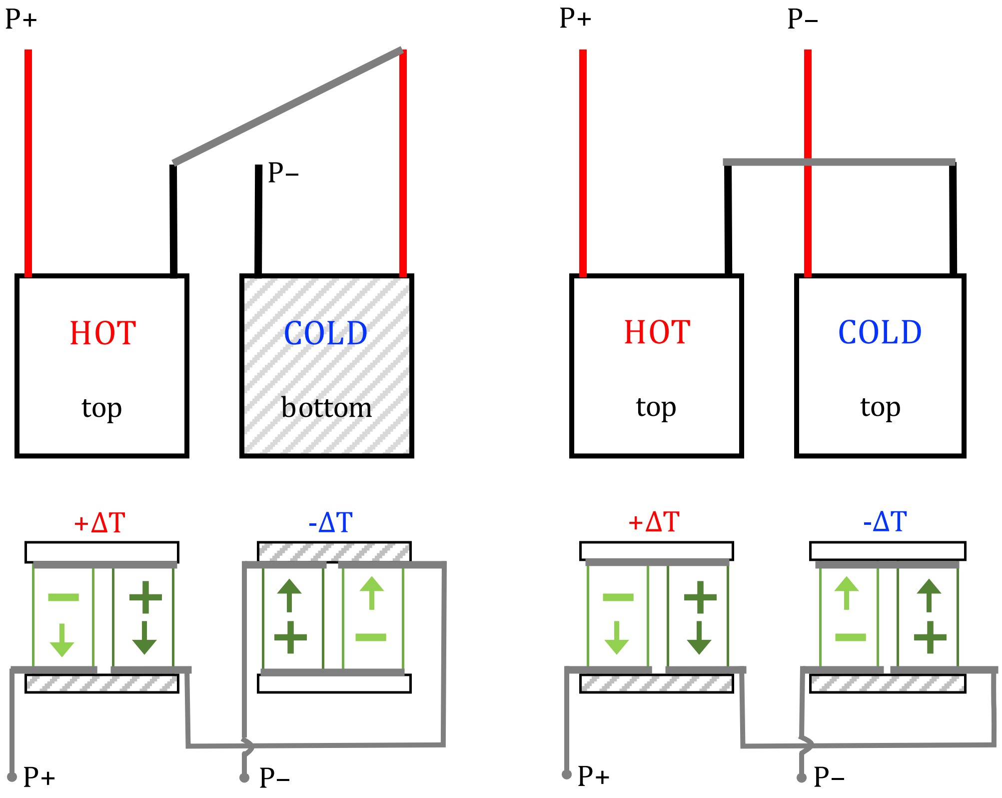

Figure 3.4: Peltier element wiring N_2 setup, illustrating the two options for connecting the elements to a single power source, as well as a schematic of carrier flow to demonstrate the necessity of proper wiring to obtain a ΔT. (left) Standard series connection requires one Peltier element to be upside-down for one surface to get hot and the other cold. (right) Mirrored series connection required if Peltier elements are both placed right side-up. The "bottom" of the Peltier element is the side to which the leads are soldered to the end connection pads, or as indicated by the manufacturer in the case of a sealed element.

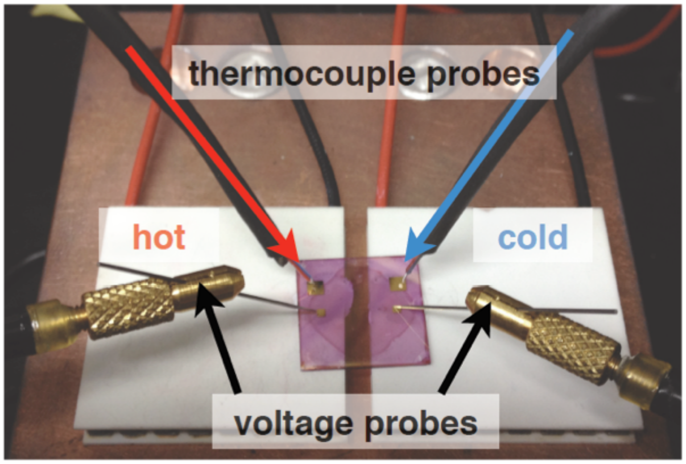

Figure 3.5: Close-up of the experimental setup in the N_2 glove box.

molded connector (SMPW-T-M, Omega Engineering).

To ensure good thermal contact, the thermocouple probe bead was dipped into a minimum amount of heat sink paste (ZnO and silicone oil). To minimize contamination and any unintended interactions between the polymer sample and the heat sink paste, thermocouples were placed on 1x1mm contact pads adjacent to the voltage probe contacts, and when possible, a drier (higher ZnO:silicone oil ratio) heat sink paste was used. The contact pads and voltage probe contacts were deposited by thermal evaporation.

3.3.4 Visualization

The probe station is equipped with a stick microscope terminated in a CCD camera to aid in the placement of the microprobes on the sub-mm contact pads. Illumination was provided by the fluorescent glove-box light and by an in-line source fitted to the microscope. The CCD camera was attached to an articulating elbow fashioned from optomechanic post assemblies (ThorLabs) to enable visualization of the entire sample stage. The camera feed was connected to a small monitor on the outside of the glove box.

3.3.5 Feedthroughs

A KF-40 port with four grounded BNC feedthroughs was installed in the side of the glovebox for voltage and current source-measure capabilities. The thermocouple connection was made by a KF-40 port with four type-T thermocouple connection pairs terminated in loops (TFT4TN00008B, Kurt J. Lesker). For ease of thermocouple probe replacement and rearrangement, the loop terminations in the glovebox were wired to type-T miniature molded female connectors (Omega). The air side loops were connected to extension grade type-T thermocouple wire with an attached miniature molded connector (male). The extension wire was then color-coded with tape on both sides of the port. An S-Video feedthrough was also made to connect the microscope camera to the monitor air-side.

3.4 Variable Temperature Vacuum Probe Station

In order to measure the temperature-dependent properties of materials over a large temperature range, a new removable chuck was developed for the variable temperature vacuum probe station (LakeShore TTP-X).* The probe station is equipped with a cold stage with cartridge heaters and a LN_2 bayonet port, and is controlled by a LakeShore 332 Temperature Controller. The cold stage allows sample measurements to be taken

---

*The page numbers in this section will refer to the LakeShore Cryotronics TTP-4 manual, which is available in .pdf form and a hard copy in lab. The TTP-4 is sufficient for TTP-X operation and maintenance, with few exceptions.

77K to 400K or 475K depending on the sample holder (see manual pg. 39 for standard sample holder limitations). The vacuum in the probe station can reach to about 10^{-5} Torr with the turbo pumping system.

3.4.1 Thermoelectric Sample Holder

3.4.1.1 Initial Version

A custom thermoelectric sample holder was made building on the footprint of the grounded sample holder (Model DC 0097, SH-1.25-G, LakeShore Cryotronics). A flat copper base was machined and the surface was lapped for flatness and smoothness. At first, the thermoelectric stage was made in the same way as the inert atmosphere probe station - with two 10mm metallized Peltier elements (04801-9G30-18RB, Custom Thermoelectric) spaced 5mm apart. The Peltier elements were secured to the copper with double-sided thermal tape. The Peltier elements were wired mirrored in series as to produce a temperature difference when powered. The end wires were terminated at a single inline package (SIP) pin strip. This iteration of the sample holder had major flaws and did not pass the initial test run. This configuration was not rated for the power required to maintain a temperature gradient in this system; it is unclear whether the point of failure was a Peltier element or the pin and socket connector. Additionally, the Peltier elements are fragile and made of brittle materials and the frequent cycling of the vacuum chamber pressure cause delamination of a lead from one of elements.

3.4.1.2 Final Version

Shown in Figures 3.6 and 3.7 . The final custom thermoelectric sample holder was also made upon a flat copper base. Instead of Peltier elements, two copper blocks were machined and bored to receive cartridge heaters. The two copper blocks were placed

5mm apart and secured with small strips of thermally conductive double-sided tape. During the test runs, the copper heater blocks were secured to the copper base plate with thermally conductive tape covering the entire area of the block heater. It was determined that the heat sinking effect from the cold plate was too large to maintain a 5K temperature gradient. After experimenting with various interface materials, it was found that thin glass standoffs affixed with Scotch tape on each end of the copper block ($\sim 40\%$ block area contacting the chuck) enabled the block heaters to maintain a temperature difference of at least 5K, and that the steady-state temperature difference was established relatively quickly (< 5 minutes).

A high-watt density stainless steel cartridge heater (CSS-01115/120V, Omega Engineering) was inserted into each bored hole, lubricated with thermal paste to increase thermal contact and reduce movement within the bore. A heat sink compound that is specially formulated for use at low temperatures (Arctic Silver Ceramique 2) was used in favor of regular heat sink compound. This compound operates as low as -150°C (123K) without seizing, allowing measurements at low temperatures. Most heat sink compounds are only rated to -40°C (233K), resulting in extremely poor heat transfer at low temperatures. The heater lead pairs were terminated with Molex MicroFit power connector pins and housing, which can handle up to 5A (connectors) and 105°C. It is reasonable to assume that the connector housing will not reach much higher than 100°C as it will not be mounted on any part of the chuck or probe station, and only thermally connected to the heater chuck via the cartridge leads. It is to be noted that the choice of dual heater blocks to replace Peltier pelements required an adjustment to the thermopower measurement procedure, which will be discussed in the Measurements section 3.5.2.2.

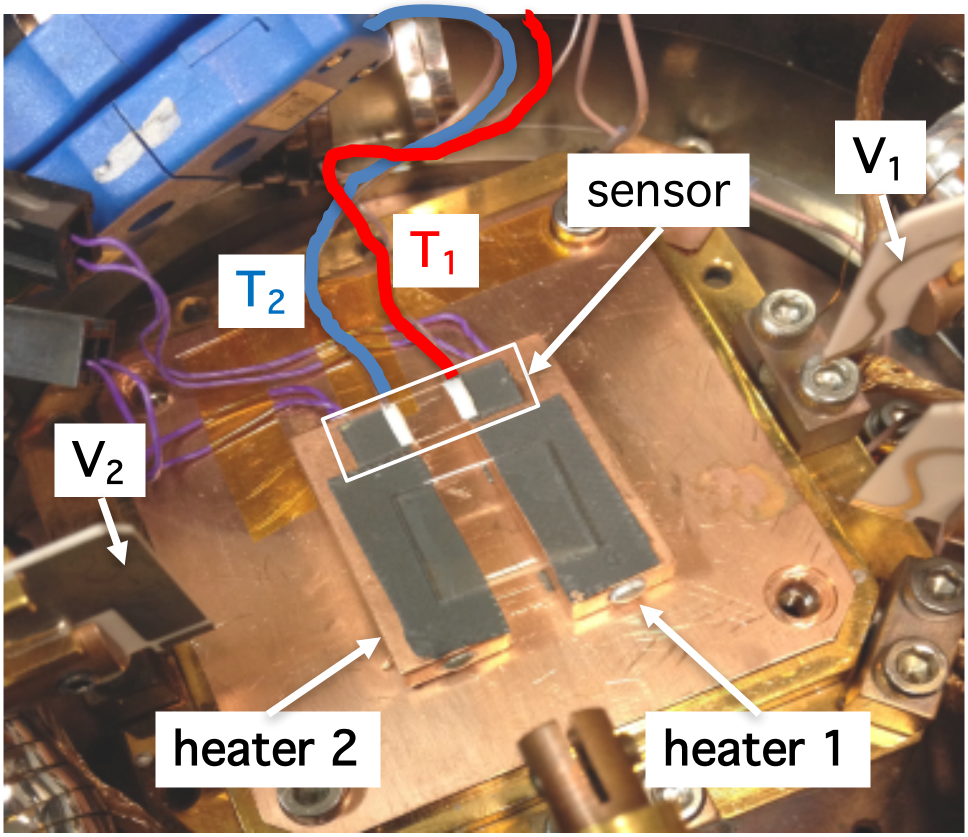

Figure 3.6: Close up of variable-temperature thermoelectric measurement stage. A 1.5×1.5 cm^2 glass slide spans the heaters to give a sense of scale and how to place a sample. The thermocouple wire and sensor are emphasized for clarity. The probes measuring V_1 and V_2 are part of the vacuum probe station.

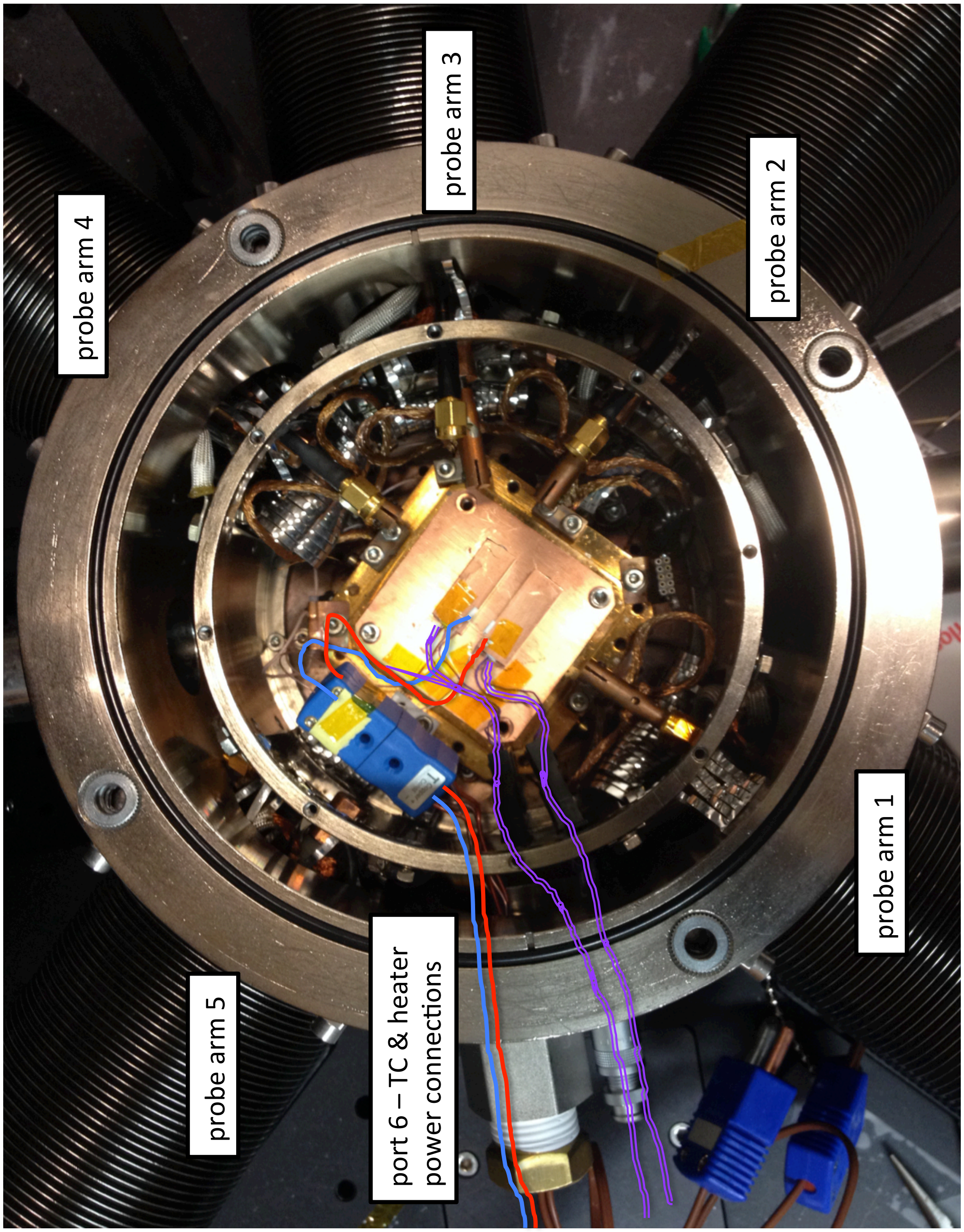

Figure 3.7: Variable temperature thermoelectric measurement stage and feedthroughs. The probe arm numbers are indicated on the vacuum chamber cover. The thermocouple wire and heater power connections are emphasized for clarity. The wires from the port plate are fed through an opening in the inner heat shield before connecting to the thermocouple stage.

3.4.2 Temperature Sensor

The temperature difference ΔT is measured with a demountable sensor consisting of two thermocouples permanently mounted to a quartz substrate. A 3x15mm quartz substrate was cut from the same 0.5mm thick quartz substrates used for the polymer samples. The thermocouples are mounted 5mm apart with a thermally conducting, electrically insulating two-part epoxy (Arctic Alumina™ Thermal Adhesive, Arctic Alumina), using 5mm wide Kapton tape as a mask during the first epoxy curing stage as indicated by the adhesive instructions.

The thermocouples are mounted on quartz, the same substrate material that the polymer thin film is cast on, in order to ensure that the temperature measured by the thermocouples is representative of the temperature experienced by the polymer thin film. If the thin film were to be deposited on a substrate with significantly different thermal conductivity, it would be prudent to make an additional sensor out of the desired substrate to compensate. For example, in an oxidized silicon wafer, the Si thermal conductivity $\kappa = 1.31 \times 10^2$ W/m-K, which is two orders of magnitude more thermally conducting, dominates over SiO_2 ($\kappa = 1.1 - 1.4$ W/m-K). Sapphire, which has been used as an alternative electrically insulating substrate for optical measurements of these same polymer thin films, also has a much higher thermal conductivity ($\kappa = 28$ W/m-K).

3.4.3 Feedthroughs

A custom feedthrough plate was made to be installed in place of the blank port on the vacuum probe station. The feedthrough plate consists of a panel-mount LEMO connector (ERA.1S.304.CLL, LEMO) for power connections to the two cartridge heaters and a hermetic type-T thermocouple wire feedthrough (PFT2NPT-2T, Omega Engineering) to enable the thermocouples to be connected directly to the temperature monitor instrument

(1529 Chub-E4 Standards Thermometer, Fluke Calobration).

3.5 Measurement Procedures (LabView) and Analysis (IgorPro)

3.5.1 Electrical Conductivity

As mentioned in previous sections, electrical conductivity is measured using a linear 4-point probe (4pp) geometry. The measurement procedure is identical for both inert room-temperature and vacuum variable-temperature electrical conductivity measurements. The current I_{source} is sourced across the outer electrodes and the resultant potential V_{meas} is measured across the inner contacts. I_{source} is stepped over $\pm I_{max}$ in equal steps (usually 11 data points symmetric about $I_{source} = 0$) with voltage measured at each discrete current value, e.g. $I_{source}(\text{nA}) = [-10, -9, -8, -7, ..., 0, ..., 7, 8, 9, 10]$. Each sample is measured at least 3 times with varying I_{source} ranges. The sheet resistance $R_S = V/I$ is taken from the slope m of the V-I curve, which is output in the data file.

In the inert room-temperature system, the ambient temperature is noted from the average of Ch1 and Ch2 of temperature monitor and entered by the user in the LabView GUI to be recorded in the output file. In the vacuum variable-temperature system, the base temperature for each conductivity measurement is automatically recorded at the beginning of the current sweep. After all measurements have been done on the sample, the thickness is measured by atomic force microscopy (AFM) (Asylum MFP-3D) by scratching the film and measuring the step height. Finally, with V-I slope $m = dV/dI$ and thickness d known, the conductivity is calculated using Equation 3.2: $\sigma = ({}^{dI}/_{dV})\ln(2)/\pi d$.

3.5.2 Seebeck Coefficient

The procedure to measure Seebeck coefficient in the vacuum probe station differs from that of the inert N_2 atmosphere probe station due to the use of copper block heaters in the former instead of Peltier elements in the latter.

3.5.2.1 Inert Room-Temperature Setup

To measure the Seebeck coefficient in the room-temperature inert set-up, the Seebeck voltage is measured at a series of ΔT values symmetric about $\Delta T = 0$. The Peltiers were source with increasing power such that $\Delta T \approx \pm 4\text{K}, \pm 2\text{K}, 0\text{K}$. Once each ΔT value is steady state (~ 75 s), 5 data points $(\Delta T, \Delta V)$ are recorded. There is also an option in the LabView .vi to record data continuously. The collection of the time dependence of the temperature difference and Seebeck voltage is useful if the data is noisy and allows for signal averaging or a large data set to more accurately determine trends. This method additionally helps determination of transient effects, which may appear as hysteresis or look like time-reversal symmetry breaking (forwards and backwards scan not identical). The Seebeck coefficient is extracted from the negative slope of the recorded $(\Delta T, \Delta V)$ values: $\alpha = -\Delta V / \Delta T$. The LabView .vi automatically calculates the slope after each ΔT step and the final Seebeck coefficient is recorded in the output file. Also recorded is the "dark voltage," which is the potential at $\Delta T = 0$. There is expected to be a small systematic dark voltage from instrumentation and cabling (a few V), while a higher dark voltage is indicative of a larger chemical potential due to other effects besides the electronic Seebeck effect.

3.5.2.2 Vacuum Variable-Temperature Setup

As mentioned, the variable-temperature setup has two copper block heaters to provide the ΔT instead of Peltier elements. As a result, the average sample temperature changes upon heating of a copper block, contrary to Peltier elements, where the average sample temperature is constant throughout the measurement. This is illustrated in Fig. 3.8a., where the blue regions highlight where T_{avg} (dashed line, right) is constant. Therefore, it is most accurate to calculate the Seebeck coefficient from data taken at steady state $\pm\Delta T$, where T_{avg} is constant. For the majority of the samples measured, the rise time of the Seebeck voltage was on par with the rise time of the temperature difference, indicating that the limiting process to obtain steady state was simply thermal equilibrium.

The Seebeck coefficient calculated from the slope of the V-T curve assumes that the Seebeck coefficient of the material is constant over the maximum ΔT of the sample. In practice, the particular samples measured had a locally flat temperature dependence of the Seebeck coefficient, so for ”well-behaved” samples taking the slope over the entire dataset results in the same Seebeck coefficient within the error of the system (15% max). ”Well-behaved” samples are those where the signal is much greater than any noise, and where the $\pm\Delta T$ are inversely identical. An example of an ideal run is shown in Fig. 3.8.

To ensure that the extracted Seebeck coefficient is extracted from a single average temperature, measurements are taken at only two ΔT steady-state values with the same T_{avg} via the following procedure (and shown in Fig. 3.8): One side of the sample is heated up to create a temperature difference $-\Delta T$, and is held until T_1, T_2, ΔT, and T_{avg} are steady state with time. The heat is then removed and the sample returns to $\Delta T = 0$. The other side is heated up to create a temperature gradient in the opposite direction, $+\Delta T$ and held until all temperatures are steady-state. The $(\Delta T, \Delta V)$ data points after steady-state has been reached are then used to calculate the Seebeck coefficient from the

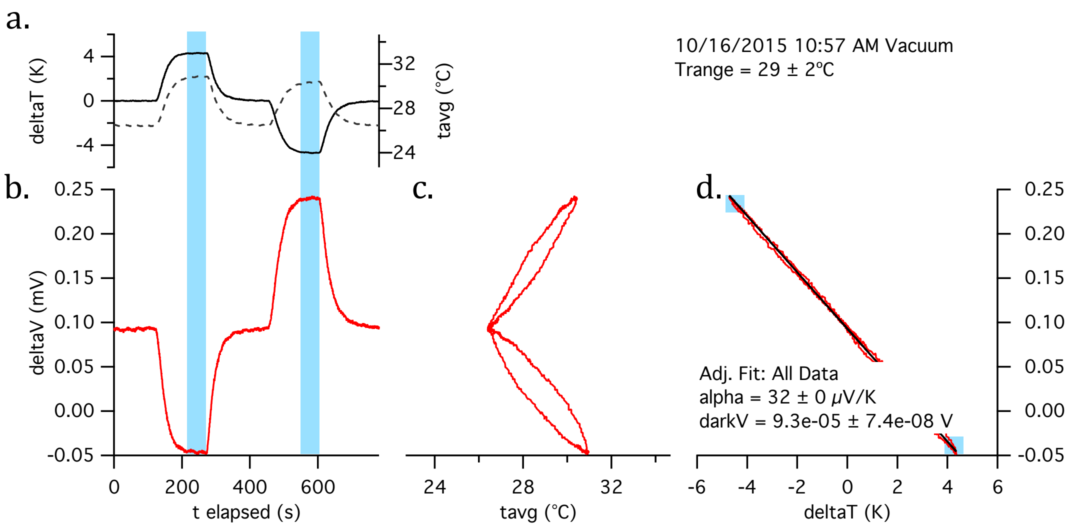

Figure 3.8: Representative data of Seebeck measurement taken under vacuum. This data is from the as-cast F_4TCNQ vapor-doped PBTTT-C_{14} sample presented in Chapter 4 . This run was taken near room temperature (29°C, 302 K), as indicated by the inset top-right text annotation which also includes the date/time stamp for the run. (a.) Solid curve is $\Delta T = T_2 - T_1$ (left axis), dashed curve is average of T_1 and T_2 (T_{avg}, right axis). (b.) Raw Seebeck voltage vs. time. (c.) Raw Seebeck voltage vs. T_{avg}. (d.) ΔV vs ΔT, with linear fit of data as the solid line. Inset text includes data run details (top) and fit results (bottom). Blue regions highlight where ΔT and ΔV are steady-state and the data points used for the linear fit used to calculate α.

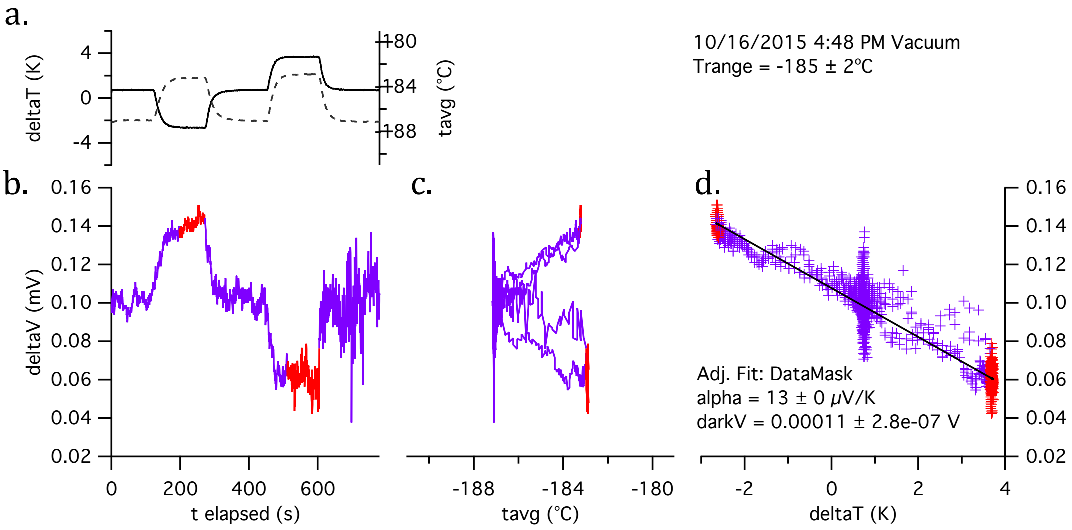

Figure 3.9: Representative data of Seebeck measurement taken under vacuum at low temperature. This data is from the same sample as in Fig. 3.8, the as-cast F_4TCNQ vapor-doped PBTTT-C_{14} sample presented in Chapter 4 , taken at -185°C (88 K). Noisy data is more likely at low temperature, and requires more careful analysis to extract meaningful Seebeck data from a signal with significant baseline noise. Red data points are those used to calculate the linear fit.

slope of a linear fit: $\alpha = -\Delta V/\Delta T$.

The LabView program has an enabled automatic procedure, with user inputs for the heater on/off times (See FIGURE). Unchecking the box labeled **Auto** enables the user to adjust the heaters manually, which is useful for measuring unusual behavior or testing new procedures. The smaller 'stop' button (**abort**) will abort the run without saving any data. The small 'ok' button (**Finished**) will abort the automated run before it is finished as well as save the existing run data, and will stop and save a manual run. The automatic run procedure was used to obtain the data in Figure 3.8, and is best explained in by looking at Figure 3.10.

1. t_0(s) **Acquire baseline - both heaters off** ($\Delta T = 0$)
2. t_{ON}(s) **Heater 1 ON** (40V, $\Delta T \approx -4$K)
3. t_{OFF}(s) **Heater 1 OFF** ($\Delta T = 0$)
4. t_{ON}(s) **Heater 2 ON** (40V, $\Delta T \approx +4$K)
5. t_{OFF}(s) **Heater 2 OFF** ($\Delta T = 0$)

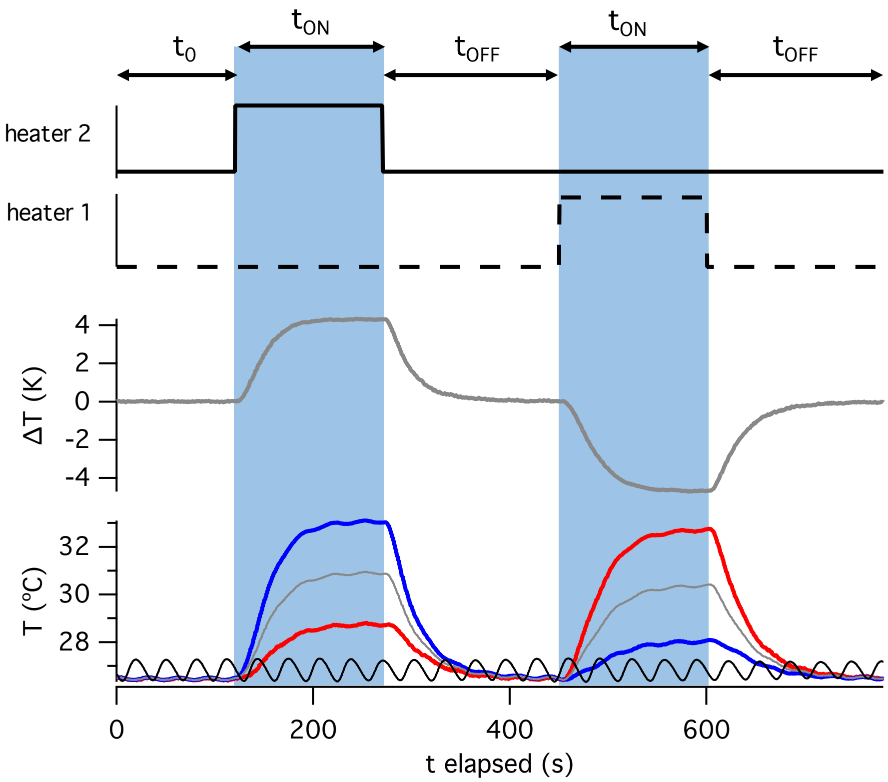

Figure 3.10: Automatic procedure available in .vi for measuring Seebeck coefficient in the variable-temperature vacuum probe station.

Chapter 4

Transport in Heterogeneous Polymers

Portions of this chapter are published in or adapted from the following authored and co-authored publications, with appropriate permissions:

[80] J. E. Cochran, M. J. N. Junk, **A. M. Glaudell**, P. L. Miller, J. S. Cowart, M. F. Toney, C. J. Hawker, B. F. Chmelka, and M. L. Chabinyc, Molecular Interactions and Ordering in Electrically Doped Polymers: Blends of PBTTT and F4TCNQ, *Macromolecules*, vol. 47, 68366846, Oct. 2014. *Adapted with Permission.* Copyright 2014 American Chemical Society

[35] **A. M. Glaudell**, J. E. Cochran, S. N. Patel, and M. L. Chabinyc, Impact of the Doping Method on Conductivity and Thermopower in Semiconducting Polythiophenes, *Advanced Energy Materials*, vol. 5, 1401072, Oct. 2015. *Adapted with Permission.* Copyright 2014 John Wiley and Sons

[95] S. N. Patel, **A. M. Glaudell**, D. Kiefer, and M. L. Chabinyc, Increasing the Thermoelectric Power Factor of a Semiconducting Polymer by Doping from the Vapor Phase, *ACS Macro Lett.*, vol. 5, 268272, Feb. 2016. *Adapted with Permission.* Copyright 2014 American Chemical Society

4.1 Introduction

The universal empirical relationship discussed in previous chapters $\alpha \propto \sigma^{-1/4}$ applies over a very large conductivity range. While much of the data lies within a decade of the trend in the context of the library of data points, individual sample sets can reveal steeper trends than the empirical law. For example, P3HT/F_4TCNQ with a P3HHT additive has a much steeper increase in power factor vs. conductivity than $PF \propto \sigma^{1/2}$, as shown in Figure 4.1, but overall under performs (but within error) the empirical prediction, and does so at very low electrical conductivity.[1] On the other hand, PEDOT-based materials, which are the current best-performing polymeric thermoelectric materials, are consistently higher performers than the empirical relationship would predict, also with a generally steeper PF vs. conductivity relationship, illustrated in Figure 4.2.[2–4] Much of the performance gains can be attributed to the ability to increase both electrical conductivity and Seebeck coefficient simultaneously with dopant, treatment, or processing. If we are to develop better thermoelectric materials, it would be judicious and efficient to understand the physical origins of the superior performance of PEDOT. An alternative is to deliberately try to break out from $\alpha \propto \sigma^{-1/2}$ in our well-studied PBTTT-F_4TCNQ system, ultimately aiming to be able to engineer a simultaneous increase in electrical conductivity and Seebeck coefficient.

Many previous works have speculated that the origin of the divergence of electronic and thermoelectric behavior from transport models at high carrier concentrations is due to a fundamental change in disruption of the electronic landscape. The electronic environment can be perturbed by disruption of the local structure, whether by altering the crystalline structure or by introduction of defects leading to electronic traps.[87,90,155–157] The structural-electronic perturbation competes with any increase in carrier concentration with doping, the results of which are difficult to predict. To rationally and sys-

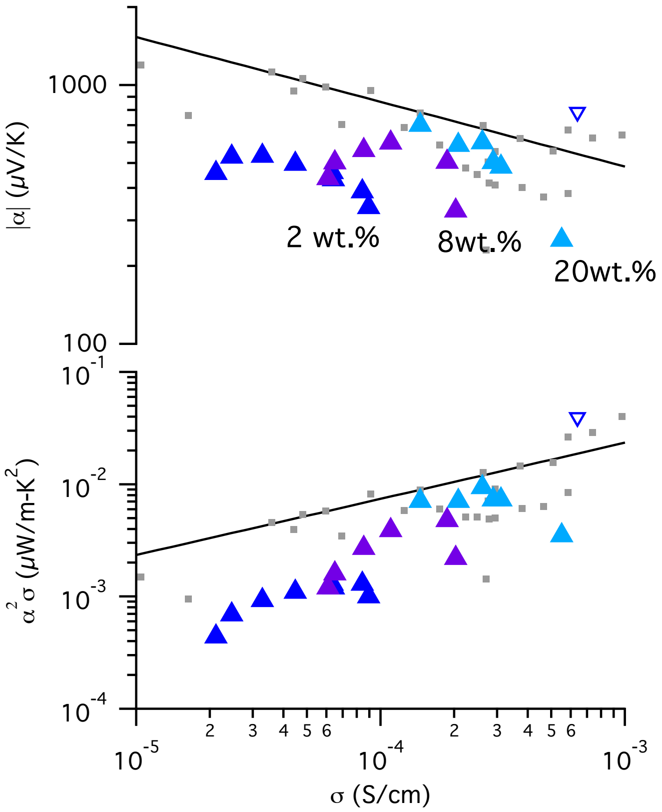

Figure 4.1: Thermoelectric properties of P3HT with increasing wt.%P3HHT as indicated, from [1]. As σ increases, α decreases more rapidly than the empirical trend (line) predicts.

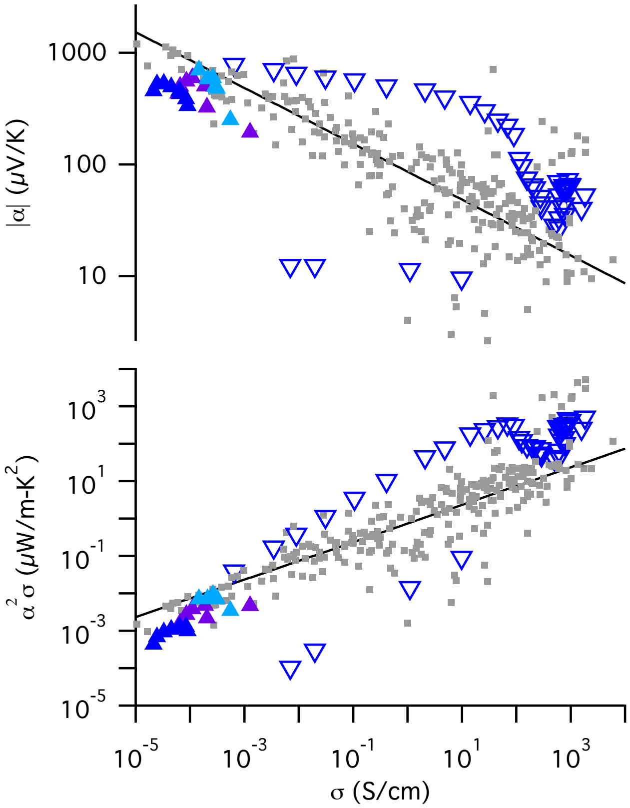

Figure 4.2: Thermoelectric properties of various PEDOT compounds vs. σ, showing consistent overperformance over the general trend.[2–4] While α decreases with σ, it does so at a much slower rate, even in the case of non-optimized samples.

tematically explore the effects of doping on charge transport, we will present electronic, thermoelectric, and structural results of PBTTT doped with F_4TCNQ , either via solution or from F_4TCNQ vapor.

Having reached the physical limit of doping PBTTT-C_{14} with F_4TCNQ by solution (10% by weight is approximately 1:4 F_4TCNQ:repeat unit of PBTTT-C_{14}) covered in and ref. [35], a new processing mechanism was tried in order to improve the electronic and thermoelectric properties. We previously found that by doping PBTTT after film casting, the PBTTT microstructure can be optimized prior to doping, without significant structural changes upon doping.[95] While that work concerned other dopants, (tridecafluoro-1,1,2,2-tetrahydrooctyl)trichlorosilane ($C_8H_4F_{13}SiCl_3$) (FTS) and 4-ethylbenzene sulfonic acid (EBSA), previous microstructural characterization of PBTTT doped with F_4TCNQ from solution suggests that introduction of F_4TCNQ itself would not significantly perturb the microstructure of the pristine cast film, which we in fact confirm.

Vapor doping of PBTTT-C_{14} with F_4TCNQ also enables full saturation of the thin film with F_4TCNQ, to the solubility limit of F_4TCNQ. Full saturation occurs after a relatively short amount of time, and is highly stable over time when kept under N_2. Figure 4.3 demonstrates the effects of vapor doping. After 5 minutes of F_4TCNQ exposure on 20 nm of PBTTT, most of the film turned highly transparent. This is attributed to possible increased thickness at the edges of the film, but is more likely due to the sample chamber. Shortly after exposure, the electrical conductivity σ was measured, $\sigma = 220$ S/cm. After one month stored under N_2, the rest of the film has turned transparent, and the conductivity has not changed ($\sigma = 212$ S/cm). The completion of film bleaching suggests that the F_4TCNQ can diffuse over time, homogenizing the local density of F_4TCNQ molecules across the film. The fact that the electrical conductivity stays the same over a month later and diffusion of F_4TCNQ strongly supports the assumption that vapor doping easily allows full saturation of the PBTTT thin film with F_4TCNQ.

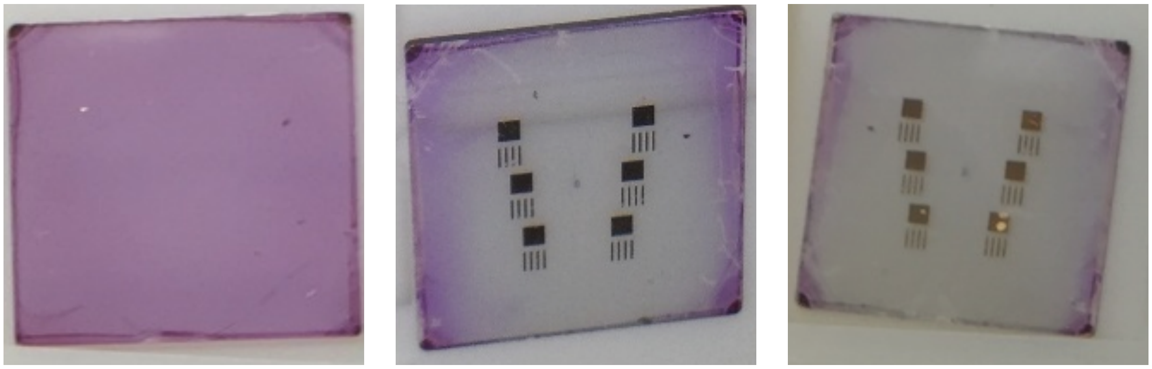

Pristine PBTTT, ~20 nm

PBTTT−F_4TCNQ, Day 1
(5 min. exposure)
σ = 220 S/cm

PBTTT−F_4TCNQ, 1 mo. later
(5 min. exposure)
σ = 212 S/cm

Figure 4.3: Images of PBTTT before and after F_4TCNQ vapor. After 5 min. of exposure to F_4TCNQ the film is almost entirely transparent. One month later it is completely transparent, with no significant reduction in σ.

Additionally, films exposed to F_4TCNQ vapor beyond 10 minutes began to show crystallized F_4TCNQ on the surface of the film, as evidenced by a slight yellow cast of residual F_4TCNQ on the otherwise transparent film. UV-vis-NIR spectroscopy also shows the presence of a peak around 400nm seen in Figure 4.4, which we attribute to unionized F_4TCNQ in excess on the surface of the film. The feature around 800nm correlates to the charge transfer state between PBTTT and F_4TCNQ, and overall the vapor doped film is in good agreement with previous results on heavily solution doped PBTTT.[80]

We can also assume that the 10wt.% (25 mol.%, or 1 F_4TCNQ for every 4 PBTTT repeat unit) is at the solubility limit of F_4TCNQ . This gives us a nice sample set with similar doping levels, and the only thing that can be reasonably assumed to be changing between the solution-doped sample and the vapor-doped samples is morphology/microstructure.

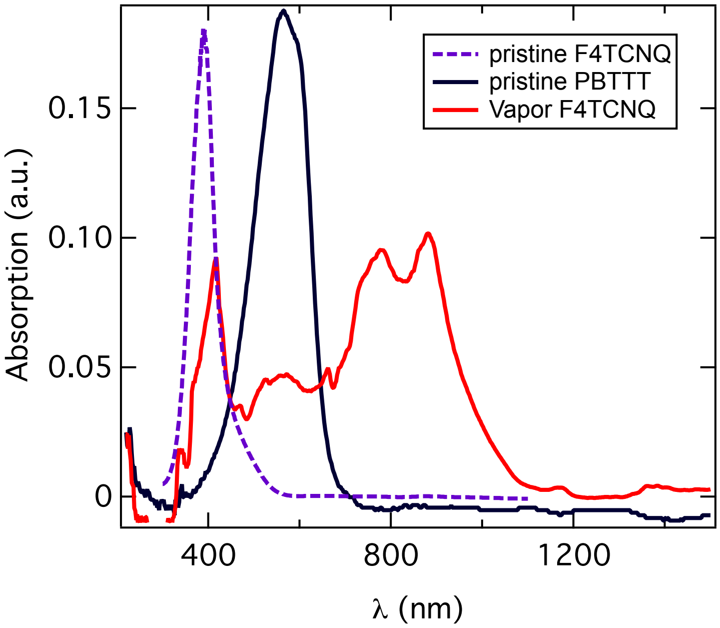

Figure 4.4: UV-vis-NIR spectroscopy of F_4TCNQ vapor-doped PBTTT (red) compared to pristine PBTTT (black) and F_4TCNQ (purple dashed). Pristine and vapor–doped PBTTT samples were measured by Kelly Peterson and Dr. Shrayesh Patel, Chabinyc Group. Pristine F_4TCNQ spectra was reported in [80].

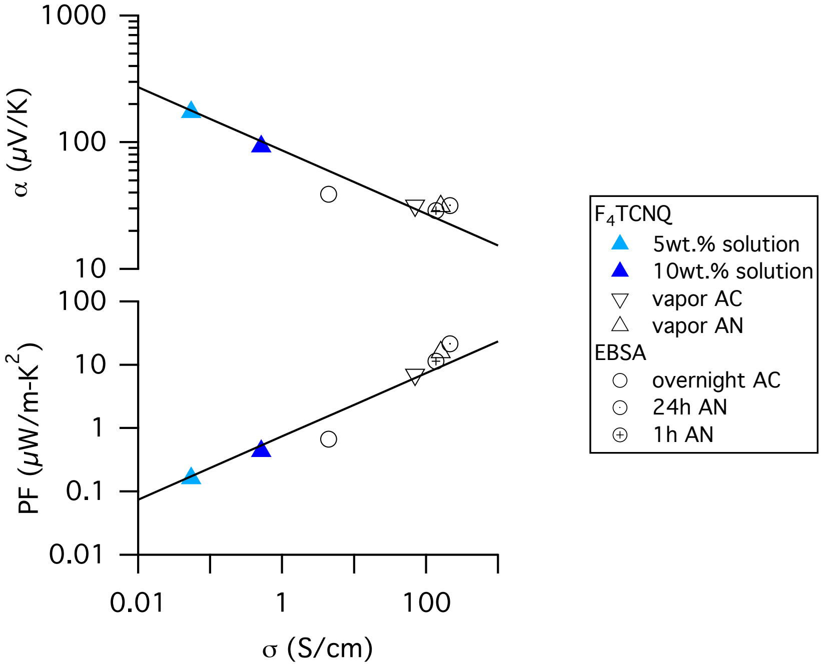

Figure 4.5: Seebeck coefficient α and power factor PF vs. electrical conductivity σ at room temperature ($\sim$ 300K) for PBTTT-C_{14} doped with F_4TCNQ (solution or vapor) or EBSA (immersion). Solid line is empirical relationship $\alpha = (k_B/e)(\sigma/\sigma_\alpha)^{-1/4}$ and corresponding $PF \propto \sigma^{1/2}$.

4.2 Controlling transport pathway independent of doping

Grazing Incidence Wide Angle X-Ray Spectroscopy (GIWAXS) of thin films can access length scales on the order of Angstroms ($<$ 10nm). The crystalline regions of PBTTT-C_{14} are accessible at this length scale, so we can get an idea of the extent of change in the local order upon doping. PBTTT-C_{14} is highly textured in the z-direction, sitting edge-on to the substrate as schematically illustrated in Figure 4.6. Diffraction for neat PBTTT, F_4TCNQ solution-doped (10wt.%) PBTTT, and F_4TCNQ vapor-doped PBTTT is shown in Figure 4.7. Three orders of alkyl stacking peaks can be seen along q_z, corresponding to a primary alkyl stacking distance of $d_{100} = 21.4$ Å for neat PBTTT. The π-π spacing is calculated from the outer peak on q_{xy}, where $d_{\pi\text{-}\pi} = 3.65$ Å, which is in good agreement with literature values.[80] By eye, there appears to be minimal change in the alkyl and π-π distances between neat PBTTT and either of the doped samples. Calculation of peak shift confirms minimal change, with $\sim$ 1 Å expansion of alkyl stacking upon doping, and $<$ 0.2Å contraction of the π-π spacing, as noted in Figure 4.7.

Resonant Soft X-ray Scattering (RSoXS) of thin films can probe correlations on the order of $\sim$100 nm. By using a polarized beam, we can also get information on domain orientation, as described in [158]. Domain spacing d can be extracted from peak q values (spacing $d = 2\pi/q$). We can also quantify domain spacing with oriented correlation length (OCL), where OCL= $d/2$.

To determine the effect of annealing on long-range order of undoped (neat) PBTTT-C_{14}, the domain spacing was determined for various annealing temperatures (as cast, 80°C, 150°C, and 180°C), shown in Figure 4.8. "As cast" films in Figure 4.8 were not heated in any way after casting. It is common to refer to samples as "as cast" while still subjecting them to a "soft" anneal of 80°C to remove residual solvent, under the

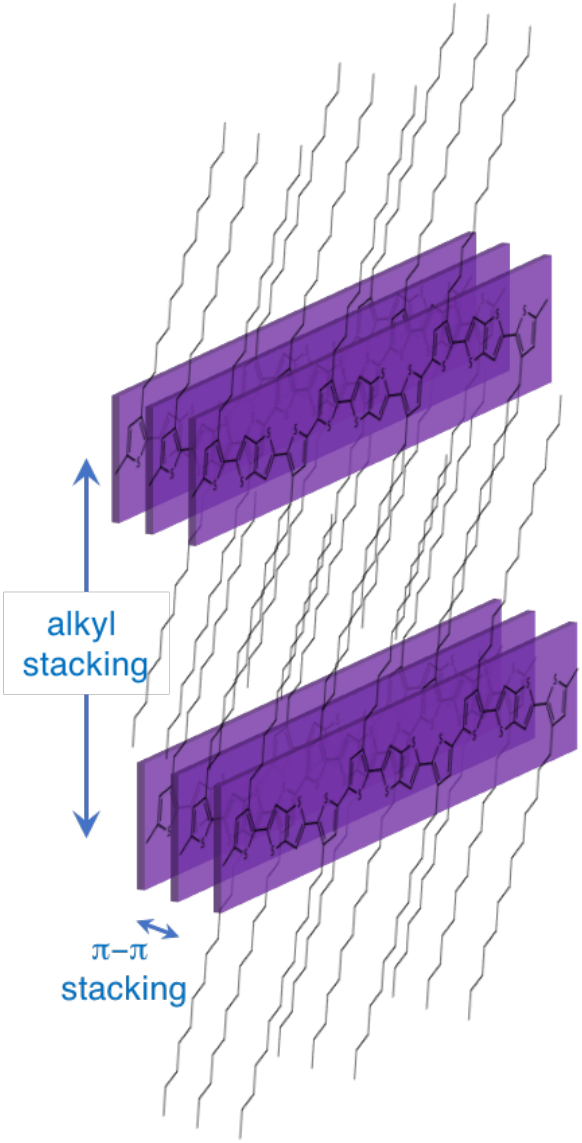

Figure 4.6: Anisotropy of PBTTT-C_{14}. PBTTT-C_{14} are dominantly edge-on such that alkyl stacking is in the $\hat{z}$ direction.

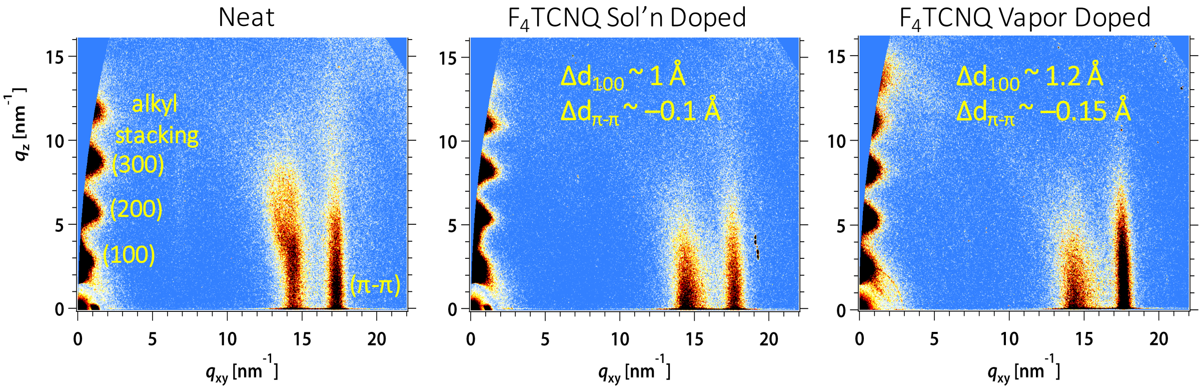

Figure 4.7: GIWAX of (left) neat PBTTT-C_{14}, (center) F_4TCNQ solution-doped PBTTT-C_{14}, and (right) F_4TCNQ vapor-doped PBTTT-C_{14}. Diffraction and analysis was done by Dr. Shrayesh Patel in the Chabinyc Group at Stanford Synchrotron Radiation Laboratory, Beamline 11-3.

assumption that the morphology does not change at that low of a temperature over a short period of time (10-30 minutes). We can see that the the scattering for as cast and 80°C sample peak at nearly the same q, corresponding to $d \sim 100$ nm (OCL= 50 nm), validating this assumption. It is known that F_4TCNQ is relatively stable in PBTTT-C_{14} up to annealing temperatures of 150°C for solution doped samples. Finally, the first transition temperature of PBTTT is around 180°C, so we expect a difference in the OCL from as cast to samples annealed at 180°C. Indeed, we see that the correlation length nearly quadruples from 50 nm upon annealing at 180°C, and conclude that annealing temperature affects the final long-range correlation in neat PBTTT.

To compare the effect of doping method on long-range correlations, the domain spacing was measured for F_4TCNQ-saturated PBTTT-C_{14} , either solution-doped at 10wt.% prior to casting, or from the vapor phase onto neat PBTTT, shown in Figure 4.9. For this survey, two films of neat PBTTT were annealed at 180°C. One film was measured neat, and the other was subject to F_4TCNQ vapor for 10 minutes. The solution-doped sample was annealed at 150°C after casting from a 10wt.% F_4TCNQ solution. The vapor doped sample has a slightly larger OCL than neat PBTTT ($\sim$ 215 vs. 190 nm), suggesting that the domain correlation is relatively unchanged, if not slightly improved, when doped via F_4TCNQ vapor. On the other hand, solution-doping of PBTTT clearly limits the domain correlation to OCL $\sim$ 40nm, which is on par with as cast PBTTT shown previously.

A reasonable explanation for the limited OCL when doping via solution is that the polymer-dopant interaction locks in the microstructure upon casting (or prior, in solution). F_4TCNQ is relatively stable in PBTTT upon annealing at 150°C, despite being a highly volatile small molecule.[35, 80, 159] We also know that the charge-transfer reaction between PBTTT and F_4TCNQ begins in solution prior to any film processing.,[80] indicating a strong polymer-dopant interaction. Owing to this stability, annealing at 150°C does not appear to enable the correlation lengths seen in neat PBTTT annealed at the same tempearature (Fig. 4.8).

Comparing to the vapor-doped case, the dopant is introduced after an optimal microstructure is established, and F_4TCNQ is able to diffuse from the surface into the film for (macroscopically) homogenous doping. The fact that F_4TCNQ is able to successfully infiltrate through the thin film over the doping period also supports our assertion that the 10wt.% (1:4 ratio) sample and the vapor doped sample have the same amount of F_4TCNQ within them, and differ only in long-range correlation length.

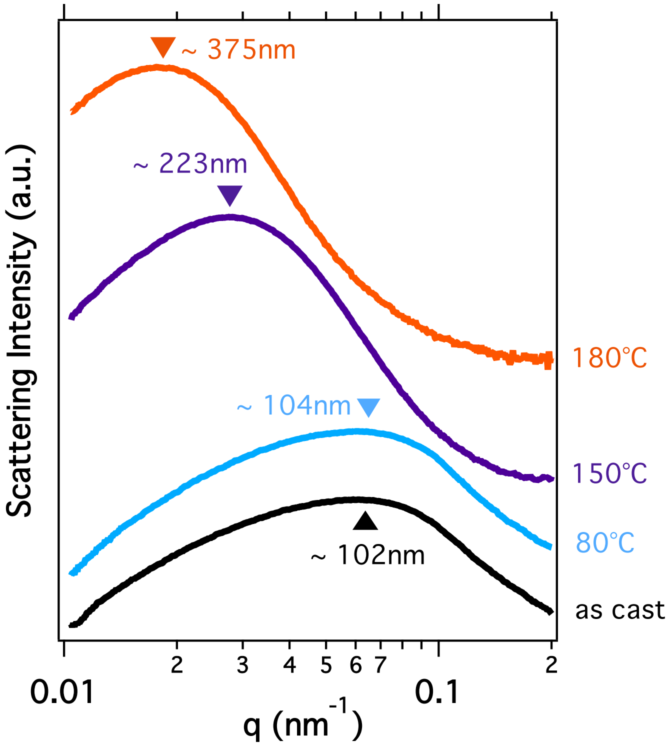

Figure 4.8: RSoX of neat PBTTT-C_{14} vs. annealing temperatures of 80°C (”soft” anneal), 150°C, and 180°C. Spacing ($2\pi/q$) is indicated for each annealing temperature. Each sample was annealed for 10 minutes. Diffraction and analysis was done by Dr. Shrayesh Patel in the Chabinyc Group at the Advanced Light Source at Lawrence Berkeley National Laboratory, Beamline 11.0.1.

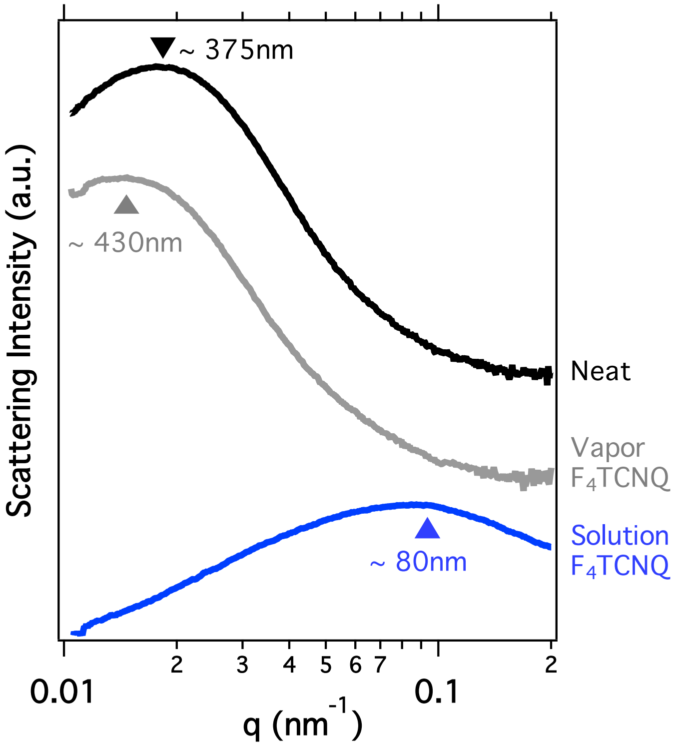

Figure 4.9: RSoX of annealed PBTTT vs. F_4TCNQ doping method, either from the vapor phase or from 10wt.% solution. Spacing $(2\pi/q)$ is indicated for each curve. Neat and vapor doped samples were annealed (prior to doping) at 180°C, solution-doped sample was annealed at 150°C. Diffraction and analysis was done by Dr. Shrayesh Patel in the Chabinyc Group at Advanced Light Source at Lawrence Berkeley National Laboratory, Beamline 11.0.1.

4.3 Temperature dependence of electrical conductivity

The $\sigma(T)$ data for each sample was initially fit to the standard Mott transport equation below, where σ_0 the characteristic conductivity, T_0 is the characteristic temperature related to the activation energy $E_A = T_0 k_B$, and γ is and given by the dimensionality d of variable range hopping (3, 2, or 1-D) such that $\gamma = 1/(d+1)$, or $\gamma = 1$ for thermally-assisted nearest-neighbor hopping. Each of these parameters will be discussed in depth in this section.

$$\sigma = \sigma_0 \exp\left[-\left(\frac{T_0}{T}\right)^{\gamma}\right] \tag{4.1}$$

To find the best reasonable fit of γ, each data set was fit for the possible γ values ($\gamma = {}^1\!/\!_4, {}^1\!/\!_3, {}^1\!/\!_2, 1$) with σ_0 and T_0 as free parameters. The curve was additionally fit freely (free parameters: σ_0, T_0, and γ) as confirmation. For many of the $\sigma(T)$ data sets, multiple γ values yielded an acceptable fit. To narrow down to an appropriate single γ value, the free fit was taken into account, and σ_0 and T_0 must also be physically based on their interpretation within a given transport model. Figure 4.10 shows the best fit curve to each of the $\sigma(T)$ data sets. Table 4.1 summarize the fit parameters for the best-fit γ, as well as the free γ fits. The 5wt.% doped sample fits well to $\gamma = 1$, and the 10wt.% sample lies in-between $\gamma = {}^1\!/\!_2$ and 1. The vapor-doped samples all exhibit a $\gamma = {}^1\!/\!_2$ dependence. It is essential to note that $\gamma = {}^1\!/\!_2$ seen here is not uniquely attributable to a single transport mechanism, and we will evaluate the validity of a few transport mechanisms that yield this dependence.

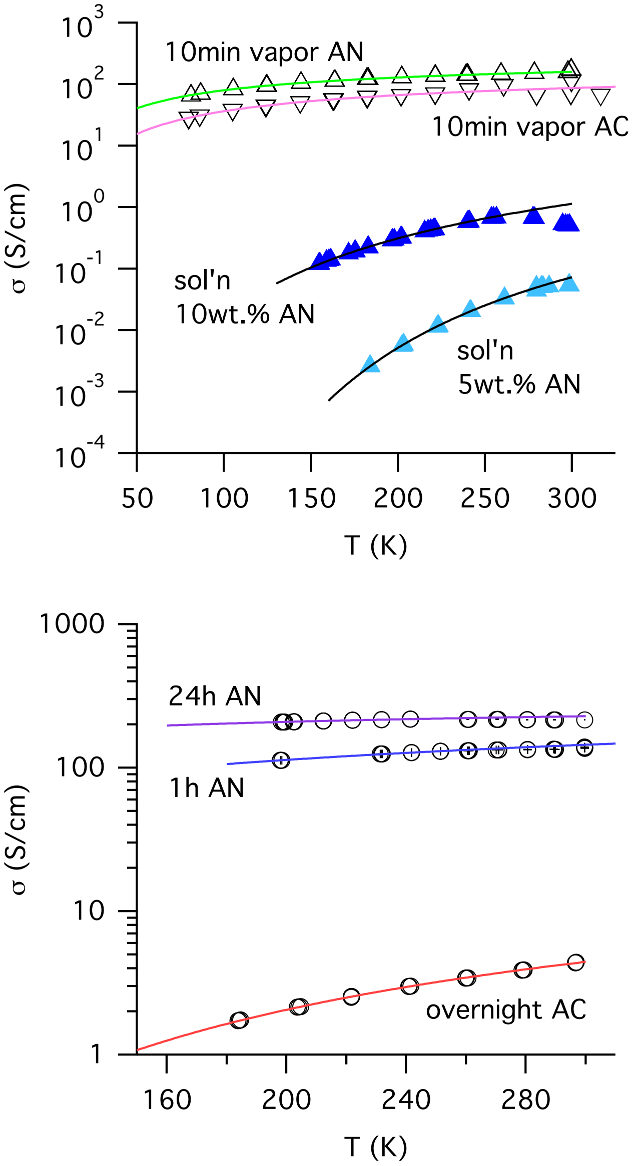

Figure 4.10: $\sigma(T)$ data and best fits for F_4TCNQ-doped (top) and EBSA-doped (bottom) PBTTT.

Table 4.1: Best fits to Mott Eqn.4.1 for F_4TCNQ-doped PBTTT. The parameters shown for each sample are extracted from the best fit(s) for that sample with $\gamma = 1, 1/2, 1/3, 1/4$. The completely free fit for each sample, where γ, σ_0, and T_0 were all free variables, is also shown (in grey italics).

Sample	γ	σ_0	σ**(300K)** (S/cm)		T_0	E_A	**a$_0$**		
Condition		(S/cm)	data	from fit	(K)	(eV)	(Å)	(# RU)	(# thio.)
from solution									
5 wt.%	1	14	0.05	0.07	1587	0.137	101	7.5	25.9
	0.955	*20*		*0.07*	*1821*	*0.157*	*74*	*5.5*	*19.0*
10 wt.%	1	235	0.5	2.2	1396	0.120	6	0.4	1.5
	1/2	362		1.13	9968	0.859	4	0.3	1
	0.642	*77*		*1.1*	*2849*	*0.246*	*19*	*1.4*	*4.9*
from vapor									
AC	1/2	284	70	87	423	0.036	5	0.4	1.3
	0.490	*295*		*87*	*452*	*0.039*	*5*	*0.4*	*1.3*
AN	1/2	408	160	160	267	0.023	4	0.4	1.0
	0.594	*335*		*158*	*185*	*0.016*	*4*	*0.4*	*1.0*

Table 4.2: Best fits of $\alpha(T)$ to different transport models for F_4TCNQ doped PBTTT

Sample Condition	**Mobility Edge** $\alpha(T) \propto T^{-1}$		**Linear** $\alpha(T) \propto T$		**VRH** $\alpha(T) \propto T^{-1}$	
	$E_F - E_V$	A	$\alpha(0K)$	$\left.\frac{d \ln N(E)}{dE}\right\vert_{E_F}$	$\alpha(0K)$	$\left.\frac{d \ln N(E)}{dE}\right\vert_{E_F}$ (eV^{-1})
	(eV)		(μV/K)	(eV^{-1})	(μV/K)	$T_0(\gamma = 1/2)$	$T_0(\gamma = 1/4)$
from solution							
5wt.%	-0.022	2.8	55	52	-38	19	0.6
			0	81	0	15	0.5
10wt.%	-0.012	1.5	23	30	-29	19	0.9
			0	81	0	15	0.6
from vapor							
AC	-0.003	0.4	6	12	-11	32	4.6
			0	16	0	22	3.2
AN	-0.002	0.4	6	12	-8	38	7.4
			0	15	0	28	5.5

4.3.1 Mobility-Edge Transport: $\gamma = 1$

The mobility-edge (ME) transport model is commonly used to explain transport in polymeric systems that exhibit thermally-activated hopping, such that $\gamma = 1$ in Eqn. 4.1. The "mobility edge" of the ME transport model is an energy separating localized from extended states, with transport occurring as carriers are thermally excited out of the localized states into the extended states. In the context of the semicrystalline microstructure of PBTTT and other high-mobility polymers, the extended states are associated with the ordered regions while the localized states are within the surrounding disordered barrier regions.[160] The solution-doped samples do exhibit thermally-activated hopping, with the 5wt.% sample showing a very strong $\gamma = 1$ dependence, and with the 10wt.% sample having $1/2 \leq \gamma \leq 1$. To evaluate the validity of the mobility-edge hopping as an appropriate charge transport model in these two cases, we look at what meaningful parameters can be extracted from σ_0 and T_0 in Equation 4.1.

The temperature dependence of the conductivity σ has been derived by others considering transport before (localized states, "above" for hole transport) and beyond (extended states, "below" for hole transport) the mobility edge.[161] For carriers excited from localized to extended states at E_V, the conductivity is given by $\sigma = \sigma_0 \exp(-E_A/k_BT)$, where the activation energy to extended states is $E_A = E_F - E_V$, giving $T_0 = E_A/k_B$ from Eqn. 4.1. For carriers excited *into* localized states with hopping transport near the band edge E_B, $\sigma = \sigma_1 \exp[-(E_A + w_1)/k_BT]$, where w_1 is the activation energy for hopping between localized states. The hopping energy w_1 is expected to weakly decrease with temperature but is considered negligible to E_A. Some discussions of the mobility-edge model in polymers restrict transport to carriers in localized states that temporarily become mobile after excitation into extended states, thus assuming that the localized tail states have zero effective mobility $\mu_L = 0$ and there is no transport between localized states. It is usually assumed that σ_1 described above is orders of magnitude smaller than σ_0 with an exponential band tail.

In the Mott model, the parameter σ_0 is in one approximation is given by $\sigma_0 = Ce^2/\hbar a$, where a is the distance between localized states, and the constant C is generally between 0.025 and 0.1.[161] Assuming a coordination number $z = 6$ with the presence of vertical disorder, $C = 0.026$, yielding $\sigma_0 \sim 150$ S/cm for $a = 4$Å.[161] In the simpler case of no vertical disorder and coordination number z, $C = 0.06(6/z)^2$, with $\sigma_0 \sim 360$ S/cm for $a = 4$Å.[123] Considering the anisotropic microstructure of PBTTT, we might reasonably estimate that there is some degree of lateral disorder, and approximate the coordination number of 4, given no coordination on the alkyl-stacking direction, and reasonable coordination along the chain and in the $\pi - \pi$ direction. This results in $C \sim 0.026(6/4)^2 = 0.06$, resulting in a similar value as the simplest case, $\sigma_0 \sim 350$ S/cm for $a = 4$Å. It is not expected that this definition of σ_0 is particularly exact, but it does provide a sense of the order of magnitude. The distance between localized states is reasonably bound by the molecular structure of PBTTT: a cannot be less than the span of a single thiophene or approximately $1/4$ of a repeat unit (RU) ($a \geq\sim 4$Å), nor can it be larger than the maximum conjugated polymer length, assumed from the molecular weight M_n(PBTTT-C_{14}) = 24000 ($a \leq 46$nm, 34RU). this gives approximate restrictions on σ_0 as the minimum metallic conductivity: $6 \leq \sigma_0 \leq 700$ S/cm. From Table 4.1, it is clear that all of our samples fall within this restriction, indicating that Mott-type hopping is not ruled out by the parameters themselves.

4.3.2 Mott Variable-Range Hopping: $1/4 \leq \gamma \leq 1/2$

The Mott model for variable range hopping has been used to explain transport in inorganic and polymeric systems where $\sigma(T) \propto \exp(-1/T^\gamma)$, where γ is given by the dimensionality ($d = 1, 2,$ or 3): $\gamma = 1/(d+1)$, such that $\gamma = {}^1\!/\!_4, {}^1\!/\!_3, {}^1\!/\!_2$.[123] For variable range hopping, T_0 is the Mott parameter: $T_{Mott} = 18/k_B L_C^3 N(E_F)$, where L_C is the localization length, and $N(E_F)$ is the number density of states (DOS) at the Fermi level. In general, variable range hopping is appropriate when $T_0/T >> 1$. If we assume strictly Mott VRH for the highly-doped samples, $\gamma = {}^1\!/\!_2$ suggests 1D variable range hopping, which doesn't seem the most appropriate given the multidimensionality of transport in PBTTT. Pure 1D VRH would suggest that transport only occurs along the chain, when in fact $\pi - \pi$ transport can be significant. This will be addressed later in the discussion of quasi-1D VRH. In the Mott model, no direct relationship exists between σ_0 and T_0. However, the inverse correlation present in the experimental results (see Figure **??**) is not surprising in the context of variable range hopping, because a high DOS at the Fermi level would give high room-temperature conductivity (large σ_0) and a small Mott parameter.

4.3.3 Efros-Shklovskii Variable Range Hopping: $\gamma = {}^1\!/\!_2$

Efros-Shklovskii variable range hopping (ES VRH) also yields a $\gamma = {}^1\!/\!_2$ dependence for conductivity, and has been explored in the context of similar polymer systems, including polypyrrole, polyaniline, and polythiophenes.[40,90] ES hopping is a modification of Mott variable range hopping, but also considers the Coulomb interaction between the hole and electron left behind, leading to a depletion in the DOS around the Fermi energy.[162,163] The parameter T_0 for ES hopping has a different form than traditional Mott hopping: $T_{ES} = 2.8e^2/\kappa k_B L_C$, where κ is the dielectric constant and L_C is again the localization length. It has also been employed with an anisotropic wavefunction to reproduce an experimental correlation between σ_0 and T_0, or between σ(300K) and T_0 for a compilation of polyacetylene samples.[164]

To assess the validity of ES hopping for the systems studied here, we will compare our data to literature treatments of P3HT with ES hopping. Wang et al. using ionic-liquid gated transistor geometry to study transport in P3HT at carrier densities up to very high hole densities ~ 0.2 holes/monomer.[90] The temperature-dependent resistivity $(\rho(T) = 1/\sigma(T))$ was measured at at gate voltages $V_G = -0.3V to -1.0V$, corresponding a hole density range $p \sim 10^{20}$ to 10^{21}cm^{-3}. Temperature-dependent conductivity exhibited $\gamma = 1/2$ at lower hole densities, and at low temperatures for higher hole densities. For high doping loads, $\gamma = 1/4$ was observed above a crossover temperature $T_X < 25$K and decreasing with increasing doping, corresponding to $T_X = 16T_{ES}^2/T_{Mott}$. T_{ES} was extracted from $\sigma(T)$ measurements, while L_C was able to be calculated from magnetoresistance measurements. The dielectric constant was then calculated from the T_{ES} definition using these two parameters. In summary, they found that ES VRH was an appropriate model for transport in electrochemically gated P3HT, when the induced charge density was less than where $T_{ES} > 400$K, localization length L_C <100Å, and relative dielectric constant $\kappa < 10$. We can compare these findings to the samples of ours that exhibited $\gamma = 1/2$ dependence. $T_0 > 400$K for 10wt.% solution-doped, and just barely so for the as-cast vapor doped sample, while $T_0 = 267$ for the annealed sample.

Samples doped to saturation with F$_4$TCNQ (10wt.% and vapor-doped) can be assumed to have a similar DOS with the crystallites given that the local structure does not change dramatically between the two doping methods. Thus, $N(E_F)$ can be reasonably assumed to be the same in each sample. With this restriction, we can estimate a relative localization length L_C from $T_0 = T_{Mott}$. Using T_0 extracted with $\gamma = 1/2$ (listed in Table 4.1), the localization length L_C is $\sim 3.3\times$ larger for the vapor-doped annealed sample than the 10wt.% sample. The ratio of correlation lengths in RSOX shows OCL(vapor) as $\sim 6\times$ OCL(10wt.%). On the other hand, if we arbitrarily decide that ES VRH is a more appropriate description of charge transport such that $T_0 = T_{ES}$ for $\gamma = 1/2$, L_C(vapor) is up to $\sim 40\times$ larger than in solution doping assuming κ is similar for the two cases.

4.3.4 Quasi-1D Variable Range Hopping & Percolation Effects

Quasi-1D variable range hopping has been used to explain $\sigma \propto \exp(-\sqrt{T})$ dependence in highly conducting polymers such as polyaniline (PANI) and PEDOT:PSS.[88, 89, 165] Going back to the original Mott hopping equation $\gamma = {}^{1}\!/_{2}$ implies 1D variable range hopping. While the nature of a single polymer chain is 1-dimensional (intrachain or parallel conduction), interchain coupling and crystallinity can increase the dimensionality of the system. In the most general terms, a quasi-1D disordered system (DS) consists of N 1-dimensional chains bundled parallel to each other and coupled, and the 1D chains may have a certain degree of energetic or structural disorder.[166] This simple definition highly resembles the microstructure of the crystalline regions of our polymer system and is worth taking a look at. For a general picture of 1D chains, in the weak coupling limit, the electronic states remain localized in 1D due to chain disorder. However, when coupling approaches the scattering rate due to chain disorder, the electronic states can become 3-dimensional in general, but may retain a degree of chain-direction anisotropy. Basically, if the rate that a carrier can jump to another chain is on the order of or larger than the rate a carrier encounters chain disorder, the carrier can jump before it is scattered and becomes delocalized.

The electronic conduction between chains $\sigma_\perp$ for weak interchain coupling in quasi-1D VRH is given by:[165]

$$\sigma_\perp = \sigma_0 \exp\left[-\left(\frac{T_0}{T}\right)^{\gamma}\right] \tag{4.2}$$

T_0 is **not** T_{Mott} in this case, but is defined as $T_0 = 16/k_B L_\parallel N(E_F) z$, where $L_\parallel$ is the localization length along the chain and z is the number of nearest-neighbor chains. Hopping along the chain is thermally-activated nearest neighbor hopping $\sigma_\parallel(T) \propto \exp(-1/T)$. It is noted that in this model, exclusively in-chain hopping is more difficult than interchain hopping at the largest potential scattering sites, the macroscopic $\sigma_\parallel$ (i.e. conductivity measured along the bundle of chains) is expected to have interchain temperature dependence $\sigma_{\parallel}(T) \propto \exp[-(T_0/T)^{1/2}]$.

To link the quasi-1D VRH theoretical treatment of 1D chain bundles with the PBTTT microstructure, we can equate the some of the disorder in the 1D chain to breaks in conjugation. The breaks in conjugation can be due to chain perturbations or ends, or simply associated with the persistence length of the polymer in the solid, where chain bends define domain boundaries or similar. This somewhat rectifies the theoretical treatment with the stiff chain picture of the polymeric bundles. However, our PBTTT thin films are deposited without alignment, and are not strained to induce long-range alignment. Macroscopically our PBTTT thin films are isotropic, with randomly oriented crystallites in-plane, and highly textured out-of-plane, so the picture of quasi-1D disordered system is not sufficient to explain macroscopic electronic conductivity. Recently, the temperature-dependent properties of PEDOT:PSS were evaluated in the context of a percolating network of filamentary structures, which more closely resemble the anisotropic quasi-1D DS discussed above.[89] It is suggested that the conductivity is dominated by the filaments and not limited by the filament connections. As mentioned previously, percolative transport also yields $\gamma = 1/2$ temperature dependence.[167] The cartoon model of PBTTT morphology has crystalline regions linked to each other via tie-chains of polymer, traversing the disordered non-crystalline barrier regions. These tie-chains complete a more direct percolation path between crystallites and can be considered analogous to the filamentary structures. Hypothetically if there were no tie-chains connecting the ordered regions to each other, transport might be better compared to inter-cluster hopping, where metallic islands are separated by an insulating matrix. Coincidentally, inter-cluster hopping also yields $\gamma = 1/2$ temperature dependence of conductivity.

4.4 Temperature dependence of the thermopower

The Seebeck coefficient is related directly to the conductivity denisty of states via the following relation for an arbitrary density of states:[102]

$$\alpha = -\frac{k_B}{e}\int \frac{E - E_F}{k_B T}\frac{\sigma(E)}{\sigma}dE \tag{4.3}$$

The entropy a carrier contributes to the thermopower is proportional to its' contribution to conduction as $\sigma(E)/\sigma$. The conductivity DOS $\sigma(E)$ takes different forms depending on the transport mechanism, but has a general form $\sigma(E) = eg(E)\mu(E)f(E)[1 - f(E)]$. This relation takes different forms depending on the transport mechanism, and the final $\alpha(T)$ has been derived previously for various hopping mechanisms, which will be discussed below. Figure 4.11 shows the temperature-dependent thermopower data plotted vs $T^{-1}, T^{1/2}$ and T.

For thermally-activated hopping / mobility-edge transport ($\sigma \propto \exp(-1/T)$), the Seebeck coefficient is inversely proportional to temperature:[102]

$$\alpha = \frac{k_B}{e}\left[\frac{E_F - E_V}{k_B T} + A\right] \tag{4.4}$$

A is the scattering paramter and generally between 2 and 4, and is weakly temperature dependent. Notice that for hole transport, $\alpha > 0$, so $\alpha(T)$ should decrease with increasing temperature given that $E_F > E_V$ for p-type semiconductors. Clearly, we can see this is not the case for the strongly thermally-activated ($\sigma \propto \exp(-1/T)$) 5wt.% sample, or any of the samples studied here, indicating that at the very least, the dominant transport mechanism in not mobility-edge like.

For d-dimensional variable-range hopping ($\gamma = 1/(d + 1)$), the thermopower is given

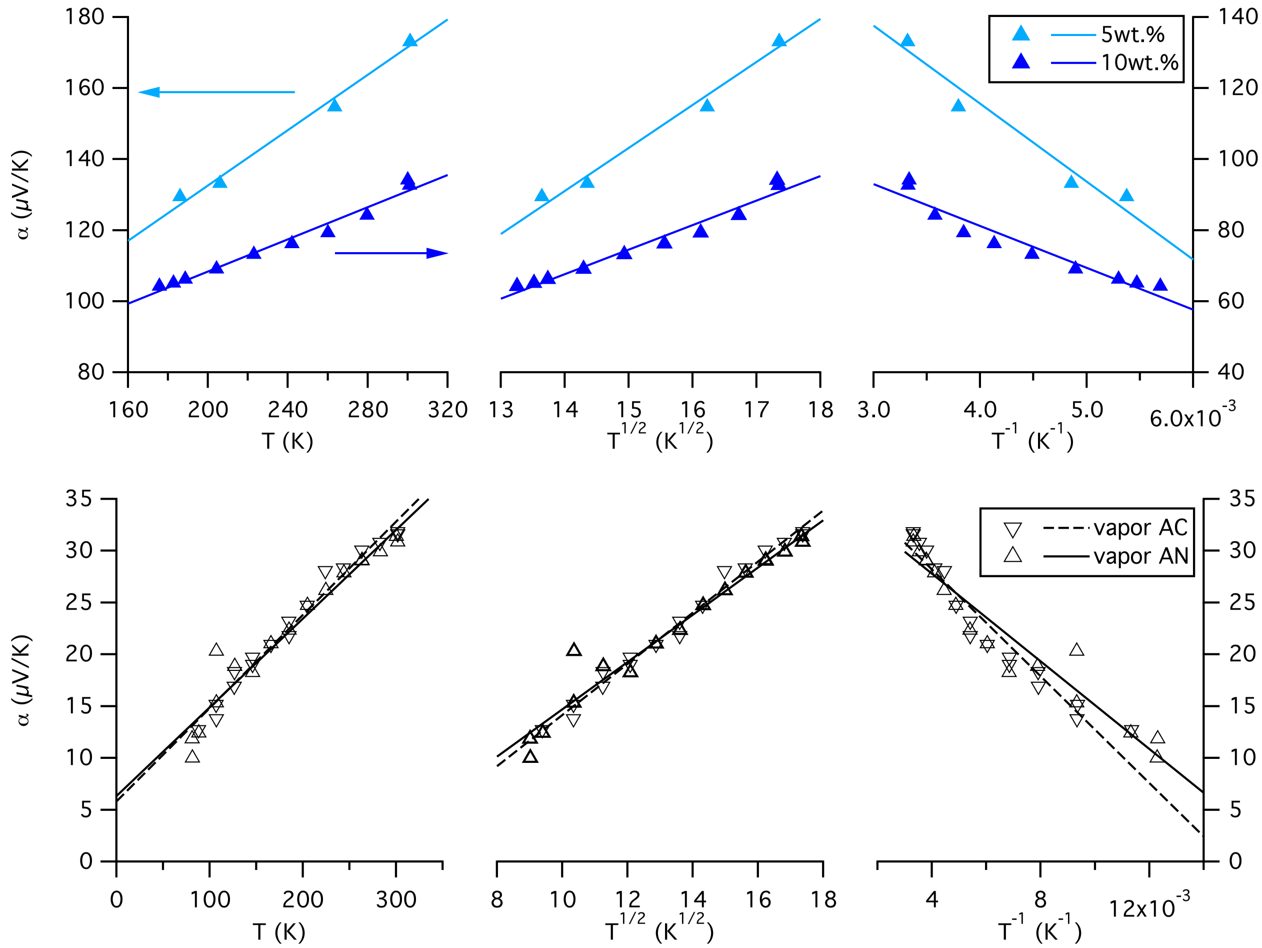

Figure 4.11: Temperature-dependent thermopower data for F_4TCNQ solution-doped (top) and vapor-doped (bottom) PBTTT, plotted vs. T, $T^{1/2}$, and T^{-1}. Linear fits to α vs each temperature dependence are also shown ($\alpha(0K) = 0$ fits shown as grey lines).

by the following:

$$\alpha_{hop}(T) = \frac{1}{2}\frac{k_B}{e}\left(\frac{\Delta_{hop}^2}{k_B T}\right)\frac{d\ln N(E)}{dE}\bigg|_{E_F} \tag{4.5}$$

where Δ_{hop} is the mean hopping energy, $\Delta_{hop} \propto (k_B T)(T_0/T)^{\gamma}$, with γ and T_0 are from the Mott $\sigma(T)$ (Eqn. 4.1). For $\gamma = 1/4$ for 3D variable range hopping, the familiar relation is obtained:

$$\alpha_{hop}(T) = \zeta\frac{k_B^2}{e}(T_0 T)^{1/2}\frac{d\ln N(E)}{dE}\bigg|_{E_F} \tag{4.6}$$

where ζ is a constant between 0.12 and 0.5 depending on the derivation. On the other hand, for $\gamma = 1/2$ as it is in ES VRH, $\alpha(T)$ is constant with temperature:

$$\alpha_{hop}(T) = \zeta\frac{k_B^2}{e}T_0\frac{d\ln N(E_F)}{dE}\bigg|_{E_F} \tag{4.7}$$

In the case that the hopping energy is less than $k_B T$ (26meV at 300K), the thermopower is linear with T and depends only of the slope of the DOS at the Fermi energy:[102]

$$\alpha = \frac{k_B^2}{e}T\frac{d\ln N(E)}{dE}\bigg|_{E_F} \tag{4.8}$$

The highly conducting vapor-doped samples have T_0 near or below room-temperature, suggesting that $\alpha(T) \propto T$ would be expected. Table 4.2 summarizes the extractable fit parameters for each of the discussed temperature dependancies.

4.5 Temperature for optimal performance

With the ability to evaluate the temperature dependence of electrical conductivity $\sigma(T)$ and thermopower $\alpha(T)$ of our materials, we can estimate a temperature range for op-

Table 4.3: Summary of room temperature (300K) data and maximum $PF(T)$ calculations. T_{PF} is the interpolated temperature at which PF maximizes, σ and α are the corresponding interpolated values.

Sample Condition	**σ(300K)** S/cm	**α(300K)** μV/K	**PF(300K)** μW/m-K^2	**T_{PF}** K	**σ_{PF}** S/cm	**α_{PF}** μV/K	**PF_{max}** μW/m-K^2
F_4TCNQ							
from solution							
5wt.%	0.054	173	0.162	302	0.054	174	0.163
10wt.%	0.509	92.7	0.437	278	0.668	83.7	0.467
from vapor							
AC	70.2	31.6	7.02	301	92.3	31.7	9
AN	160	31.4	15.7	300	169	31.0	16
EBSA							
immersion time							
overnight (AC)	4.4	38.9	0.669	300	4.48	37.4	0.627
24h (AN)	215	31.7	21.6	312	171	32.2	18
1h (AN)	136	28.9	11.4	289	135	27.8	10

timal thermoelectric performance, such that power factor is maximum. The temperature-dependent power factor $PF(T)$ was calculated from the spline interpolations of the $\sigma(T)$ and the $\alpha(T)$ data, as shown for each sample in Figures 4.12 and 4.13. Figures 4.14 summarizes the calculated $PF(T)$, and Table 4.3 summarizes the thermoelectric parameters σ, α, and PF at 300K, and at the temperature at which PF is maximum, T_{PF}. With the exception of the 10wt.% sample, the maximum power factor PF_{max} occurred at approximately 300K. The 10wt% sample has a maximum power factor ($PF_{max} = 0.5\mu$W/m-K^2) at 278K, which corresponds to an anomalous maximum in the electrical conductivity σ at the same temperature.

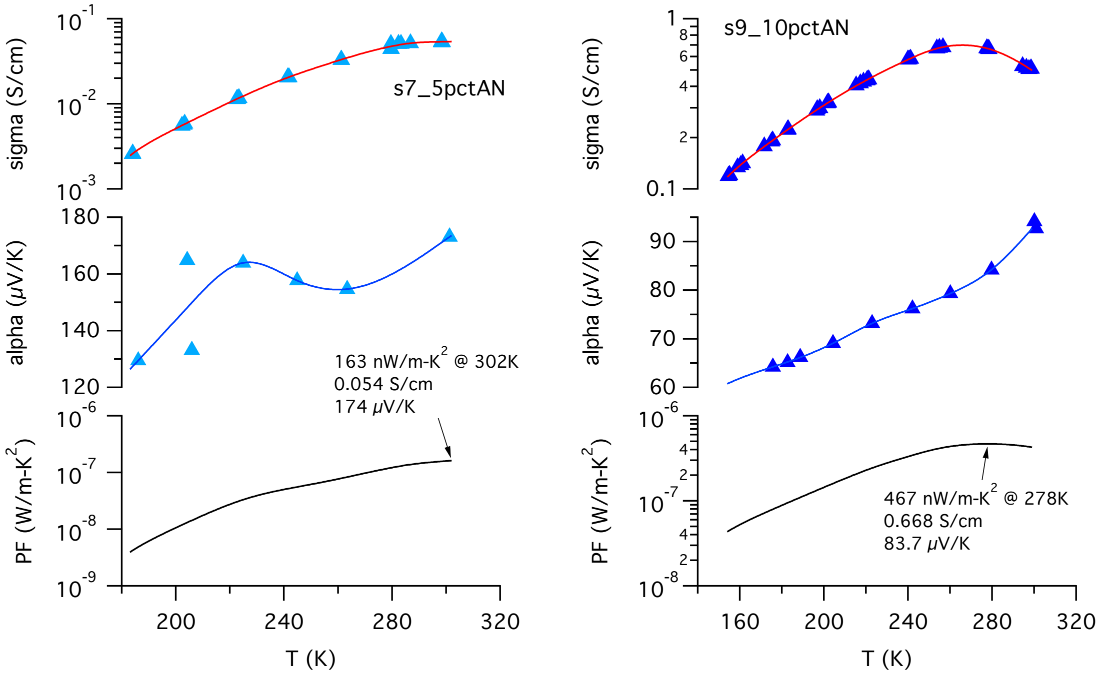

(a) F_4TCNQ 5wt.% solution doped (b) F_4TCNQ 10wt.% solution doped

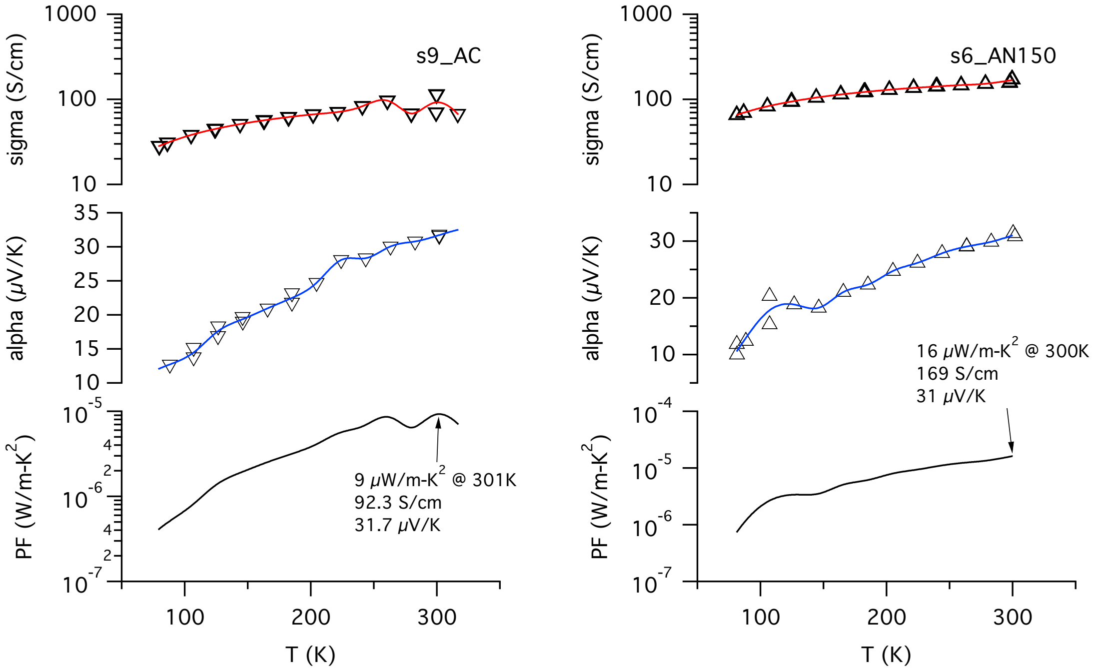

(c) F_4TCNQ vapor, AC (d) F_4TCNQ vapor, AN

Figure 4.12: Temperature-dependent power factor $PF(T)$ calculated from the interpolated $\sigma(T)$ and $\alpha(T)$ data for F_4TCNQ-doped PBTTT.

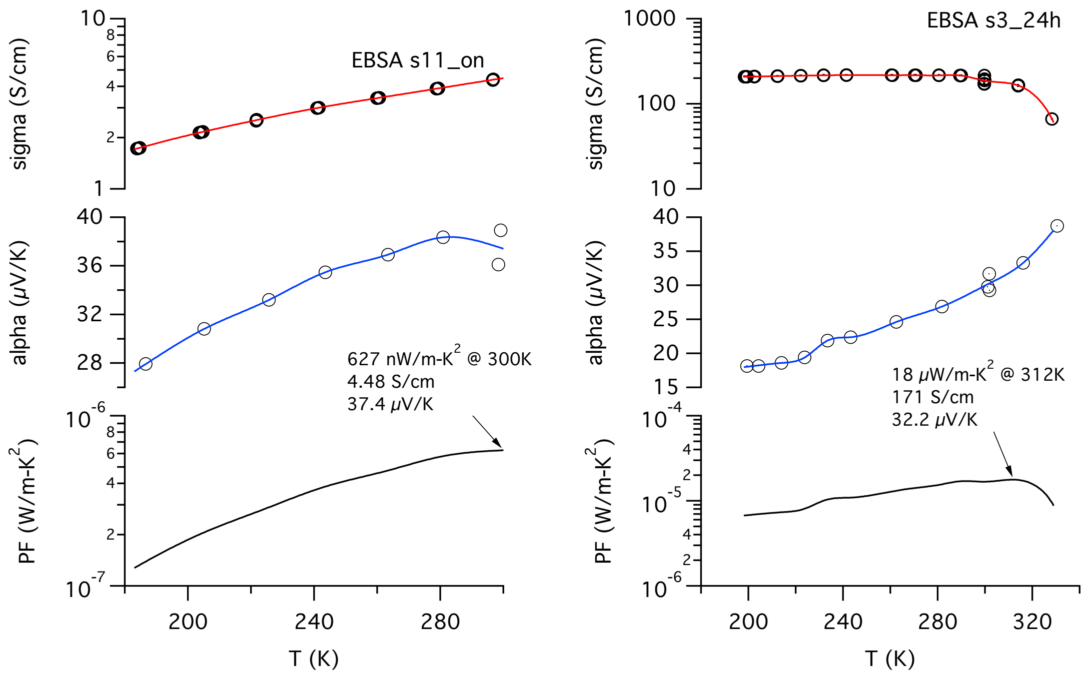

(a) EBSA immersion, overnight (b) EBSA immersion, 24h AN

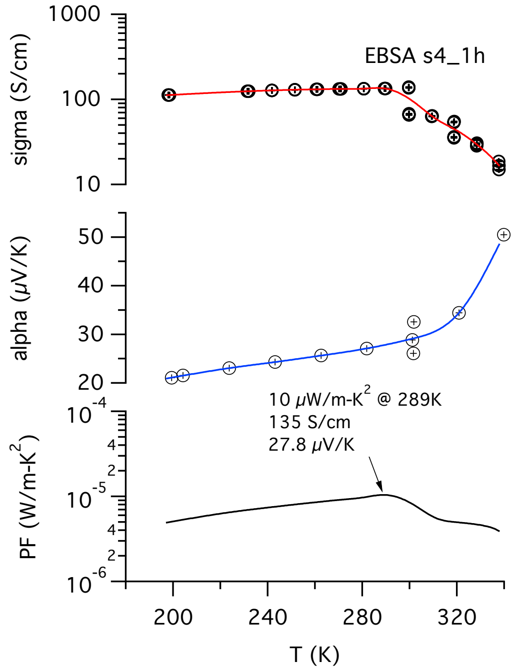

(c) EBSA immersion, 1h AN

Figure 4.13: Temperature-dependent power factor $PF(T)$ calculated from the interpolated $\sigma(T)$ and $\alpha(T)$ data for EBSA-doped PBTTT.

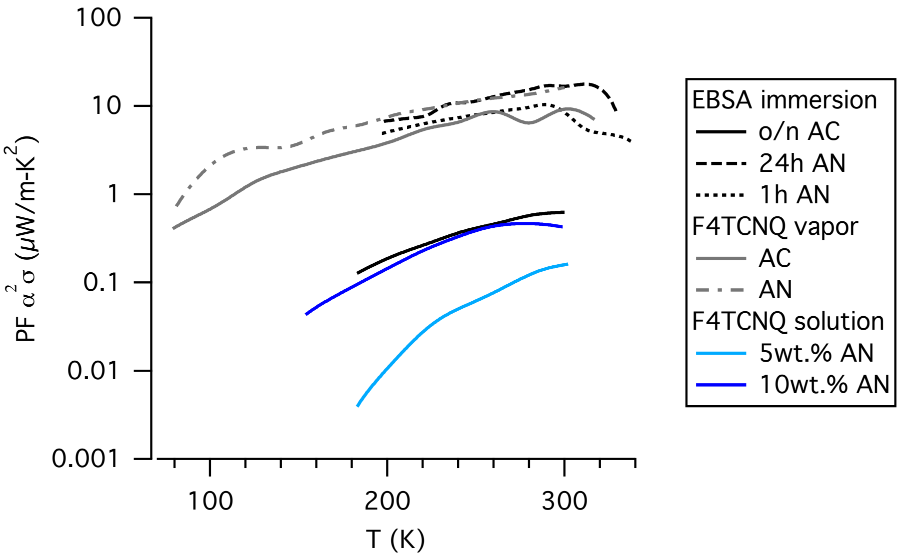

Figure 4.14: Summary of power factor $\alpha^2\sigma$ vs. T.

4.6 Experimental

4.6.1 Doping and processing methods

PBTTT-C_{14} was doped with F_4TCNQ either in solution or post-deposition by vapor. For solution-doped samples, a 1-5 mg/mL F_4TCNQ solution was added to 5 mg/mL PBTTT-C_{14} to obtain the appropriate weight percent dopant solution (5 or 10wt.% F_4TCNQ). The doped solution was kept at and spin-cast onto a cleaned quartz substrate, yielding ~ 50nm thick thin films. For vapor-doped samples, neat PBTTT-C_{14} samples were spin-cast at identical conductions. As-cast (AC) films were heated at 80°C for 10 minutes under N_2 to drive out any remaining solvent. Annealed (AN) films were baked at 150°C for 10 minutes under N_2. gold contacts for linear four-point probe conductivity and for thermopower measurements were thermally evaporated as a final step for solution-doped samples, or before doping for vapor-doped samples. To obtain vapor-doped samples, prepared neat PBTTT-C_{14} samples were mounted on the plastic lid of

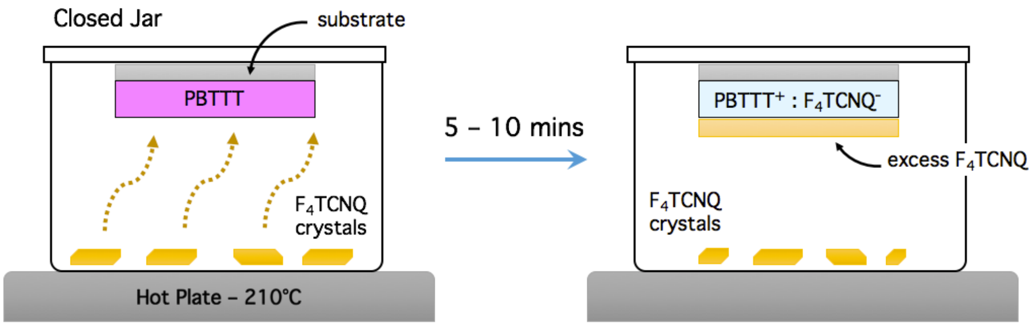

Figure 4.15: Schematic of F_4TCNQ doping from the vapor phase.

a small glass jar containing F_4TCNQ crystals, and the jar was placed on a hot plate at under nitrogen, shown in Figure 4.15. To stop doping after the designated time period, the lid wtih the sample was immediately removed (and replaced with a temporary lid as not to dope the surrounding environment), and quenched on an aluminum platen.

EBSA-doped samples were doped post-deposition by immersion. A solution was prepared in a shallow glass petri dish and the prepared neat PBTTT-C_{14} film was submerged and covered with an foil-covered petri dish lid to prevent evaporation of the solution and any spurious photo-degredation. After the designated time period, the sample was removed and rinsed with 2 mL of acetonitrile to remove excess EBSA from the surface.

4.7 Acknowledgements

The vapor doping study was done in collaboration with Dr. Shrayesh Patel (Chabinyc Group), who was an equal contributor in interpreting the overall results of the study. Much of the experimental work was carried out by Dr. Shrayesh Patel, with the assistance of Kelly Peterson, of the Chabinyc Group, as indicated below. Dr. Patel created the vapor doping apparatus and procedure as described in Fig. 4.15, and measured the stability of vapor doping in Fig. 4.3, as well as provided the images.

UV-vis-NIR Spectrometry

- Experiments were carried out in part by Dr. Shrayesh Patel and Kelly Peterson, Chabinyc Group UC Santa Barbara.
- Experiments were in part carried out in the Materials Research Lab TEMPO Facility. The MRL Shared Experimental Facilities are supported by the MRSEC Program of the NSF under Award No. DMR 1121053; a member of the NSF-funded Materials Research Facilities Network (`www.mrfn.org`).

RSoXS - Resonant Soft X-Ray Scattering

- Experiments were carried out and analyzed by Dr. Shrayesh Patel, Chabinyc Group UC Santa Barbara.
- Experiments were carried out at the Advanced Light Source, Beamline 11.0.1, and is supported by the Director, Office of Science, Office of Basic Energy Sciences, of the U.S. Department of Energy under Contract No. DE-AC02-05CH11231.

GIWAXS - Grazing Incidence Wide Angle X-Ray Spectroscopy

- Experiments were done and analyzed by Dr. Shrayesh Patel, Chabinyc Group UC Santa Barbara.
- Experiments were carried out at the Stanford Synchrotron Radiation Lightsource (SSRL), on Beamline 11-3. Use of the Stanford Synchrotron Radiation Lightsource, SLAC National Accelerator Laboratory, is supported by the U.S. Department of Energy, Office of Science, Office of Basic Energy Sciences, under Contract DE-AC02-76SF00515.

Chapter 5

Transient Effects in Thermopower Measurements

5.1 PANI-PAAMPSA

Polyaniline (PANI) compounds have also been exampled as conducting polymers and in composites for thermoelectric applications,[44,46,48] due to their moderate to high conductivity when doped with polymer acids . Practically, processing these materials are limited by poor solubility of molecular-acid doped PANI in many common solvents. By template synthesizing PANI with the polymer acid poly(2-acrylamido-2-methylpropanesulfonic acid) (PAAMPSA), solubility is increased and PANI-PAAMPSA (shown in Figure 5.1 is easily processable from aqueous dispersions.[168,169] Unlike PEDOT-based compounds, PANI is doped by protonation, usually from an acid, to have a moderate intrinsic electrical conductivity σ (<1 S/cm), which can be improved by processing.

In collaboration with Prof. Yuen-Lynn Loo at Princeton University, the thermoelectric properties of PANI-PAAMPSA were investigated. They previously found that post-processing of PANI-PAAMPSA with dichloroacetic acid (DCA) improved the electrical conductivity by over two orders of magnitude, from ∼ 0.4 S/cm to 40 S/cm,.[168] Pristine PANI-PAAMPSA films are solvent-annealed in DCA at 100 °C, and then baked at 170 °C to remove the DCA. Characterization after treatment with DCA reveals that the DCA allows dramatic structural relaxation on multiple length scales. This is attributed to the DCA reducing electrostatic interactions between PANI and PAAMPSA, dissolving the PANI-PAAMPSA colloidal nanoparticles, extending PANI chain conformation and reducing film roughness (from ∼60 to ∼4nm). Similar approaches of structural modification due to post-treatment have been shown to improve simultaneously the electrical conductivity and the thermopower.[3]

5.1.1 Effect of environment and DCA treatment on σ and α of PANI

The electrical conductivity of PANI was measured under air, nitrogen, and vacuum and was found to be sensitive to environment. Pristine PANI-PAAMPSA is relatively air-stable and has a moderate electrical conductivity on the order of 0.01 to 0.1 S/cm in air at room temperature. The conductivity of PANI-PAAMPSA is known to be very sensitive to synthesis and processing, so a large variation is not unexepected. Interestingly, the electrical conductivity is notably lower in an inert nitrogen environment, indicating some sensitivity to humidity or oxygen. DCA-treated PANI-PAAMPSA showed increased conductivity (Figure 5.2, in agreement with previously published results).[168] The DCA also potentially increases protonation and could increase carrier concentration as well as morphological effects.

To determine if the Seebeck coefficient showed the same sensitivity to environment, the thermopower of pristine and DCA-treated PANI-PAAMPSA was also measured in air, nitrogen, and vacuum (∼10^{-5} torr). Unfortunately, the data taken under nitrogen

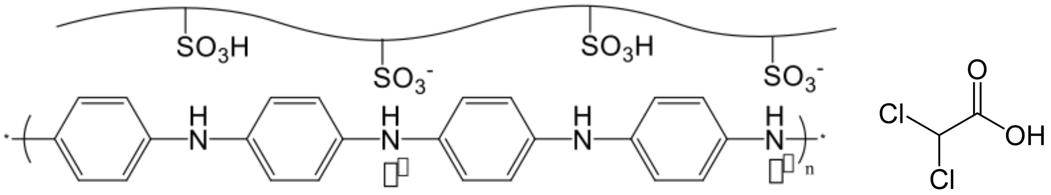

Figure 5.1: Structure of PANI-PAAMPSA (left) and dichloroacetic acid (DCA, right).

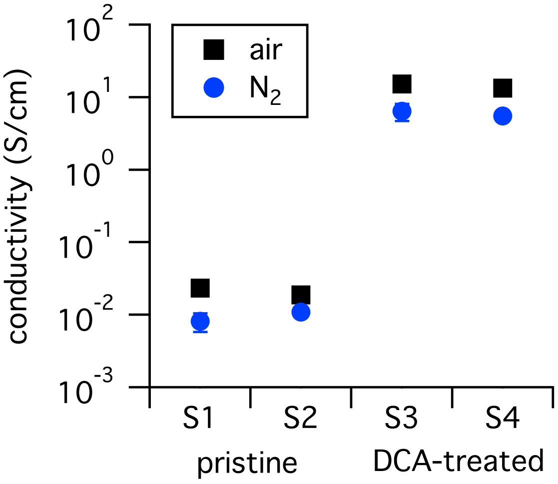

Figure 5.2: Electrical conductivity of pristine (Samples 1 & 2) and DCA-treated (Samples 3 & 4) PANI-PAAMPSA. Each sample was measured at room temperature in air and under nitrogen.

was too noisy to extract a meaningful Seebeck coefficient (Fig. 5.3), for reasons which will be discussed in the next section. Significant scatter is still present when measured in air (Fig. **??**), but a clear linear trend between ΔV and ΔT emerges. The most striking feature was that PANI-PAAMPSA in air appears to be n-type, whereas from the molecular picture one would not expect electron mobility to be significant, let alone dominate in the material. To confirm that the sign and magnitude of the Seebeck were real, the thermopower measurement was run $+\Delta T \rightarrow -\Delta T$ and then $-\Delta T \rightarrow +\Delta T$, with the same result.

The thermopower measurements were repeated in air and N_2 for DCA-treated PANI-PAAMPSA. The DCA treatment flipped the sign of the Seebeck coefficient in air, from -5.9µV/K to +4.6 µV/K. There was significantly less scatter for the DCA sample measured in air. Unlike the pristine samples, DCA-treated samples does indeed have a readable thermopower signal under nitrogen, shown in Fig. 5.4. To improve the accuracy of the fit, multiple runs were taken at different ranges and directions of ΔT. Finally, DCA-treated PANI-PAAMPSA was measured under vacuum, exhibiting a slight increase in Seebeck coefficient coinciding with a slight decrease in electrical conductivity within the same sample, where the magnitude of the decrease was still within the scatter of the sample-to-sample measurements.

Initial thermopower measurements of pristine PANI-PAAMPSA were taken under nitrogen only, with disheartening results for untreated PANI-PAAMPSA. There was an enormous amount of scatter in the data such that any existing signal was masked, as shown in Figure 5.6. The usual room-temperature Seebeck protocol (Fig.5.6a) of recording 5 data points after ΔT is steady-state had no clear trend, with peak-to-peak Seebeck voltage noise of nearly 0.6 mV. To possibly draw out a better baseline from the scatter, all data points were recorded (Fig.5.6b), with similar results. To confirm the previous results, multiple subsequent runs were done over different ΔT ranges (Fig.5.6c). Each

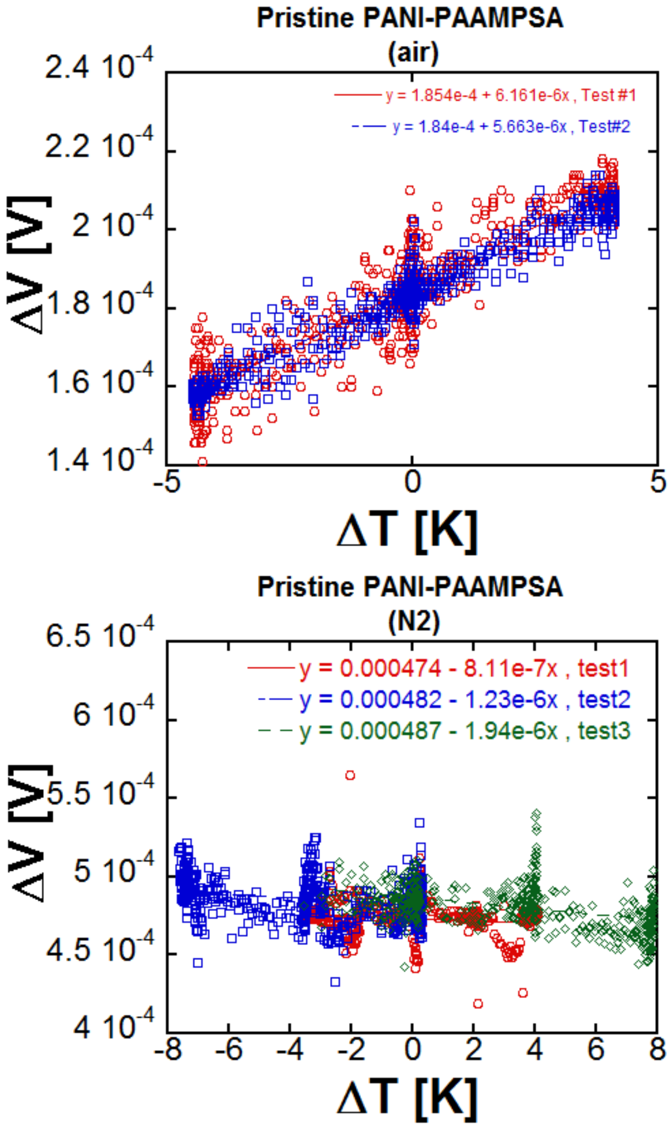

Figure 5.3: Thermopower measurements of pristine PANI-PAAMPSA in (top) air and (bottom) N_2. Linear fits to $\Delta V/\Delta T$ yield $\alpha(air) = -5.9\mu$V/K, $\alpha(N_2) = +1.3\mu$V/K.

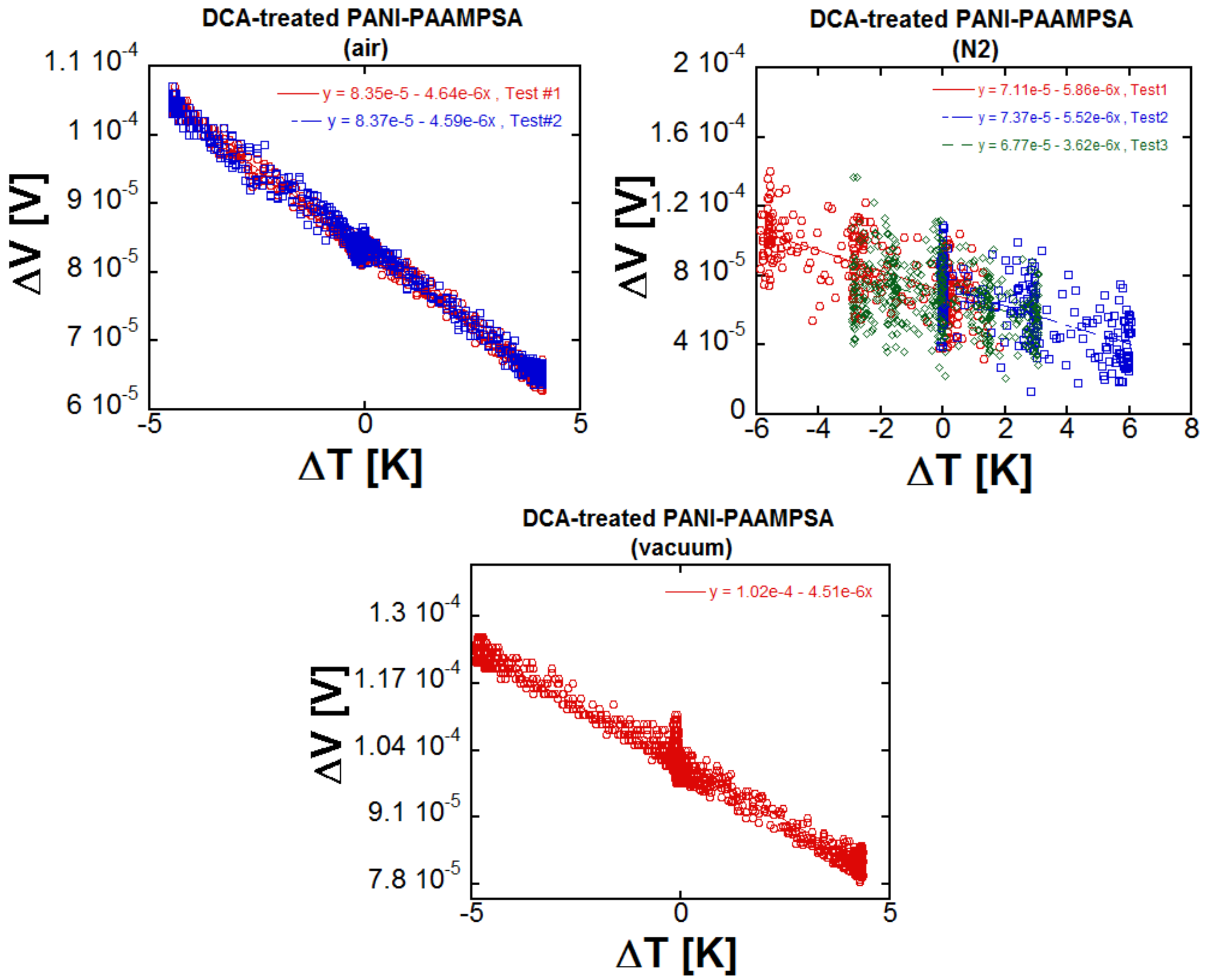

Figure 5.4: Thermopower measurements of DCA-treated PANI-PAAMPSA in (top left) air, (top right) N_2, and (bottom) under vacuum. Linear fits to $\Delta V/\Delta T$ yield $\alpha(air) = 4.6\mu$V/K, $\alpha(N_2) = 5\mu$V/K, $\alpha(vac) = 4.5\mu$/K.

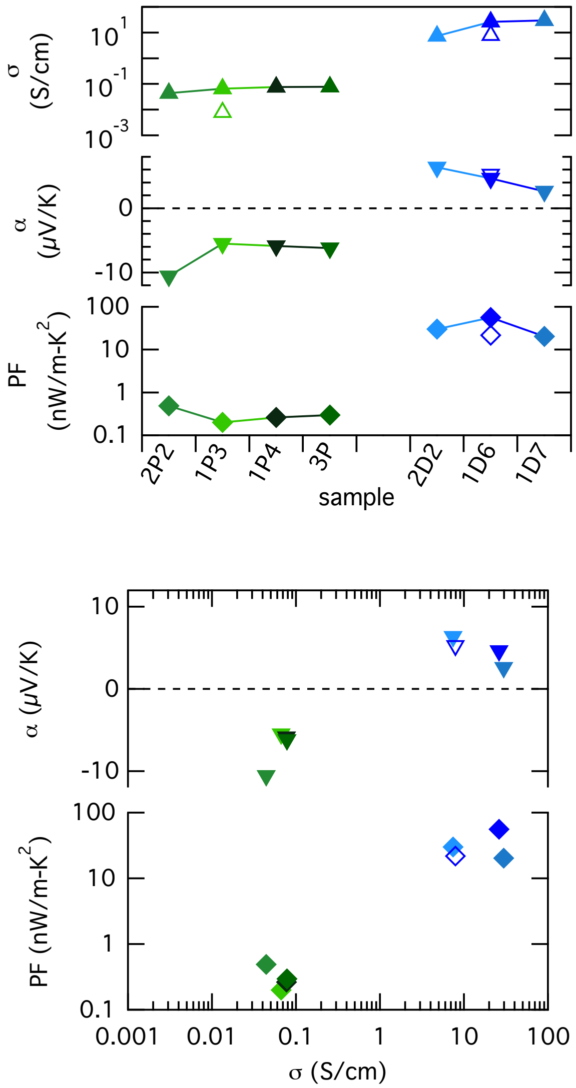

Figure 5.5: Electrical conductivity σ, Seebeck coefficient α, and power factor PF for 4 pristine (greens) and 3 DCA-treated (blues) PANI-PAAMPSA samples. Open symbols were taken under vacuum, all others were measured in air. (Top) σ, α, and PF for each sample. (Bottom) α and PF vs. σ, clearly illustrating that DCA treatment increases electrical conductivity and the Seebeck coefficient simultaneously.

of the plots in Figure 5.6 were different samples measured on different days, but all had $\Delta V(\Delta T = 0)$ (a so-called "dark voltage") on the order of 1mV.

To rule out the measurement system as a systematic cause of noise greater than signal, a reference sample of indium tin oxide (ITO) was measured. ITO is a transparent material with high carrier concentration, and it is expected to have a very low Seebeck coefficient. It is clear from Figure 5.6d that the measurement system has low enough resolution to measure Seebeck voltages approaching 0 μV/K, with little scatter for $\alpha_{\text{ITO}} \sim 4-6\mu$V/K. In the case that the resistivity of the sample is very high, measurement of the Seebeck voltage becomes unreliable due to the voltmeter impedance nearing that of the device under test. Although the electrical conductivity does decrease from air to nitrogen environments, the increased impedance does not approach that of the source-measure unit.

Clearly, the scatter was due to the sample, the origin unknown. One initial hypothesis was that if the Seebeck coefficient was very small due to dual carrier conduction, small fluctuations in environment may cause amplified oscillations of the hole-electron equilibrium, causing the sign of the Seebeck coefficient to oscillate about zero. Further measurements are needed to determine the origin of the scatter as well as the sign-change flip.

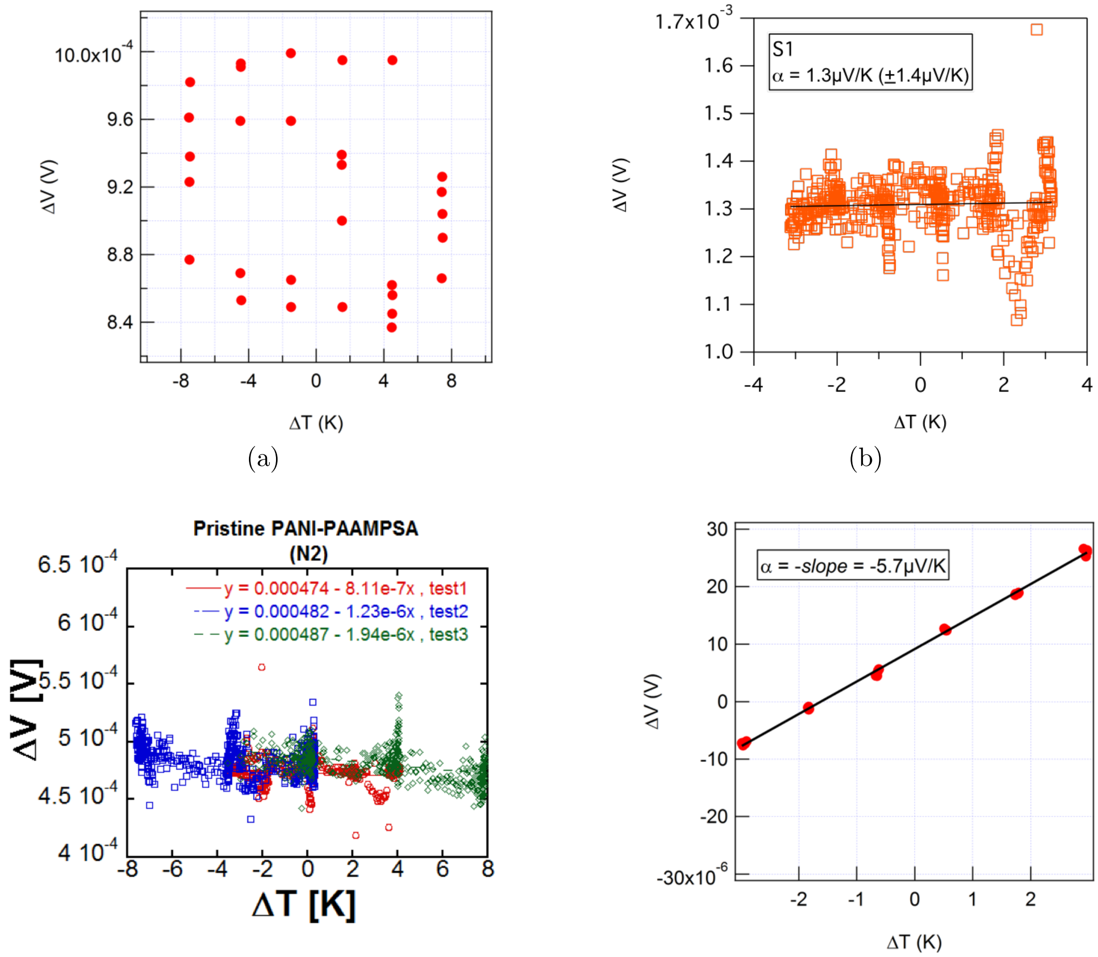

(a) (b)

(c) (d)

Figure 5.6: Highly scattered thermopower measurements of pristine PANI-PAAMPSA under N_2: (a) Five Seebeck voltage data points at each ΔT, (b) Seebeck voltages recorded continuously, (c) Seebeck voltage recorded over 3 separate runs of different ΔT ranges. The thermopower of ITO (d) demonstrates the ability to measure Seebeck coefficients <10 mV.

5.2 Transient thermopower in PEDOT:PSS

PANI is doped by protonation of backbone. To uncover if the transient behavior was due to this or DCA itself, PEDOT:PSS (shown in Figure 5.7, which is doped differently, was also treated with DCA. The results were that DCA had a similar effect on the present transient effects seen in pristine PEDOT:PSS, but these transients took a very different form. To illustrate the extent of these effects, thermopower curves of a single sample of pristine PEDOT:PSS were taken back-to-back, and then the following day. Figure 5.8 The first measurement of Day 1 (Fig. 5.8a) showed an extreme reduction of the Seebeck voltage at $+\Delta T$. There was also a sharp rise of 0.26 mV in the baseline (dark voltage) over time. The final red flag was that the Seebeck voltage was lagging the temperature gradient, and did not reach steady-state with respect to the baseline over the steady-state ΔT.

The measurement was repeated in reverse order ($+\Delta T$ first) to determine if any of these effects were dependent on which way the temperature was poled first, time spent under ΔT, or total elapsed time, shown in Figure 5.8c. To account for the extreme lag of the Seebeck response, the time that each heater was on was extended by 1 minute in an effort to allow ΔV to reach steady-state. There still was a steady drift in the $\Delta T = 0$

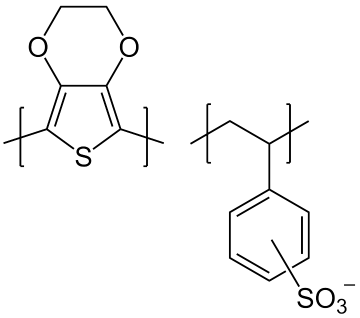

Figure 5.7: Molecular structure of PEDOT:PSS

voltage to a lesser extent (~0.08 mV), and the $+\Delta T$ Seebeck voltage was still suppressed compared to $-\Delta T$.

The final measurement was repeated again as in the first one ($-\Delta T$ first), with a longer time recording the background Seebeck voltage prior to any temperature gradients, as shown in Figure 5.8e. The initial background voltage continued to be higher than in the previous measurement, but there was noticeably less drift prior to any temperature gradient applied, and over the entire measurement. A small degree of anisotropy for $\pm\Delta T$ remained, and their shapes were still noticeably different shapes. What was interesting is the evolution of the baseline during the $\Delta T = 0$ time periods. The baseline shift from the beginning to the end of the measurement has a discontinuous jump before and after the first temperature gradient applied ($-\Delta T$), but remains stable after that, even through the $+\Delta T$ period.

After being left overnight in air in the dark, the pristine PEDOT:PSS sample was measured similarly to the previous day. The same general trends from measurement to measurement were still seen: suppression of ΔV during $+\Delta T$, lag in Seebeck voltage response, and a gradually increasing baseline. Most noticably in Day 2, ΔV was the wrong polarity during the $+\Delta T$ period. Naively, one might think that *somehow* the thermopower of PEDOT:PSS is positive p-type during $\Delta T < 0$, and negative n-type during $\Delta T > 0$, which since the PEDOT:PSS sample is not macroscopically poled, is basically impossible. However, one might reasonably interpret this as suppression of ΔV taken to an extreme. The fact that the Seebeck response is the wrong sign but decreases in ”wrongness” over long time periods definitively points to multiple competing processes that take place on very different time scales, which would be consistent with the presence of an ionic Seebeck effect.[170,171]

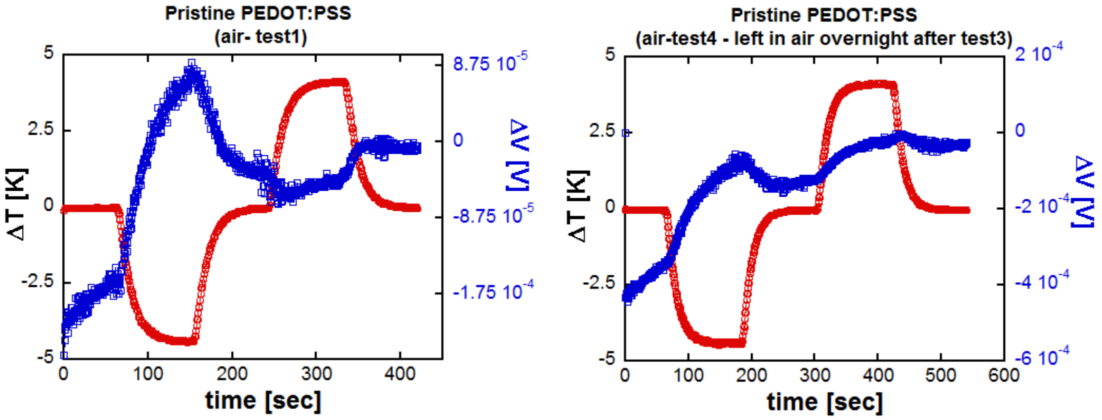

(a) Day 1 - Test 1 (b) Day 2 - Test 1

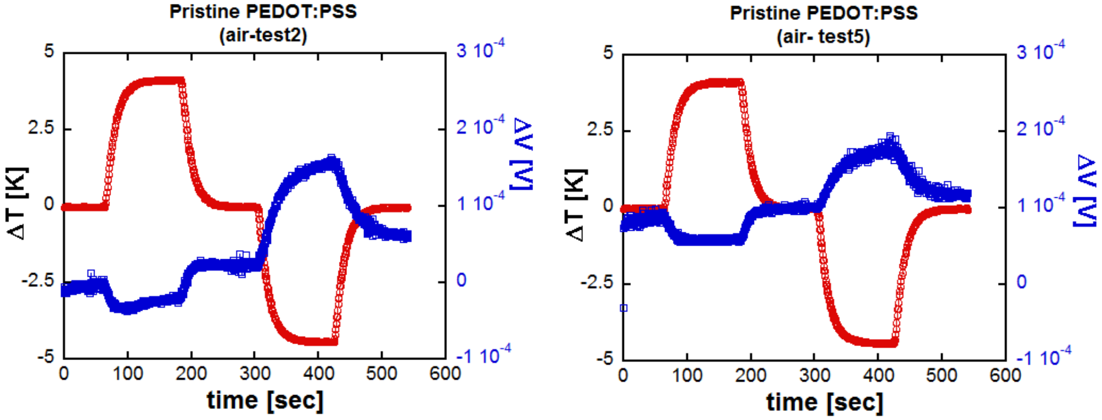

(c) Day 1 - Test 2 (d) Day 2 - Test 2

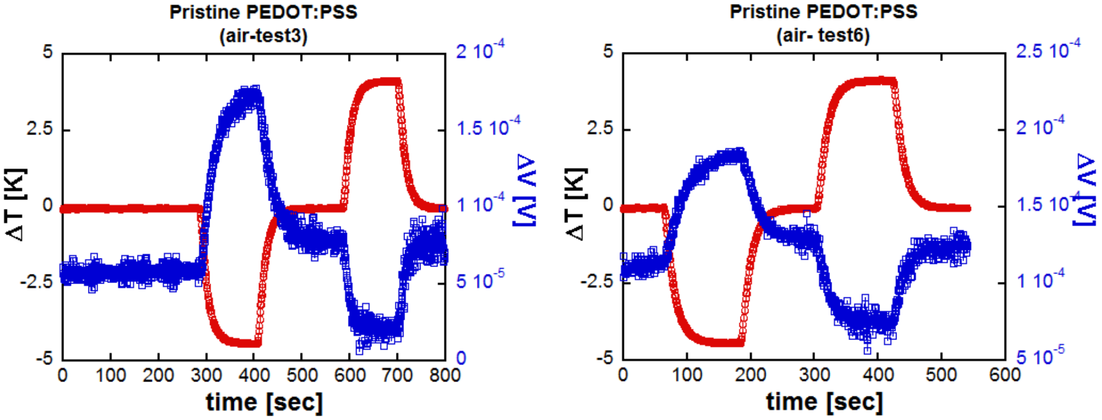

(e) Day 1 - Test 3 (f) Day 2 - Test 3

Figure 5.8: Thermopower measurements over time of pristine PEDOT:PSS - ΔT (left axis, red circles) and ΔV (right axis, blue squares). Tests 1, 2, and 3 of each day were taken one after another with minimal time in between.

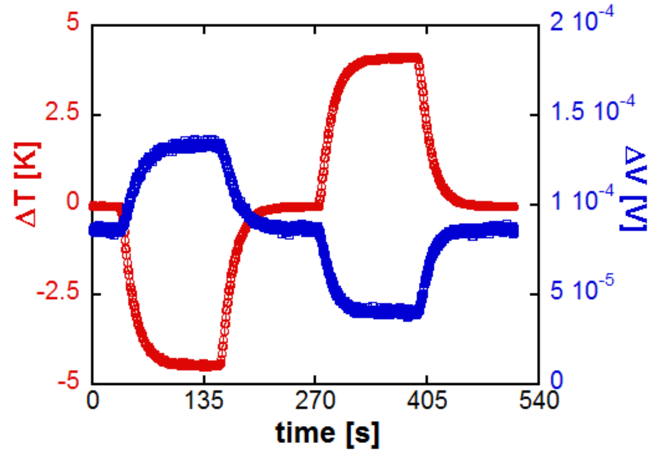

Figure 5.9: ΔT and Seebeck voltage ΔV over time for DCA-treated PEDOT:PSS. Sample is well-behaved, exhibiting no obvious ionic effects.

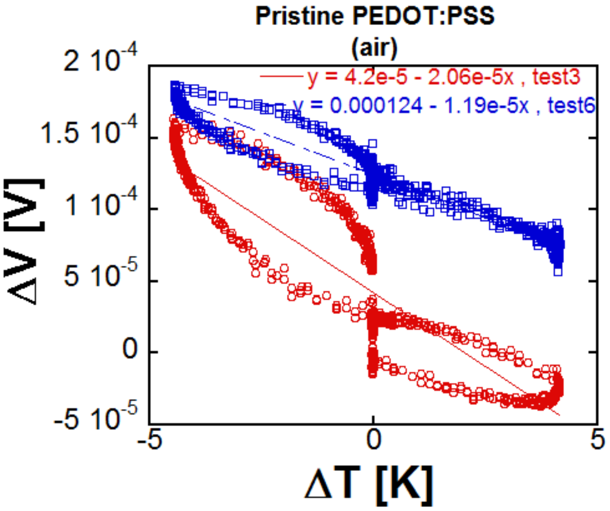

(a) Pristine PEDOT:PSS, Day 1 (red - from Fig. 5.8e) and Day 2 (blue - from Fig. 5.8f). Linear fit over all data points results in α(Day 1) = 21 µV/K, α(Day 2) = 12 µV/K.

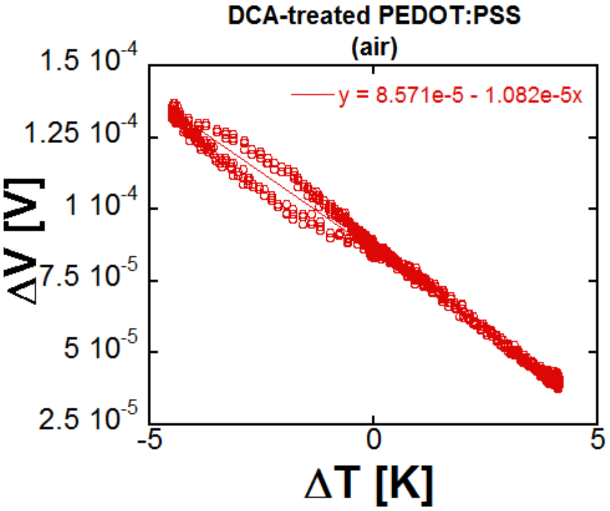

(b) DCA-treated PEDOT:PSS. α = 11 µV/K from linear fit.

Figure 5.10: Seebeck curves for (a) pristine and (b) DCA-treated PEDOT:PSS. The lobe-like features correspond with shifting baselines and/or significant lag in Seebeck response.

5.3 Acknowledgements

The study that contributed to this chapter was done in collaboration with Melda Sezen and Prof. Yueh-lin (Lynn) Loo, Princeton University, and William Chang and Prof. Rachel Segalman, UC Santa Barbara. Ms. Sezen and Prof. Loo provided expertise on PANI and the PANI:PAAMPSA system. All PANI:PAAMPSA and PEDOT samples were fabricated by Ms. Sezen, who also assisted with taking thermoelectric measurements. Mr. Chang and Prof. Rachel Segalman provided expertise on PEDOT:PSS and ionic effects.

Thank you to Prof. G. Jeffrey Snyder, (Caltech) Northwestern University, for helpful discussions and assistance in identifying the source of the highly scattered thermopower measurements. Prof. Snyder's expertise in thermoelectric materials was instrumental in interpreting the often non-ideal thermoelectric properties of our polymeric systems.

Bibliography

[1] J. Sun, M.-L. Yeh, B. J. Jung, B. Zhang, J. Feser, A. Majumdar, and H. E. Katz, “Simultaneous Increase in Seebeck Coefficient and Conductivity in a Doped Poly(alkylthiophene) Blend with Defined Density of States,” *Macromolecules*, vol. 43, pp. 2897–2903, Mar. 2010.

[2] O. Bubnova, Z. U. Khan, A. Malti, S. Braun, M. Fahlman, M. Berggren, and X. Crispin, “Optimization of the thermoelectric figure of merit in the conducting polymer poly(3,4-ethylenedioxythiophene),” *Nature Materials*, vol. 10, pp. 429–433, May 2011.

[3] G.-H. Kim, L. Shao, K. Zhang, and K. P. Pipe, “Engineered doping of organic semiconductors for enhanced thermoelectric efficiency,” *Nature Materials*, vol. 12, pp. 719–723, May 2013.

[4] O. Bubnova, Z. U. Khan, H. Wang, S. Braun, D. R. Evans, M. Fabretto, P. Hojati-Talemi, D. Dagnelund, J.-B. Arlin, Y. H. Geerts, S. Desbief, D. W. Breiby, J. W. Andreasen, R. Lazzaroni, W. M. Chen, I. Zozoulenko, M. Fahlman, P. J. Murphy, M. Berggren, and X. Crispin, “Semi-metallic polymers,” *Nature Materials*, vol. 13, no. 2, p. 190, 2014.

[5] B. Russ, A. M. Glaudell, J. J. Urban, M. L. Chabinyc, and R. A. Segalman, “Organic Thermoelectrics for Conformal Energy Harvesting and Personal Comfort,” *Nature Reviews Materials, in revisions*, 2016.

[6] A. M. Glaudell, R. A. Schlitz, and M. L. Chabinyc, *Innovative Thermoelectric Materials*, ch. Seebeck Coefficient and Electrical Conductivity Optimization in Polymers. Imperial College Press, England, 2014 (*In Press*).

[7] L. Dou, J. You, Z. Hong, Z. Xu, G. Li, R. A. Street, and Y. Yang, “25th Anniversary Article: A Decade of Organic/Polymeric Photovoltaic Research,” *Advanced Materials*, vol. 25, pp. 6642–6671, Dec. 2013.

[8] T. N. Ng, D. E. Schwartz, L. L. Lavery, G. L. Whiting, B. Russo, B. Krusor, J. Veres, P. Bröms, L. Herlogsson, N. Alam, O. Hagel, J. Nilsson, and C. Karlsson, “Scalable printed electronics: an organic decoder addressing ferroelectric non-volatile memory,” *Scientific Reports*, vol. 2, p. 585, 2012.

[9] K. T. Kamtekar, A. P. Monkman, and M. R. Bryce, "Recent Advances in White Organic Light-Emitting Materials and Devices (WOLEDs)," *Advanced Materials*, vol. 22, pp. 572–582, Feb. 2010.

[10] S. Holliday, J. E. Donaghey, and I. McCulloch, "Advances in Charge Carrier Mobilities of Semiconducting Polymers Used in Organic Transistors," *Chemistry of Materials*, vol. 26, pp. 647–663, Jan. 2014.

[11] J. E. Anthony, "Functionalized Acenes and Heteroacenes for Organic Electronics," *Chemical Reviews*, vol. 106, pp. 5028–5048, Dec. 2006.

[12] M. Bendikov, F. Wudl, and D. F. Perepichka, "Tetrathiafulvalenes, Oligoacenenes, and Their Buckminsterfullerene Derivatives: The Brick and Mortar of Organic Electronics," *Chemical Reviews*, vol. 104, pp. 4891–4946, Nov. 2004.

[13] H. J. Son, F. He, B. Carsten, and L. Yu, "Are we there yet? Design of better conjugated polymers for polymer solar cells," *Journal of Materials Chemistry*, vol. 21, no. 47, p. 18934, 2011.

[14] A. Salleo, R. J. Kline, D. M. DeLongchamp, and M. L. Chabinyc, "Microstructural Characterization and Charge Transport in Thin Films of Conjugated Polymers," *Advanced Materials*, vol. 22, no. 34, pp. 3812–3838, 2010.

[15] D. M. DeLongchamp, R. J. Kline, D. A. Fischer, L. J. Richter, and M. F. Toney, "Molecular Characterization of Organic Electronic Films," *Advanced Materials*, vol. 23, pp. 319–337, Jan. 2011.

[16] P. M. Chaikin, R. L. Greene, S. Etemad, and E. Engler, "Thermopower of an isostructural series of organic conductors," *Physical Review B*, vol. 13, pp. 1627–1632, Feb. 1976.

[17] P. M. Chaikin and G. Beni, "Thermopower in the correlated hopping regime," *Physical Review B*, vol. 13, pp. 647–651, Jan. 1976.

[18] J. B. Torrance, "The difference between metallic and insulating salts of tetracyanoquinodimethone (tcnq): how to design an organic metal," *Accounts of Chemical Research*, vol. 12, no. 3, pp. 79–86, 1979.

[19] A. Shakouri and S. Li, "Thermoelectric Power Factor for Electrically Conductive Polymers," *18th International Conference on Thermoelectrics*, pp. 402–406, 1999.

[20] T. Schimmel, G. Denninger, W. Riess, J. Voit, M. Schwoerer, W. Schoepe, and H. Naarmann, "Proceedings of the international conference on science and technology of synthetic metals high- polyacetylene: Dc conductivity between 14 mk and 300 k," *Synthetic Metals*, vol. 28, no. 3, pp. D11 – D18, 1989.

[21] L. Groenendaal, F. Jonas, D. Freitag, H. Pielartzik, and J. R. Reynolds, "Poly(3,4-ethylenedioxythiophene) and Its Derivatives: Past, Present, and Future," *Advanced Materials*, vol. 12, pp. 481–494, Apr. 2000.

[22] "Frequently Asked Questions About Our Cooling and Heating Technology." Tellurex Corporation, 2010.

[23] G. J. Snyder and E. S. Toberer, "Complex thermoelectric materials," *Nature Materials*, vol. 7, no. 2, pp. 105–114, 2008.

[24] M. Beekman, D. T. Morelli, and G. S. Nolas, "Better thermoelectrics through glass-like crystals," *Nature Materials*, vol. 14, pp. 1182–1185, Nov. 2015.

[25] A. Shakouri, "Recent Developments in Semiconductor Thermoelectric Physics and Materials," *Annual Review of Materials Research*, vol. 41, no. 1, pp. 399–431, 2011.

[26] V. Coropceanu, J. Cornil, D. A. da Silva Filho, Y. Olivier, R. Silbey, and J.-L. Brédas, "Charge Transport in Organic Semiconductors," *Chemical Reviews*, vol. 107, pp. 926–952, Apr. 2007.

[27] J. L. Bredas and G. B. Street, "Polarons, bipolarons, and solitons in conducting polymers," *Accounts of Chemical Research*, vol. 18, pp. 309–315, Oct. 1985.

[28] J. E. Anthony, A. Facchetti, M. Heeney, S. R. Marder, and X. Zhan, "n-Type Organic Semiconductors in Organic Electronics," *Advanced Materials*, vol. 22, no. 34, pp. 3876–3892, 2010.

[29] X. Guo, M. Baumgarten, and K. Müllen, "Designing -conjugated polymers for organic electronics," *Progress in Polymer Science*, vol. 38, pp. 1832–1908, Dec. 2013.

[30] J. Mei and Z. Bao, "Side Chain Engineering in Solution-Processable Conjugated Polymers," *Chemistry of Materials*, vol. 26, pp. 604–615, Jan. 2014.

[31] M. Chabinyc, "Thermoelectric polymers: Behind organics' thermopower," *Nat Mater*, vol. 13, no. 2, pp. 119–121, 2014.

[32] A. J. Heeger, S. Kivelson, J. R. Schrieffer, and W. P. Su, "Solitons in conducting polymers," *Rev. Mod. Phys.*, vol. 60, pp. 781–850, Jul 1988.

[33] R. Noriega, J. Rivnay, K. Vandewal, F. P. V. Koch, N. Stingelin, P. Smith, M. F. Toney, and A. Salleo, "A general relationship between disorder, aggregation and charge transport in conjugated polymers," *Nature Materials*, vol. 12, pp. 1038–1044, Nov. 2013.

[34] D. Venkateshvaran, M. Nikolka, A. Sadhanala, V. Lemaur, M. Zelazny, M. Kepa, M. Hurhangee, A. J. Kronemeijer, V. Pecunia, I. Nasrallah, I. Romanov, K. Broch, I. McCulloch, D. Emin, Y. Olivier, J. Cornil, D. Beljonne, and H. Sirringhaus, "Approaching disorder-free transport in high-mobility conjugated polymers," *Nature*, vol. 515, no. 7527, pp. 384–388, 2014.

[35] A. M. Glaudell, J. E. Cochran, S. N. Patel, and M. L. Chabinyc, "Impact of the Doping Method on Conductivity and Thermopower in Semiconducting Polythiophenes," *Advanced Energy Materials*, vol. 5, p. 1401072, Oct. 2015.

[36] Y. Xuan, X. Liu, S. Desbief, P. Leclère, M. Fahlman, R. Lazzaroni, M. Berggren, J. Cornil, D. Emin, and X. Crispin, "Thermoelectric properties of conducting polymers: The case of poly(3-hexylthiophene)," *Physical Review B*, vol. 82, no. 11, p. 115454, 2010.

[37] R. B. Aïch, N. Blouin, A. Bouchard, and M. Leclerc, "Electrical and Thermoelectric Properties of Poly(2,7-Carbazole) Derivatives," *Chemistry of Materials*, vol. 21, pp. 751–757, Feb. 2009.

[38] Q. Zhang, Y. Sun, W. Xu, and D. Zhu, "What To Expect from Conducting Polymers on the Playground of Thermoelectricity: Lessons Learned from Four High-Mobility Polymeric Semiconductors," *Macromolecules*, p. 609, Jan. 2014.

[39] C. O. Yoon, R. M., D. Moses, and A. J. Heeger, "Transport near the metal-insulator transition: Polypyrrole doped with PF_{6}," *Physical Review B*, vol. 49, pp. 10851–10863, Apr. 1994.

[40] C. Yoon, M. Reghu, D. Moses, A. Heeger, Y. Cao, T.-A. Chen, X. Wu, and R. Rieke, "Hopping transport in doped conducting polymers in the insulating regime near the metal-insulator boundary: polypyrrole, polyaniline and polyalkylthiophenes," *Synthetic Metals*, vol. 75, pp. 229–239, Dec. 1995.

[41] J. Paloheimo, K. Laakso, H. Isotalo, and H. Stubb, "Conductivity, thermoelectric power and field-effect mobility in self-assembled films of polyanilines and oligoanilines," *Synthetic Metals*, vol. 68, pp. 249–257, Feb. 1995.

[42] Y. Nogami, H. Kaneko, T. Ishiguro, A. Takahashi, J. Tsukamoto, and N. Hosoito, "On the metallic states in highly conducting iodine-doped polyacetylene," *Solid State Communications*, vol. 76, pp. 583–586, Nov. 1990.

[43] A. B. Kaiser, "Thermoelectric power and conductivity of heterogeneous conducting polymers," *Physical Review B*, vol. 40, no. 5, pp. 2806–2813, 1989.

[44] G. P. Moriarty, K. Briggs, B. Stevens, C. Yu, and J. C. Grunlan, "Fully Organic Nanocomposites with High Thermoelectric Power Factors by using a Dual-Stabilizer Preparation," *Energy Technology*, vol. 1, pp. 265–272, Apr. 2013.

[45] D. Kim, Y. Kim, K. Choi, J. C. Grunlan, and C. Yu, “Improved Thermoelectric Behavior of Nanotube-Filled Polymer Composites with Poly(3,4-ethylenedioxythiophene) Poly(styrenesulfonate),” *ACS Nano*, vol. 4, pp. 513–523, Jan. 2010.

[46] K. Choi and C. Yu, “Highly Doped Carbon Nanotubes with Gold Nanoparticles and Their Influence on Electrical Conductivity and Thermopower of Nanocomposites,” *PLoS ONE*, vol. 7, p. e44977, Sept. 2012.

[47] C. Yu, K. Choi, L. Yin, and J. C. Grunlan, “Light-Weight Flexible Carbon Nanotube Based Organic Composites with Large Thermoelectric Power Factors,” *ACS Nano*, vol. 5, pp. 7885–7892, Oct. 2011.

[48] C. Yu, Y. S. Kim, D. Kim, and J. C. Grunlan, “Thermoelectric Behavior of Segregated-Network Polymer Nanocomposites,” *Nano Letters*, vol. 8, pp. 4428–4432, Dec. 2008.

[49] C. Cho, B. Stevens, J.-H. Hsu, R. Bureau, D. A. Hagen, O. Regev, C. Yu, and J. C. Grunlan, “Completely Organic Multilayer Thin Film with Thermoelectric Power Factor Rivaling Inorganic Tellurides,” *Advanced Materials*, vol. 27, pp. 2996–3001, May 2015.

[50] T. Inabe, H. Ogata, Y. Maruyama, Y. Achiba, S. Suzuki, K. Kikuchi, and I. Ikemoto, “Electronic structure of alkali metal doped C60 derived from thermoelectric power measurements,” *Physical Review Letters*, vol. 69, no. 26, pp. 3797–3799, 1992.

[51] Z. H. Wang, A. W. P. Fung, G. Dresselhaus, M. S. Dresselhaus, K. A. Wang, P. Zhou, and P. C. Eklund, “Electron-electron interactions and superconducting fluctuations in weakly localized K_{3}C_{60},” *Physical Review B*, vol. 47, pp. 15354–15357, June 1993.

[52] M. Sumino, K. Harada, M. Ikeda, S. Tanaka, K. Miyazaki, and C. Adachi, “Thermoelectric properties of n-type C-60 thin films and their application in organic thermovoltaic devices,” *Applied Physics Letters*, vol. 99, Aug. 2011.

[53] Y. Sun, P. Sheng, C. Di, F. Jiao, W. Xu, D. Qiu, and D. Zhu, “Organic Thermoelectric Materials and Devices Based on p- and n-Type Poly(metal 1,1,2,2-ethenetetrathiolate)s,” *Advanced Materials*, vol. 24, pp. 932–937, Feb. 2012.

[54] H. J. Goldsmid, “The Electrical Conductivity and Thermoelectric Power of Bismuth Telluride,” *Proceedings of the Physical Society*, vol. 71, p. 633, Apr. 1958.

[55] B. Poudel, Q. Hao, Y. Ma, Y. Lan, A. Minnich, B. Yu, X. Yan, D. Wang, A. Muto, D. Vashaee, X. Chen, J. Liu, M. S. Dresselhaus, G. Chen, and Z. Ren, “High-Thermoelectric Performance of Nanostructured Bismuth Antimony Telluride Bulk Alloys,” *Science*, vol. 320, pp. 634–638, May 2008.

[56] R. Venkatasubramanian, E. Siivola, T. Colpitts, and B. O'Quinn, "Thin-film thermoelectric devices with high room-temperature figures of merit," *Nature*, vol. 413, pp. 597–602, Oct. 2001.

[57] H. Sirringhaus, "25th Anniversary Article: Organic Field-Effect Transistors: The Path Beyond Amorphous Silicon," *Advanced Materials*, vol. 26, pp. 1319–1335, Mar. 2014.

[58] M. V. Fabretto, D. R. Evans, M. Mueller, K. Zuber, P. Hojati-Talemi, R. D. Short, G. G. Wallace, and P. J. Murphy, "Polymeric Material with Metal-Like Conductivity for Next Generation Organic Electronic Devices," *Chemistry of Materials*, vol. 24, pp. 3998–4003, Oct. 2012.

[59] A. J. Heeger, "Semiconducting and Metallic Polymers: The Fourth Generation of Polymeric Materials," *The Journal of Physical Chemistry B*, vol. 105, pp. 8475–8491, Sept. 2001.

[60] B. J. Worfolk, S. C. Andrews, S. Park, J. Reinspach, N. Liu, M. F. Toney, S. C. B. Mannsfeld, and Z. Bao, "Ultrahigh electrical conductivity in solution-sheared polymeric transparent films," *Proceedings of the National Academy of Sciences*, vol. 112, pp. 14138–14143, Nov. 2015.

[61] K. Walzer, B. Maennig, M. Pfeiffer, and K. Leo, "Highly Efficient Organic Devices Based on Electrically Doped Transport Layers," *Chemical Reviews*, vol. 107, pp. 1233–1271, Apr. 2007.

[62] J. Zaumseil and H. Sirringhaus, "Electron and Ambipolar Transport in Organic Field-Effect Transistors," *Chemical Reviews*, vol. 107, pp. 1296–1323, Apr. 2007.

[63] T. D. Anthopoulos, G. C. Anyfantis, G. C. Papavassiliou, and D. M. de Leeuw, "Air-stable ambipolar organic transistors," *Applied Physics Letters*, vol. 90, Mar. 2007.

[64] D. M. de Leeuw, M. M. J. Simenon, A. R. Brown, and R. E. F. Einerhand, "Stability of n-type doped conducting polymers and consequences for polymeric microelectronic devices," *Synthetic Metals*, vol. 87, pp. 53–59, Feb. 1997.

[65] B. J. Jung, N. J. Tremblay, M.-L. Yeh, and H. E. Katz, "Molecular Design and Synthetic Approaches to Electron-Transporting Organic Transistor Semiconductors," *Chemistry of Materials*, vol. 23, pp. 568–582, Feb. 2011.

[66] B. Russ, M. J. Robb, F. G. Brunetti, P. L. Miller, E. E. Perry, S. N. Patel, V. Ho, W. B. Chang, J. J. Urban, M. L. Chabinyc, C. J. Hawker, and R. A. Segalman, "Power Factor Enhancement in Solution-Processed Organic n-Type Thermoelectrics Through Molecular Design," *Advanced Materials*, vol. 26, pp. 3473–3477, June 2014.

[67] R. A. Schlitz, F. G. Brunetti, A. M. Glaudell, P. L. Miller, M. A. Brady, C. J. Takacs, C. J. Hawker, and M. L. Chabinyc, “Solubility-Limited Extrinsic n-Type Doping of a High Electron Mobility Polymer for Thermoelectric Applications,” *Advanced Materials*, vol. 26, pp. 2825–2830, May 2014.

[68] H. Shi, C. Liu, Q. Jiang, and J. Xu, “Effective Approaches to Improve the Electrical Conductivity of PEDOT: PSS: A Review,” *Advanced Electronic Materials*, vol. 1, no. 4, 2015.

[69] B. Winther-Jensen and K. West, “Vapor-Phase Polymerization of 3,4-Ethylenedioxythiophene: A Route to Highly Conducting Polymer Surface Layers,” *Macromolecules*, vol. 37, pp. 4538–4543, June 2004.

[70] P. Wei, T. Menke, B. D. Naab, K. Leo, M. Riede, and Z. Bao, “2-(2-Methoxyphenyl)-1,3-dimethyl-1h-benzoimidazol-3-ium Iodide as a New Air-Stable n-Type Dopant for Vacuum-Processed Organic Semiconductor Thin Films,” *Journal of the American Chemical Society*, vol. 134, pp. 3999–4002, Mar. 2012.

[71] S. Guo, S. B. Kim, S. K. Mohapatra, Y. B. Qi, T. Sajoto, A. Kahn, S. R. Marder, and S. Barlow, “n-Doping of Organic Electronic Materials using Air-Stable Organometallics,” *Advanced Materials*, vol. 24, pp. 699–+, Feb. 2012.

[72] B. Lussem, M. Riede, and K. Leo, “Doping of organic semiconductors,” *Physica Status Solidi a-Applications and Materials Science*, vol. 210, pp. 9–43, Jan. 2013.

[73] J. Li, G. Zhang, D. M. Holm, I. E. Jacobs, B. Yin, P. Stroeve, M. Mascal, and A. J. Moulé, “Introducing Solubility Control for Improved Organic P-Type Dopants,” *Chemistry of Materials*, vol. 27, pp. 5765–5774, Aug. 2015.

[74] C. Chan, E.-G. Kim, J.-L. Brédas, and A. Kahn, “Molecular n-Type Doping of 1,4,5,8-Naphthalene Tetracarboxylic Dianhydride by Pyronin B Studied Using Direct and Inverse Photoelectron Spectroscopies,” *Advanced Functional Materials*, vol. 16, pp. 831–837, Apr. 2006.

[75] F. Li, M. Pfeiffer, A. Werner, K. Harada, K. Leo, N. Hayashi, K. Seki, X. Liu, and X.-D. Dang, “Acridine orange base as a dopant for n doping of C[sub 60] thin films,” *Journal of Applied Physics*, vol. 100, no. 2, p. 023716, 2006.

[76] F. Li, A. Werner, M. Pfeiffer, K. Leo, and X. Liu, “Leuco Crystal Violet as a Dopant for n-Doping of Organic Thin Films of Fullerene C $_{60}$,” *The Journal of Physical Chemistry B*, vol. 108, pp. 17076–17082, Nov. 2004.

[77] B. D. Naab, S. Guo, S. Olthof, E. G. B. Evans, P. Wei, G. L. Millhauser, A. Kahn, S. Barlow, S. R. Marder, and Z. A. Bao, “Mechanistic Study on the Solution-Phase n-Doping of 1,3-Dimethyl-2-aryl-2,3-dihydro-1h-benzoimidazole

Derivatives," *Journal of the American Chemical Society*, vol. 135, pp. 15018–15025, Oct. 2013.

[78] K. Shi, F. Zhang, C.-A. Di, T.-W. Yan, Y. Zou, X. Zhou, D. Zhu, J.-Y. Wang, and J. Pei, "Toward High Performance n-Type Thermoelectric Materials by Rational Modification of BDPPV Backbones," *Journal of the American Chemical Society*, vol. 137, pp. 6979–6982, June 2015.

[79] B. Russ, M. J. Robb, B. C. Popere, E. E. Perry, C.-K. Mai, S. L. Fronk, S. N. Patel, T. E. Mates, G. C. Bazan, J. J. Urban, M. L. Chabinyc, C. J. Hawker, and R. A. Segalman, "Tethered tertiary amines as solid-state n-type dopants for solution-processable organic semiconductors," *Chem. Sci.*, vol. 7, no. 3, pp. 1914–1919, 2016.

[80] J. E. Cochran, M. J. N. Junk, A. M. Glaudell, P. L. Miller, J. S. Cowart, M. F. Toney, C. J. Hawker, B. F. Chmelka, and M. L. Chabinyc, "Molecular Interactions and Ordering in Electrically Doped Polymers: Blends of PBTTT and F4tcnq," *Macromolecules*, vol. 47, pp. 6836–6846, Oct. 2014.

[81] D. T. Duong, C. Wang, E. Antono, M. F. Toney, and A. Salleo, "The chemical and structural origin of efficient p-type doping in P3ht," *Organic Electronics*, vol. 14, pp. 1330–1336, May 2013.

[82] M. Winokur, Y. B. Moon, A. J. Heeger, J. Barker, D. C. Bott, and H. Shirakawa, "X-Ray Scattering from Sodium-Doped Polyacetylene: Incommensurate-Commensurate and Order-Disorder Transformations," *Physical Review Letters*, vol. 58, pp. 2329–2332, June 1987.

[83] M. J. Winokur, P. Wamsley, J. Moulton, P. Smith, and A. J. Heeger, "Structural evolution in iodine-doped poly(3-alkylthiophenes)," *Macromolecules*, vol. 24, pp. 3812–3815, June 1991.

[84] K. Tashiro, M. Kobayashi, T. Kawai, and K. Yoshino, "Crystal structural change in poly(3-alkyl thiophene)s induced by iodine doping as studied by an organized combination of X-ray diffraction, infrared/Raman spectroscopy and computer simulation techniques," *Polymer*, vol. 38, pp. 2867–2879, June 1997.

[85] C.-K. Mai, B. Russ, S. L. Fronk, N. Hu, M. B. Chan-Park, J. J. Urban, R. A. Segalman, M. L. Chabinyc, and G. C. Bazan, "Varying the ionic functionalities of conjugated polyelectrolytes leads to both p-and n-type carbon nanotube composites for flexible thermoelectrics," *Energy & Environmental Science*, 2015.

[86] C.-K. Mai, R. A. Schlitz, G. M. Su, D. Spitzer, X. Wang, S. L. Fronk, D. G. Cahill, M. L. Chabinyc, and G. C. Bazan, "Side-Chain Effects on the Conductivity, Morphology, and Thermoelectric Properties of Self-Doped Narrow-Band-Gap

Conjugated Polyelectrolytes," *Journal of the American Chemical Society*, vol. 136, no. 39, pp. 13478–13481, 2014.

[87] P. Pingel and D. Neher, "Comprehensive picture of p-type doping of P3ht with the molecular acceptor F4tcnq," *Physical Review B*, vol. 87, p. 115209, Mar. 2013.

[88] Z. H. Wang, C. Li, E. M. Scherr, A. G. MacDiarmid, and A. J. Epstein, "Three dimensionality of "metallic" states in conducting polymers: Polyaniline," *Physical Review Letters*, vol. 66, pp. 1745–1748, Apr. 1991.

[89] K. van de Ruit, R. I. Cohen, D. Bollen, T. van Mol, R. Yerushalmi-Rozen, R. A. J. Janssen, and M. Kemerink, "Quasi-One Dimensional in-Plane Conductivity in Filamentary Films of PEDOT:PSS," *Advanced Functional Materials*, vol. 23, pp. 5778–5786, Dec. 2013.

[90] S. Wang, M. Ha, M. Manno, C. Daniel Frisbie, and C. Leighton, "Hopping transport and the Hall effect near the insulator–metal transition in electrochemically gated poly(3-hexylthiophene) transistors," *Nature Communications*, vol. 3, p. 1210, Nov. 2012.

[91] A. Epstein, J. Joo, R. Kohlman, G. Du, A. MacDiarmid, E. Oh, Y. Min, J. Tsukamoto, H. Kaneko, and J. Pouget, "Inhomogeneous disorder and the modified Drude metallic state of conducting polymers," *Synthetic Metals*, vol. 65, pp. 149–157, Aug. 1994.

[92] Y. H. Kim, C. Sachse, M. L. Machala, C. May, L. Müller-Meskamp, and K. Leo, "Highly Conductive PEDOT:PSS Electrode with Optimized Solvent and Thermal Post-Treatment for ITO-Free Organic Solar Cells," *Advanced Functional Materials*, vol. 21, pp. 1076–1081, Mar. 2011.

[93] J. Luo, D. Billep, T. Waechtler, T. Otto, M. Toader, O. Gordan, E. Sheremet, J. Martin, M. Hietschold, D. R. T. Zahn, and T. Gessner, "Enhancement of the thermoelectric properties of PEDOT:PSS thin films by post-treatment," *Journal of Materials Chemistry A*, vol. 1, no. 26, p. 7576, 2013.

[94] D. M. DeLongchamp, B. D. Vogt, C. M. Brooks, K. Kano, J. Obrzut, C. A. Richter, O. A. Kirillov, and E. K. Lin, "Influence of a Water Rinse on the Structure and Properties of Poly(3,4-ethylene dioxythiophene):Poly(styrene sulfonate) Films," *Langmuir*, vol. 21, pp. 11480–11483, Nov. 2005.

[95] S. N. Patel, A. M. Glaudell, D. Kiefer, and M. L. Chabinyc, "Increasing the Thermoelectric Power Factor of a Semiconducting Polymer by Doping from the Vapor Phase," *ACS Macro Letters*, vol. 5, pp. 268–272, Feb. 2016.

[96] D. T. Scholes, S. A. Hawks, P. Y. Yee, H. Wu, J. R. Lindemuth, S. H. Tolbert, and B. J. Schwartz, "Overcoming Film Quality Issues for Conjugated Polymers Doped with F $_4$ TCNQ by Solution Sequential Processing: Hall Effect, Structural, and Optical Measurements," *The Journal of Physical Chemistry Letters*, vol. 6, pp. 4786–4793, Dec. 2015.

[97] R. Lazzaroni, M. Lögdlund, S. Stafström, W. R. Salaneck, and J. L. Brédas, "The poly-3-hexylthiophene/NOPF6 system: A photoelectron spectroscopy study of electronic structural changes induced by the charge transfer in the solid state," *The Journal of Chemical Physics*, vol. 93, no. 6, p. 4433, 1990.

[98] M. Lögdlund, R. Lazzaroni, S. Stafström, W. R. Salaneck, and J.-L. Brédas, "Direct observation of charge-induced -electronic structural changes in a conjugated polymer," *Physical Review Letters*, vol. 63, pp. 1841–1844, Oct. 1989.

[99] K. Yim, G. L. Whiting, C. E. Murphy, J. J. Halls, J. H. Burroughes, R. H. Friend, and J. Kim, "Controlling Electrical Properties of Conjugated Polymers via a SolutionBased pType Doping," *Advanced Materials*, vol. 20, no. 17, pp. 3319–3324, 2008.

[100] F. J. Zhang, Y. P. Zang, D. Z. Huang, C. A. Di, X. Gao, H. N. Sirringhaus, and D. B. Zhu, "Modulated Thermoelectric Properties of Organic Semiconductors Using Field-Effect Transistors," *Advanced Functional Materials*, vol. 25, pp. 3004–3012, May 2015.

[101] S. Kola, J. H. Kim, R. Ireland, M.-L. Yeh, K. Smith, W. Guo, and H. E. Katz, "Pyromellitic Diimide–Ethynylene-Based Homopolymer Film as an N-Channel Organic Field-Effect Transistor Semiconductor," *ACS Macro Letters*, vol. 2, pp. 664–669, Aug. 2013.

[102] H. Fritzsche, "A general expression for the thermoelectric power," *Solid State Communications*, vol. 9, pp. 1813–1815, Nov. 1971.

[103] Y. W. Park, A. Denenstein, C. K. Chiang, A. J. Heeger, and A. G. MacDiarmid, "Semiconductor-metal transition in doped (CH)x: Thermoelectric power," *Solid State Communications*, vol. 29, pp. 747–751, Mar. 1979.

[104] M. Reghu, Y. Cao, D. Moses, and A. J. Heeger, "Counterion-induced processibility of polyaniline: Transport at the metal-insulator boundary," *Physical Review B*, vol. 47, pp. 1758–1764, Jan. 1993.

[105] A. B. Kaiser, "Electronic transport properties of conducting polymers and carbon nanotubes," *Reports on Progress in Physics*, vol. 64, pp. 1–49, Jan. 2001.

[106] N. Massonnet, A. Carella, O. Jaudouin, P. Rannou, G. Laval, C. Celle, and J.-P. Simonato, “Improvement of the Seebeck coefficient of PEDOT:PSS by chemical reduction combined with a novel method for its transfer using free-standing thin films,” *J. Mater. Chem. C*, vol. 2, no. 7, pp. 1278–1283, 2014.

[107] K. C. See, J. P. Feser, C. E. Chen, A. Majumdar, J. J. Urban, and R. A. Segalman, “Water-Processable Polymer-Nanocrystal Hybrids for Thermoelectrics,” *Nano Letters*, vol. 10, pp. 4664–4667, Nov. 2010.

[108] N. Massonnet, A. Carella, A. de Geyer, J. Faure-Vincent, and J.-P. Simonato, “Metallic behaviour of acid doped highly conductive polymers,” *Chem. Sci.*, vol. 6, no. 1, pp. 412–417, 2015.

[109] K. P. Pernstich, B. Rössner, and B. Batlogg, “Field-effect-modulated Seebeck coefficient in organic semiconductors,” *Nature Materials*, vol. 7, no. 4, pp. 321–325, 2008.

[110] C. J. Vineis, A. Shakouri, A. Majumdar, and M. G. Kanatzidis, “Nanostructured thermoelectrics: big efficiency gains from small features,” *Adv Mater*, vol. 22, pp. 3970–80, Sept. 2010.

[111] J. J. Urban and N. E. Coates, *Innovative Thermoelectric Materials*, ch. Polymer-CNT and Polymer-Nanowire Composites. Imperial College Press, England, 2014 (*In Press*).

[112] J. J. Urban, “Prospects for thermoelectricity in quantum dot hybrid arrays,” *Nature Nanotechnology*, vol. 10, pp. 997–1001, Dec. 2015.

[113] M. He, J. Ge, Z. Lin, X. Feng, X. Wang, H. Lu, Y. Yang, and F. Qiu, “Thermopower enhancement in conducting polymer nanocomposites via carrier energy scattering at the organic–inorganic semiconductor interface,” *Energy & Environmental Science*, vol. 5, no. 8, p. 8351, 2012.

[114] C. Zhou, C. Dun, Q. Wang, K. Wang, Z. Shi, D. L. Carroll, G. Liu, and G. Qiao, “Nanowires as Building Blocks to Fabricate Flexible Thermoelectric Fabric: The Case of Copper Telluride Nanowires,” *ACS Applied Materials & Interfaces*, vol. 7, pp. 21015–21020, Sept. 2015.

[115] Y. S. Ju, K. Kurabayashi, and K. E. Goodson, “Thermal characterization of anisotropic thin dielectric films using harmonic Joule heating,” *Thin Solid Films*, vol. 339, pp. 160–164, Feb. 1999.

[116] J. C. Duda, P. E. Hopkins, Y. Shen, and M. C. Gupta, “Exceptionally Low Thermal Conductivities of Films of the Fullerene Derivative PCBM,” *Physical Review Letters*, vol. 110, p. 015902, Jan. 2013.

[117] X. Wang, C. D. Liman, N. D. Treat, M. L. Chabinyc, and D. G. Cahill, "Ultralow thermal conductivity of fullerene derivatives," *Physical Review B*, vol. 88, p. 075310, Aug. 2013.

[118] X. Wang, V. Ho, R. A. Segalman, and D. G. Cahill, "Thermal Conductivity of High-Modulus Polymer Fibers," *Macromolecules*, vol. 46, pp. 4937–4943, June 2013.

[119] J. Liu, X. Wang, D. Li, N. E. Coates, R. A. Segalman, and D. G. Cahill, "Thermal Conductivity and Elastic Constants of PEDOT:PSS with High Electrical Conductivity," *Macromolecules*, vol. 48, pp. 585–591, Feb. 2015.

[120] A. Weathers, Z. U. Khan, R. Brooke, D. Evans, M. T. Pettes, J. W. Andreasen, X. Crispin, and L. Shi, "Significant Electronic Thermal Transport in the Conducting Polymer Poly (3, 4ethylenedioxythiophene)," *Advanced Materials*, vol. 27, no. 12, pp. 2101–2106, 2015.

[121] Q. Wei, M. Mukaida, K. Kirihara, and T. Ishida, "Experimental Studies on the Anisotropic Thermoelectric Properties of Conducting Polymer Films," *ACS Macro Letters*, vol. 3, pp. 948–952, Sept. 2014.

[122] R. R. Søndergaard, M. Hösel, and F. C. Krebs, "Roll-to-Roll fabrication of large area functional organic materials," *Journal of Polymer Science Part B: Polymer Physics*, vol. 51, pp. 16–34, Jan. 2013.

[123] N. F. Mott and E. A. Davis, *Electronic processes in non-crystalline materials.* Oxford: Oxford University Press, 1971.

[124] O. Bubnova and X. Crispin, "Towards polymer-based organic thermoelectric generators," *Energy & Environmental Science*, vol. 5, pp. 9345–9362, Oct. 2012.

[125] G. Kim and K. P. Pipe, "Thermoelectric model to characterize carrier transport in organic semiconductors," *Physical Review B*, vol. 86, p. 085208, Aug. 2012.

[126] N. Mateeva, H. Niculescu, J. Schlenoff, and L. R. Testardi, "Correlation of Seebeck coefficient and electric conductivity in polyaniline and polypyrrole," *Journal of Applied Physics*, vol. 83, no. 6, p. 3111, 1998.

[127] P. R. Newman, M. D. Ewbank, C. D. Mauthe, M. R. Winkle, and W. D. Smolyncki, "The temperature dependence and anisotropy of the thermal conductivity in polyacetylene," *Solid State Communications*, vol. 40, pp. 975–978, Dec. 1981.

[128] S. K. Yee, N. E. Coates, A. Majumdar, J. J. Urban, and R. A. Segalman, "Thermoelectric power factor optimization in PEDOT:PSS tellurium nanowire hybrid composites," *Physical Chemistry Chemical Physics*, vol. 15, no. 11, p. 4024, 2013.

[129] M. . Panzer and C. . Frisbie, “High Carrier Density and Metallic Conductivity in Poly(3hexylthiophene) Achieved by Electrostatic Charge Injection,” *Advanced Functional Materials*, vol. 16, pp. 1051–1056, May 2006.

[130] M. J. Lee, D. Gupta, N. Zhao, M. Heeney, I. McCulloch, and H. Sirringhaus, “Anisotropy of Charge Transport in a Uniaxially Aligned and Chain-Extended, High-Mobility, Conjugated Polymer Semiconductor,” *Advanced Functional Materials*, vol. 21, pp. 932–940, Mar. 2011.

[131] J.-F. Chang, J. Clark, N. Zhao, H. Sirringhaus, D. Breiby, J. Andreasen, M. Nielsen, M. Giles, M. Heeney, and I. McCulloch, “Molecular-weight dependence of interchain polaron delocalization and exciton bandwidth in high-mobility conjugated polymers,” *Physical Review B*, vol. 74, Sept. 2006.

[132] M. He, J. Li, M. L. Sorensen, F. Zhang, R. R. Hancock, H. H. Fong, V. A. Pozdin, D.-M. Smilgies, and G. G. Malliaras, “Alkylsubstituted Thienothiophene Semiconducting Materials: StructureProperty Relationships,” *Journal of the American Chemical Society*, vol. 131, pp. 11930–11938, Aug. 2009.

[133] I. McCulloch, M. Heeney, C. Bailey, K. Genevicius, I. MacDonald, M. Shkunov, D. Sparrowe, S. Tierney, R. Wagner, W. Zhang, M. L. Chabinyc, R. J. Kline, M. D. McGehee, and M. F. Toney, “Liquid-crystalline semiconducting polymers with high charge-carrier mobility,” *Nature Materials*, vol. 5, pp. 328–333, Mar. 2006.

[134] M. L. Chabinyc, L. H. Jimison, J. Rivnay, and A. Salleo, “Connecting Electrical and Molecular Properties of Semiconducting Polymers for Thin-Film Transistors,” *MRS Bulletin*, vol. 33, pp. 683–689, July 2008.

[135] W. C. Tsoi, S. J. Spencer, L. Yang, A. M. Ballantyne, P. G. Nicholson, A. Turnbull, A. G. Shard, C. E. Murphy, D. D. C. Bradley, J. Nelson, and J.-S. Kim, “Effect of Crystallization on the Electronic Energy Levels and Thin Film Morphology of P3ht:PCBM Blends,” *Macromolecules*, vol. 44, pp. 2944–2952, Apr. 2011.

[136] D. Veldman, S. C. J. Meskers, and R. A. J. Janssen, “The Energy of Charge-Transfer States in Electron Donor-Acceptor Blends: Insight into the Energy Losses in Organic Solar Cells,” *Advanced Functional Materials*, vol. 19, pp. 1939–1948, June 2009.

[137] Q. Sun, K. Park, and L. Dai, “Liquid Crystalline Polymers for Efficient Bilayer-Bulk-Heterojunction Solar Cells,” *The Journal of Physical Chemistry C*, vol. 113, pp. 7892–7897, May 2009.

[138] W. Gao and A. Kahn, “Controlled p doping of the hole-transport molecular material N,N-diphenyl-N,N-bis(1-naphthyl)-1,1-biphenyl-4,4-diamine with tetrafluorotetracyanoquinodimethane,” *Journal of Applied Physics*, vol. 94, pp. 359–366, June 2003.

[139] C. Y. Kao, B. Lee, L. S. Wielunski, M. Heeney, I. McCulloch, E. Garfunkel, L. C. Feldman, and V. Podzorov, “Doping of Conjugated Polythiophenes with Alkyl Silanes,” *Advanced Functional Materials*, vol. 19, no. 12, pp. 1906–1911, 2009.

[140] H. Sirringhaus, P. Brown, R. Friend, M. Nielsen, K. Bechgaard, B. Langeveld-Voss, A. Spiering, R. Janssen, E. Meijer, P. Herwig, *et al.*, “Two-dimensional charge transport in self-organized, high-mobility conjugated polymers,” *Nature*, vol. 401, no. 6754, pp. 685–688, 1999.

[141] J. Chen, A. Heeger, and F. Wudl, “Confined soliton pairs (bipolarons) in polythiophene: In-situ magnetic resonance measurements,” *Solid State Communications*, vol. 58, pp. 251–257, Apr. 1986.

[142] H. Tanaka, M. Hirate, S. Watanabe, and S.-i. Kuroda, “Microscopic Signature of Metallic State in Semicrystalline Conjugated Polymers Doped with Fluoroalkylsilane Molecules,” *Advanced Materials*, vol. 26, pp. 2376–2383, Apr. 2014.

[143] D. M. Rowe and G. Min, “-in plot as a thermoelectric material performance indicator,” *Journal of Materials Science Letters*, vol. 14, pp. 617–619, Jan. 1995.

[144] J. F. Kwak, T. C. Clarke, R. L. Greene, and G. B. Street, “Transport properties of heavily AsF5 doped polyacetylene,” *Solid State Communications*, vol. 31, pp. 355–358, Aug. 1979.

[145] Y.-W. Park, A. J. Heeger, M. A. Druy, and A. G. MacDiarmid, “Electrical transport in doped polyacetylene,” *The Journal of Chemical Physics*, vol. 73, no. 2, pp. 946–957, 1980.

[146] Y. W. Park, W. K. Han, C. H. Choi, and H. Shirakawa, “Metallic nature of heavily doped polyacetylene derivatives: Thermopower,” *Physical Review B*, vol. 30, pp. 5847–5851, Nov. 1984.

[147] A. J. Epstein, H. Rommelmann, R. Bigelow, H. W. Gibson, D. M. Hoffmann, and D. B. Tanner, “Role of Solitons in Nearly Metallic Polyacetylene,” *Physical Review Letters*, vol. 50, pp. 1866–1869, June 1983.

[148] M. Galtier, J. M. Gay, A. Montaner, and J. L. Ribet, “Semiconductor to metal transistion in $MoCl_5$ doped polyacetylene,” *Le Journal de Physique Colloques*, vol. 44, pp. C3–107–C3–110, June 1983.

[149] M. Przybylski, B. R. Bulka, I. Kulszewicz, and A. Proń, "Electrical transport properties of polyacetylene tetrachloroferrate - [CH(FeCl4)y]x]," *Solid State Communications*, vol. 48, pp. 893–896, Dec. 1983.

[150] J. R. Reynolds, J. B. Schlenoff, and J. C. W. Chien, "Magnetic and Transport Properties of Electrochemically Oxidized Polyacetylene," *Journal of The Electrochemical Society*, vol. 132, pp. 1131–1135, May 1985.

[151] T. E. Jones, T. R. Ogden, W. C. McGinnis, W. F. Butler, and D. M. Gottfredson, "Electronic properties of polyacetylene doped with FeCl3," *The Journal of Chemical Physics*, vol. 83, pp. 2532–2537, Sept. 1985.

[152] W. Beyer and H. Overhof, "Transport properties of doped amorphous silicon," *Solid State Communications*, vol. 31, pp. 1–4, July 1979.

[153] A. Burkov, "Measurements of Resistivity and Thermopower: Principles and Practical Realization," in *Thermoelectrics Handbook* (D. Rowe, ed.), pp. 22–1–22–12, CRC Press, Dec. 2005.

[154] B. Schumacher, H.-G. Bach, P. Spitzer, and J. Obrzut, "Electrical Properties," in *Springer Handbook of Materials Measurement Methods* (H. C. Prof, T. Saito, and L. Smith, eds.), pp. 431–484, Springer Berlin Heidelberg, 2006. DOI: 10.1007/978-3-540-30300-8_9.

[155] V. I. Arkhipov, P. Heremans, E. V. Emelianova, G. J. Adriaenssens, and H. Bässler, "Charge carrier mobility in doped semiconducting polymers," *Applied Physics Letters*, vol. 82, pp. 3245–3247, May 2003.

[156] V. Arkhipov, P. Heremans, E. Emelianova, and H. Bässler, "Effect of doping on the density-of-states distribution and carrier hopping in disordered organic semiconductors," *Physical Review B*, vol. 71, Jan. 2005.

[157] V. I. Arkhipov, E. V. Emelianova, P. Heremans, and H. Bässler, "Analytic model of carrier mobility in doped disordered organic semiconductors," *Phys. Rev. B*, vol. 72, p. 235202, Dec 2005.

[158] B. A. Collins, J. E. Cochran, H. Yan, E. Gann, C. Hub, R. Fink, C. Wang, T. Schuettfort, C. R. McNeill, M. L. Chabinyc, and H. Ade, "Polarized X-ray scattering reveals non-crystalline orientational ordering in organic films," *Nature Materials*, vol. 11, pp. 536–543, Apr. 2012.

[159] Z. Q. Gao, B. X. Mi, G. Z. Xu, Y. Q. Wan, M. L. Gong, K. W. Cheah, and C. H. Chen, "An organic p-type dopant with high thermal stability for an organic semiconductor," *Chem. Commun.*, no. 1, pp. 117–119, 2008.

[160] A. Salleo, T. W. Chen, A. R. Völkel, Y. Wu, P. Liu, B. S. Ong, and R. A. Street, “Intrinsic hole mobility and trapping in a regioregular poly(thiophene),” *Physical Review B*, vol. 70, p. 115311, Sept. 2004.

[161] N. F. Mott, *Electronic processes in non-crystalline materials.* International series of monographs on physics, Oxford: Clarendon Press, 2nd ed ed., 2012.

[162] A. L. Efros and B. I. Shklovskii, “Coulomb gap and low temperature conductivity of disordered systems,” *Journal of Physics C: Solid State Physics*, vol. 8, no. 4, p. L49, 1975.

[163] B. I. Shklovskii and A. L. Ėfros, *Electronic properties of doped semiconductors.* No. 45 in Springer series in solid-state sciences, Berlin: Springer, 1984.

[164] S. ROTH, “CHAPTER 11 - Hopping Conduction in Electrically Conducting Polymers,” in *Modern Problems in Condensed Matter Sciences* (M. P. a. B. SHKLOVSKII, ed.), vol. 28 of *Hopping Transport in Solids*, pp. 377–395, Elsevier, 1991.

[165] Z. H. Wang, E. M. Scherr, A. G. MacDiarmid, and A. J. Epstein, “Transport and EPR studies of polyaniline: A quasi-one-dimensional conductor with three-dimensional “metallic” states,” *Physical Review B*, vol. 45, pp. 4190–4202, Feb. 1992.

[166] V. N. Prigodin, Y. A. Firsov, and W. Weller, “Localization in a system of N coupled chains,” *Solid State Communications*, vol. 59, pp. 729–735, Sept. 1986.

[167] K. Maschke, H. Overhof, and P. Thomas, “On Variable Range Hopping near the Fermi Energy One-Dimensional Systems,” *physica status solidi (b)*, vol. 61, pp. 621–627, Feb. 1974.

[168] J. E. Yoo, K. S. Lee, A. Garcia, J. Tarver, E. D. Gomez, K. Baldwin, Y. Sun, H. Meng, T.-Q. Nguyen, and Y.-L. Loo, “Directly patternable, highly conducting polymers for broad applications in organic electronics,” *Proceedings of the National Academy of Sciences*, vol. 107, pp. 5712–5717, Mar. 2010.

[169] J. E. Yoo, *Understanding the Processing-Structure-Property Relationships of Water-Dispersible, Conductive Polyaniline.* PhD thesis, The University of Texas at Austin, May 2009.

[170] W. B. Chang, H. Fang, J. Liu, C. M. Evans, B. Russ, B. C. Popere, S. N. Patel, M. L. Chabinyc, and R. A. Segalman, “Electrochemical effects in thermoelectric polymers,” *ACS Macro Letters*, vol. 5, pp. 455–459, 2016.

[171] Q. Wei, M. Mukaida, K. Kirihara, Y. Naitoh, and T. Ishida, “Thermoelectric power enhancement of PEDOT:PSS in high-humidity conditions,” *Applied Physics Express*, vol. 7, p. 031601, Mar. 2014.